



TÉCNICO  
LISBOA



**An hydrofoil control system for the SR02 vessel in the  
scope of the Técnico Solar Boat Project**

**Basile Jean Belime**

Thesis to obtain the Master of Science Degree in  
**Electrical and Computer Engineering**

Supervisor: Prof. António Manuel dos Santos Pascoal

**Examination Committee**

Chairperson: Prof. João Fernando Cardoso Silva Sequeira

Supervisor: Prof. António Manuel dos Santos Pascoal

Member of the Committee: Prof. António Pedro Rodrigues Aguiar

**October 2020**



I declare that this document is an original work of my own authorship and that it fulfills all the requirements of the Code of Conduct and Good Practices of the Universidade de Lisboa.



Dedicated to the Técnico Solar Boat team



## Acknowledgments

The work done in this thesis could not be possible without the help of the complete Técnico Solar Boat team. For 4 years I have worked with incredible people within the Técnico Solar Boat project, and it was an incredible journey.

Regarding the past year, there are a few names I have to mention: David Mendes, for his help with all the communication and coding for the implementation of the hydrofoil control system, Sebastião Beirão for pushing us all to work harder and make all kinds of improvements on the boat, and finally Robin Tomaz for his knowledge about hydrofoils and for being the most patient pilot I have ever met, he spent over 150 hours sitting in the boat in the past 4 months, sometimes waiting for half an hour for me to remotely upload new firmware to the foils' microcontroller. Thank you all so much, without you the boat would definitely not be flying today.

Thank you everyone who has been part of the TSB team, thank you for making this such a great project. I wish everyone who is now involved in the project a lot of success and hope to see all future vessels flying faster, higher and better.

Thank you to all the other student teams who have so openly shared their knowledge and experience with us.

At last I would like to thank my supervisor, prof. António Pascoal, for all his help in the development of the controller.



## Resumo

Esta tese foca o projeto, implementação e teste de um sistema de controlo para a embarcação SR02 com *hydrofoils* desenvolvida no âmbito do projeto Técnico Solar Boat. Neste projeto constroem-se embarcações movidas a energia solar e por isso tem como objetivo serem o mais leve e o mais eficiente possível. Para tal tenciona-se projetar e implementar um sistema com *hydrofoils*, asas que se inserem por baixo do barco ficando submersas e criando uma força de elevação suficiente para o casco não tocar na água. Assim pode-se reduzir o arrasto da embarcação e avançar de forma mais eficiente do ponto de vista energético.

Nesta tese são estudadas todas as equações físicas que regem o sistema de forma a ser possível criar um modelo *Simulink* para poder fazer todo o tipo de simulações e analisar o comportamento da embarcação quando se encontra sobre *foils*. A partir deste modelo segue-se a implementação de um sistema de controlo que poderá regular a força de elevação gerada pelos *hydrofoils* e assim estabilizar a embarcação a uma certa altura relativamente á linha de água. Para desenhar o sistema de controlo passa-se pela procura dos vários pontos de equilíbrio do sistema, a linearização em torno de um desses pontos, e o cálculo dos ganhos mais adequados para estabilizar o sistema.

O controlador analisado é baseado num LQR (Linear Quadratic Regulator), onde é implementado um seguimento de referência, uma acção de ganho integral, um sistema de *anti wind-up* e uma implementação delta. Após ter o controlador desenhado procede-se à procura dos melhores ganhos para o sistema, tanto para um controlo de inclinação lateral como para um controlo de altura.

Ambos os controladores são testados no modelo não linear do veículo, com variações de aceleração, com ruído dos sensores e com pertubações laterais.

São depois apresentados os sensores e os atuadores implementados no sistema e a arquitetura do sistema real. E analisado parte do sistema de *software* implementado nos microcontroladores do barco que permitem flexibilidade ao piloto.

O sistema de controlo é testado nos microcontrolador para fazer testes de *hardware in the loop*. Os resultados destes testes são comparados aos dados das simulações para verificar que a implementação no sistema final foi bem feita.

Com isto tudo a embarcação seguirá para a água e serão analisados os resultados obtidos. Com base nos resultados e nas aprendizagens obtidas através dos testes são apresentadas melhorias e os resultados das mesmas. Tal como a implementação de um sistema de controlo de velocidade do veículo e um controlo de inclinação forçada.



## Abstract

This thesis focuses on the design, implementation and testing of a control system for the hydrofoil vessel SR02, developed under the Técnico Solar Boat project. In this project solar-powered vessels are built and therefore aim to be as light and efficient as possible. For this purpose it is intended to design and implement a system with *hydrofoils*, wings that are inserted underneath the boat becoming submerged and creating sufficient lift force for the hull not to touch the water. This way it is possible to reduce the drag of the boat and advance in a more energy efficient way.

In this thesis all the physical equations that govern the system are studied so that it is possible to create a *Simulink* model to be able to make all kinds of simulations and analyze the behavior of the boat when it is *foilborne*. This model is followed by the implementation of a control system that can regulate the lift force generated by the *hydrofoils* and thus stabilize the vessel at a certain height in relation to the water line. To design the control system one has to look for the various equilibrium points of the system, linearize it around one of these points, and calculate the most appropriate gains to stabilize the system.

The controller analysed is based on an LQR (Linear Quadratic Regulator), where reference tracking, integral action, anti wind-up and a delta implementation are introduced. Once the controller has been designed, the best gains for the system are sought, both for roll control and for heave control.

Both controllers are tested on the non-linear model of the vehicle, with acceleration variations, with sensor noise and with lateral disturbances.

Then the sensors and actuators implemented in the system and the actual system's architecture are presented. Part of the *software* implemented in the microcontrollers of the boat is presented.

*Hardware in the loop* tests are carried in the microcontrollers. The results of these tests are compared with the data from the simulations to verify that the implementation in the final system is well done.

With all this the vessel will proceed to the water and the results will be analyzed. Based on the tests and their results, some improvements are suggested, tested and analyzed. Such as the implementation of a speed control system and an active reference on roll control.



# Contents

Acknowledgments . . . . .	vii
Abstract . . . . .	ix
Abstract . . . . .	xi
List of Tables . . . . .	xv
List of Figures . . . . .	xvii
Nomenclature . . . . .	xxi
<b>1 Introduction</b>	<b>1</b>
1.1 Motivation . . . . .	2
1.2 Topic Overview . . . . .	3
1.3 Objectives . . . . .	4
1.4 State of the art . . . . .	4
1.4.1 Hydrofoil history . . . . .	4
1.4.2 Hydrofoil control . . . . .	6
1.5 Thesis Outline . . . . .	8
<b>2 Background</b>	<b>11</b>
2.1 Theoretical Model . . . . .	15
2.1.1 Reference frames . . . . .	15
2.1.2 Main forces . . . . .	16
2.1.3 Equations breakdown . . . . .	17
<b>3 Model</b>	<b>23</b>
3.1 Non-linear model . . . . .	23
3.2 Trimming of the Model . . . . .	26
3.3 Linearization of the Model . . . . .	29
<b>4 Controller</b>	<b>33</b>
4.1 Linear Quadratic Regulator . . . . .	33
4.1.1 General equations . . . . .	33
4.1.2 Reference following for heave . . . . .	34
4.1.3 Choosing Q and R weights . . . . .	34

4.1.4	Step responses for heave and pitch . . . . .	36
4.1.5	Integral Action . . . . .	39
4.1.6	Anti wind-up . . . . .	40
4.1.7	Delta implementation . . . . .	41
4.1.8	Gains recalibration . . . . .	42
4.1.9	Final controller vs simple LQR . . . . .	43
4.2	Controller for roll . . . . .	44
4.3	Common and differential modes . . . . .	45
<b>5</b>	<b>Simulations using the Non-linear Model</b>	<b>47</b>
5.1	Heave and pitch control simulations . . . . .	47
5.2	Roll control simulations . . . . .	51
<b>6</b>	<b>Implementation</b>	<b>55</b>
6.1	Hardware . . . . .	55
6.2	Software . . . . .	57
6.3	Hardware in the loop test . . . . .	59
<b>7</b>	<b>Results and upgrades</b>	<b>61</b>
7.1	Roll controller tests . . . . .	61
7.2	Heave and pitch controller tests . . . . .	64
7.2.1	Motor's PID upgrade . . . . .	66
7.3	Active roll reference . . . . .	70
7.4	Técnico Solar Boat Odisseia 2020 . . . . .	75
<b>8</b>	<b>Conclusions</b>	<b>77</b>
8.1	Summary . . . . .	77
8.2	Future Work . . . . .	78
<b>Bibliography</b>		<b>81</b>
<b>A Controller PCB</b>		<b>83</b>

# List of Tables

2.1	Constants used for the model . . . . .	22
3.1	Initial conditions used for trimming the model . . . . .	27
3.2	Limits of the model for steady state search . . . . .	28
3.3	Steady states values of front and rear foil's AoA and thrust for different $u$ speeds . . . . .	29
3.4	Steady states values of thrust and pitch for different fixed rear foil AoA and a $u$ speed of 7 m/s . . . . .	29
4.1	Estimates of the full ranges of the state variables for the heave model. . . . .	35
4.2	Estimates of the full ranges of the state variables for the roll model. . . . .	36



# List of Figures

1.1 SR01 in Mónaco . . . . .	1
1.2 Render of Tecnico Solar Boat's vessel where 3 foils and their corresponding struts are visible under the hull. . . . .	2
1.3 Speed versus drag curves for SR01 with and without hydrofoils. [1] . . . . .	3
1.4 Clafis dutch solar boat team using mechanical foil control [2]. . . . .	3
1.5 Hydrofoil vessel from 1906 [4]. . . . .	5
1.6 USS PEGASUS (PHM-1) US Navy Patrol Combatant Hydrofoil from the 70s [5]. . . . .	5
1.7 Surface piercing and fully submerged foils [4]. . . . .	6
1.8 Surface piercing foils from Engineers of Innovation team in Holland. . . . .	6
1.9 TU Delft Solar Boat team and their 2017 boat [7]. . . . .	6
1.10 US NAVY 1953 - The Lantern (HC-4). . . . .	7
1.11 Candela Speed Boat [10]. . . . .	8
1.12 Delft Solar Boat team's bicycle hydrofoil boat [11]. . . . .	8
2.1 The working principle of a foil and how it generates lift. . . . .	11
2.2 The hydrofoils designed for SR01 that will be used on SR02. . . . .	12
2.3 Lift coefficients for 5 different Re values, which represent 5 different speeds of the vessel. Here alpha represents the angle of attack of the foil. . . . .	13
2.4 Linear curve approximation of $C_L$ and AoA of the hydrofoils . . . . .	14
2.5 Drag curve of $C_D$ and AoA of the hydrofoils . . . . .	15
2.6 The axis orientation and the movement definitions for boats. [13] . . . . .	16
2.10 Foils distances to center of mass on the XZ plane. . . . .	21
2.11 Front foils distances to center of mass on the XY plane. . . . .	22
3.1 Model architecture of the boat on foils. . . . .	24
3.2 Boat equations block of the boat model. . . . .	25
4.1 Classical LQR block diagram. . . . .	34
4.2 LQR model with reference following on heave. . . . .	35
4.3 Front foil step response with LQR control for multiple R values. . . . .	37
4.4 First second of the front foil input value for step response with LQR control. . . . .	37
4.5 Front foil step response with LQR control for multiple gains on the $z$ entry for the $Q_h$ matrix. . . . .	38

4.6	First seconds of the front foil input value for step response with LQR control for multiple gains on the $z$ entry for the $Q_h$ matrix. . . . .	38
4.7	Pitch value for front foil step response with LQR control for multiple gains on the $z$ entry for the $Q_h$ matrix. . . . .	39
4.8	LQR model with integral action on heave. . . . .	39
4.9	LQR model with integral action on heave. . . . .	41
4.10	LQR model with delta implementation on heave. . . . .	42
4.11	Front foil step response with LQR control for multiple gains on the $q_i$ entry for the $Q_h$ matrix. . . . .	42
4.12	Bode plot of the closed loop linear system for heave and pitch. . . . .	43
4.13	Front foil step response with LQR control as in figure 4.2 (simple reference following) with error on speed sensor value at $t = 10s$ . . . . .	44
4.14	Front foil step response with LQR control as in figure 4.10 (delta implementation) with error on speed sensor value at $t = 10s$ . . . . .	44
4.15	LQR model with delta implementation on roll. . . . .	45
4.16	Common and differential modes combination. . . . .	46
5.1	Non linear model's step response. . . . .	48
5.2	Thrust variations impact on heave and pitch control. . . . .	49
5.3	Thrust variations impact on heave and pitch control. Here with an undershoot on heave. . . . .	49
5.4	Real sensors' data detrended which was used in the simulation of figure 5.5. . . . .	50
5.5	Simulations with added real sensors' data to mimic noise. . . . .	50
5.6	Non linear model's step response for roll. . . . .	51
5.7	Roll readings from sensor used as perturbations for the simulation done in 5.8. . . . .	52
5.8	Roll control simulation with outside perturbations on roll. . . . .	52
5.9	Roll control simulation with exaggerated perturbations on roll. . . . .	53
5.10	Roll control simulation with exaggerated perturbations on roll but higher slew rate on the foils' AoA. . . . .	53
6.1	Hardware diagram of the components on the vessel that allow to control the hydrofoils. . . . .	56
6.2	Positioning of the AHRS and the ultrasonic sensor on the vessel. . . . .	56
6.3	Flowchart of the different states and operating modes. . . . .	58
6.4	Comparison between LQR controller output on the microcontroller and <i>Simulink</i> for heave control. . . . .	59
7.1	First tests where no control was active and high rolls can be seen in multiple runs. . . . .	62
7.2	First test with active roll control. . . . .	62
7.3	Roll controller active and turning at cruise speed. . . . .	63
7.4	Bird view of the course taken by the boat for data of figure 7.3. . . . .	63
7.5	First test with active roll control. . . . .	64
7.6	First tests with active height control. . . . .	65

7.8 Flying with small rear AoA. . . . .	66
7.9 Scheme of how the motor is controller without PID. . . . .	67
7.10 Scheme of how the motor is controller with the new PID. . . . .	67
7.11 PID feedback loop that was implemented to keep a constant speed. . . . .	68
7.12 PID speed control results. . . . .	69
7.13 Flight data with PID speed control corresponding to figure 7.12. . . . .	69
7.14 Flying stable and doing a small turn (drone view). . . . .	70
7.15 Flight data where the boat can be seen falling sideways due to the wind. . . . .	71
7.16 Upgrade done on the roll controller with yaw rate (here GyroZ) fed back to the reference. .	71
7.17 Real data used to simulate how the roll reference would look like. As can be seen here, a lot of noise comes from the sensor. . . . .	72
7.18 Yaw rate filtered data over the raw data from the sensor. . . . .	73
7.19 Active roll reference simulation with filtered yaw rate as reference. . . . .	73
7.20 Real data with active roll reference implemented on the vessel and doing loopings at cruise speed. . . . .	74
7.21 Bird view of the course taken by the boat for data of figure 7.20. . . . .	74
7.22 Long flight during the Odisseia 2020 event. . . . .	75
7.23 Images of the boat during the Odisseia 2020 tour. . . . .	75



# Nomenclature

## Greek symbols

$\alpha_{front}$  Angle of attack of front foils.

$\alpha_{rear}$  Angle of attack of rear foil.

$\phi$  Roll Angle.

$\rho$  Density.

$\theta$  Pitch Angle.

## Roman symbols

$AoA$  Foil's angle of attack.

$C_D$  Coefficient of drag.

$C_L$  Coefficient of lift.

$CM$  Boat's centre of mass.

$D_{left}$  Front left foil's drag.

$D_{right}$  Front right foil's drag.

$D_{rear}$  Rear foil's drag.

$I_X$  Boat's moment of inertia about X axis.

$I_Y$  Boat's moment of inertia about Y axis.

$L_{left}$  Front left foil's lift.

$L_{right}$  Front right foil's lift.

$L_{rear}$  Rear foil's lift.

$X$  Surge.

$X_b, Y_b, Z_b$  Body axis.

$X_i, Y_i, Z_i$  Inertial axis.

$z$  Heave.

$\mathbf{u}$  Velocity vector.

$u, v, w$  Velocity Cartesian components.

# Chapter 1

## Introduction

Técnico Solar Boat was created by Naval engineering students of Instituto Superior Técnico (IST) in 2014. The team has since expanded and is now a group of around 30 students from a wide range of undergraduate, MSc and Phd programs.

The main goal of the team is to work on the development of a solar powered boat to participate in worldwide university competitions organized by Solar Sport One or the Monaco Yacht Club such as the Monaco Solar & Energy Boat Challenge.

The team has already participated in competitions in 2017 in Monaco and in 2018 in Holland and Monaco again. In these two years the races were done with the first prototype, SR01, built in 2017 and fine tuned in 2018.



Figure 1.1: SR01 in Mónaco

## 1.1 Motivation

Throughout all the years of existence of the Técnico Solar Boat team there has always been a key goal in mind: to build the best, most efficient and fastest boat for the competitions in which it's involved. It has always been known by the team members that in order to make this happen there would need to be a special feature on the boat: actuators in the form of hydrofoils.

Hydrofoils allow a boat to get elevated over the water line in such a way that the hull doesn't touch the water. This is one way of reducing the drag forces exerted on the boat, thus allowing it to consume less energy for the same horizontal speed. The drag reduction is the difference between the drag from the hull when not elevated from the water, and the total drag experienced only by the submerged hydrofoils and corresponding struts. The struts are rigid structures to which the foils are attached, see 1.2. The struts need to be strong enough to support the weight of the vessel.



Figure 1.2: Render of Tecnico Solar Boat's vessel where 3 foils and their corresponding struts are visible under the hull.

The difference in drag for the SR01 boat with and without hydrofoils has been explained in a thesis done by a former member of the Técnico Solar Boat team [1]. Figure 1.3 shows how hydrofoils can be in terms of improving the performance of SR01. The figure shows an abrupt fall in drag at around 5 m/s, which is the predicted take off speed.

Every year the team has attempted to implement this feature, but there has always been drawbacks that led to the team giving up on using the hydrofoils. Nonetheless hydrofoils have always been part of the work plan and all the mechanical and electrical parts are ready to be implemented on the boat. The commitment to pursue this goal is the main motivation for the work described in the present thesis.

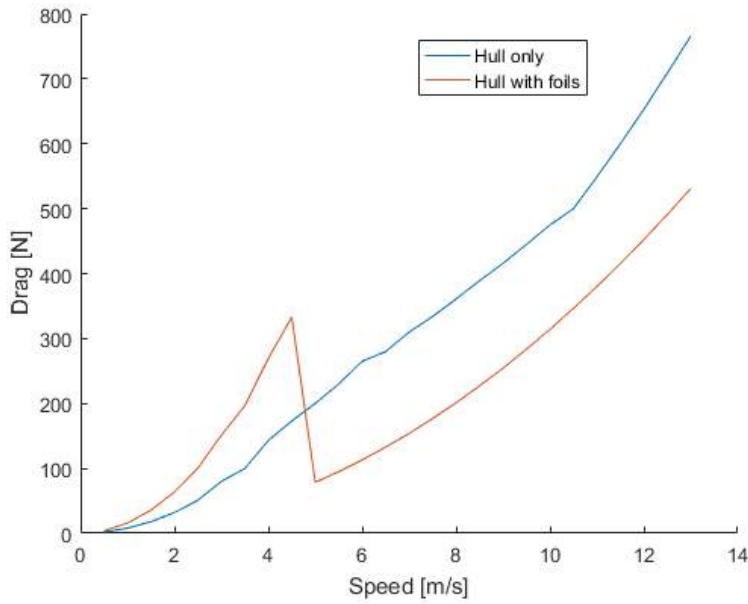


Figure 1.3: Speed versus drag curves for SR01 with and without hydrofoils. [1]

## 1.2 Topic Overview

Since 2016 the team has been working on developing a hydrofoil system. Thus far, one mechanical and one electronically controlled system had been developed, but not well enough to be implemented.

In the first year of the team's existence, a system was dimensioned with 3 foils, two at the front and one at the back, and the angles of attack of the foils were mechanically controlled. This mechanical system used floaters attached to carbon fiber tubes that moved the whole strut to which the hydrofoil was attached. Figure 1.4 illustrates a boat from a private team using this kind of foil control. Basically, the small water skates "measure" the distance of the front of the vessel to the water line.



Figure 1.4: Clafis dutch solar boat team using mechanical foil control [2].

During the season 2017/2018, new foils, lighter and more hydrodynamic, were produced with the

hope to yield a better system. This time, the control was planned to be done using a sensor to measure the boat's distance to water and another to measure roll, pitch, angular velocities and x, y, z accelerations, then small stepper motors would adjust the angle of attack of the foils according to the desired pitch, roll and height above the water.

Unfortunately, the team had major problems with the power train and there was a small mechanical part holding the foil that broke very near the time of the competitions. As a result the team did not have enough time to test the system. After the competitions the focus of the team shifted to building a new hull, SR02, and so again the hydrofoils were not implemented and tested.

Finally, for the SR02 boat (shown in figure 1.2) the team designed the control parts of the hydrofoil system in a way that it would be possible to either use a mechanical control system or an electrical control system. This boat was used for the Monaco Solar & Energy Boat Challenge [3], and finished in a great 2<sup>nd</sup> place, but still without the hydrofoils.

The SR02 is a manned vessel where heading and speed are controlled by the pilot.

The boat was tested again in October 2019 because its power train and communications were not fully functional during the race. Now everything is in place to finally use the hydrofoils, and this is a priority of the team for the 2019/2020 season.

## 1.3 Objectives

This thesis addresses the modeling and control of the SR02 solar boat using hydrofoils, with a goal of reducing the energy spent in cruising and obtaining a smooth and thus comfortable ride. The specifications call for a control system capable of maintaining the vessel above the medium water level and execute smooth transitions in altitude, while keeping pitch and roll close to 0 degrees.

In the previous years of existence of the team, some members have worked on the development of a *Simulink*-based dynamic model for the boat on hydrofoils, which proved to be extremely helpful to understand the key principles at the core of the model.

This thesis' final goal is to get the SR02 vessel to smoothly ride on hydrofoils. For that a model needs to be created, which will allow the design and validation of a controller. After the validation, the controller will be implemented on the real boat.

It is to be noted that this work is to be done on an already existing vessel with existing components. The foils, the sensors, the actuators, the hull itself, are all components that have already been designed and manufactured/acquired by the Técnico Solar Boat team.

## 1.4 State of the art

### 1.4.1 Hydrofoil history

One of the first successful hydrofoil boats was ridden in 1894 [4]. The boat was built by an inventor who knew that lift was proportional to the square of the velocity of the foil with respect to the surrounding

fluid and took advantage of this fact. According to [4], the reason for not having seen earlier boats successfully using hydrofoils was due to the lack of suitable structural materials.

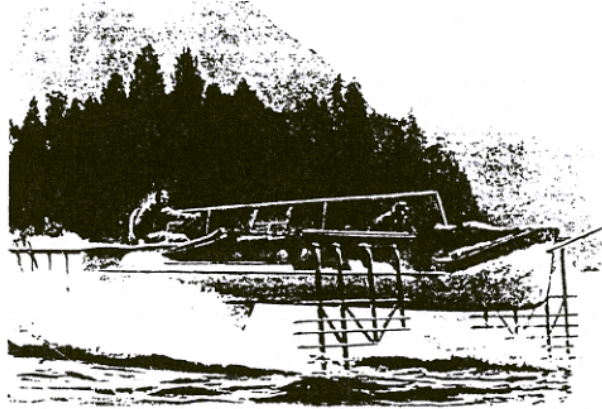


Figure 1.5: Hydrofoil vessel from 1906 [4].

Since then, hydrofoils have been used in different applications, mainly in the military [5] and in commercial [6] boats. Some have been made for public transportation, in Holland for example [5].



Figure 1.6: USS PEGASUS (PHM-1) US Navy Patrol Combatant Hydrofoil from the 70s [5].

With all the developments since the early models of hydrofoils there are now two main types of hydrofoils: surface piercing and fully submerged. The two shapes can be seen in figure 1.7. The main difference between the two is that the surface piercing does not need an active control system. This happens because as it lifts out of the water the surface area of the submerged foil reduces and thus lift reduces until it stabilizes.

The functioning of the fully submerged foil is different in a way that it will not move that much as waves don't change the submerged area of the foil, and therefore the ride is smoother. On the other hand, the functioning of fully submerged foils totally depends on an active control system, either fully mechanical or electrical sensor based.

In the context of this project there are many different types of hydrofoils systems implemented. Some teams have surface piercing foils (figure 1.8), others have fully submerged foils with electrical sensor based control (figure 1.9) and some use mechanical control systems, as seen previously in figure 1.4.

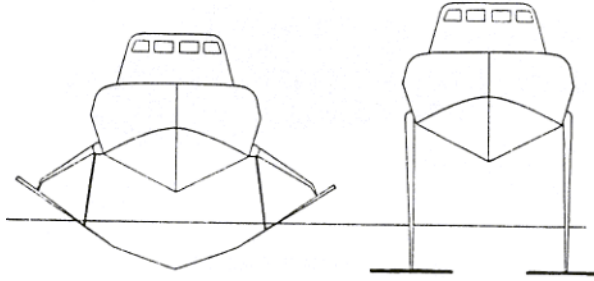


Figure 1.7: Surface piercing and fully submerged foils [4].



Figure 1.8: Surface piercing foils from Engineers of Innovation team in Holland.



Figure 1.9: TU Delft Solar Boat team and their 2017 boat [7].

### 1.4.2 Hydrofoil control

Electronic hydrofoil control systems have already been used in the military back in 1980, using gyroscopes, accelerometers, height sensors and hydraulic servo actuators [8].

There have been many different kinds of automatic control systems used. Initially, most were with mechanical control of the angle of attack of the foil. Then, manual control systems were used, there was a man-in-the-loop concept with a joystick to control the vessel's stability. Also a pneumatic system with an air-feed control system has been developed where the amount of air going to the foils was automatically controlled. All these systems are described in depth in [9].

The first electronic control known to have been used was around 1953 on a vessel called Lantern,

seen in figure 1.10. After some time with the fall of prices for electronic parts, electronic systems started to be more dominant [9].

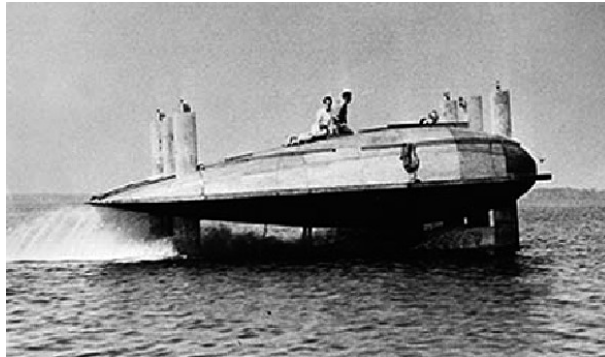


Figure 1.10: US NAVY 1953 - The Lantern (HC-4).

At the Monaco Solar & Energy Boat Challenge, most control systems are based on electronic sensors or on water skates that get lifted by the waves and therefore raise the angle of attack which in turn increases the lift force.

Both systems proved to be adequate for the races as the teams with hydrofoils managed to get great results. The use of mechanical control may be cheaper and more robust, as it depends on less parts, but it adds the drag of the water skates and is much harder to tune. The electronic control system can be tuned from the shore with proper connectivity and can be previously adapted to any boat given the main parameters of the vessel, such as weight, mass distribution and physical location of the foils relative to the boat.

After concluding some research and exchanges with other teams it's possible to say that most of the electronic control systems that have been developed are based on PID controllers. This controller has the advantage of being simple to implement but requires tuning that is usually done by trial and error. One of the disadvantages of this controller is that it only takes one input and its reference, for example height and desired height of the boat. To control height and take advantage of more measurements available, such as linear and angular velocities, data would have to be processed before being used as a PID input.

In this thesis we explore the use of a linear quadratic regulator (LQR), which basically allows us to use any variable that may have an influence on the variable that needs to be controlled. Then for every single variable we can choose how much influence we want it to have on the controller's output. This brings many advantages on the adaptability of the system, where it could work with a single measurement of height to many measurements like all the acceleration, linear and angular velocities and height.

In the market there are also some existing commercial boats such as for example the Candela Speed Boat, which uses electronic sensor based control, see figure 1.11.

Students from the TU Delft university have also developed another system which consists of only two foils, which they claim to work with the same principle as a bicycle, where the pilot maintains the boat balanced by turning the front strut [11].



Figure 1.11: Candela Speed Boat [10].



Figure 1.12: Delft Solar Boat team's bicycle hydrofoil boat [11].

## 1.5 Thesis Outline

First of all an analytic overview of the hydrofoils that were designed for the SR01 will be made. All the data used for the drag and lift coefficient of the foils and also for the struts will be analyzed. These data were provided by Aerospace Engineering students who are also members of the Técnico Solar Boat team and are the ones who projected the foils. The foils have been projected based on data from *airfoiltools*, an online database in which all kinds of different foils with various sections and shapes have their physical properties available for everyone.

After going through the foils, the physical equations of the SR02 boat, which has 2 foils at the front and 1 at the rear, will be analyzed. The main equations used are the drag, lift, angular accelerations and the X and Z accelerations. These are the equations that will lead to the *Simulink*-based model that simulates the pitch and heave of the boat.

Having the model defined it will be possible to analyze the behavior of the boat, more specifically the heave and pitch responses to changes in the foils' angle of attack (AoA). With this will also come the search of a stable operating point given the initial conditions, and around this operating point the model will be linearized.

For this boat it is known that the rear foil will be at a fixed adjustable angle, so there will be no electronic actuator on it. With this known the referenced control will either have to be a heave control or a pitch control, not both as in an ideal case. Thus another analysis will be made to know how the pitch changes relative to the speed of the vessel.

Then, having the linear model a controller is designed. Here the LQR is used and the characteristics and the results of this controller will be analyzed. Reference following on heave is also applied to seek for a controller that can stabilize the height of the vessel relative to the water line.

Finally an analysis is made of the real life tests that are made with the boat. The vessel is tested many times with different types of control, such as open loop, differential mode, common mode and a full mode where differential and common are both active. At last, some upgrades are tested such as active reference on roll, and speed control on the motors.



# Chapter 2

## Background

Figure 2.1 shows the basic principle of a foil and how it generates lift, this is the same principle that allows airplanes to fly. The difference on pressure between the bottom and the top of the foil creates this vertical force that allows to carry a certain mass. This force will depend on the speed of the foil relative to the fluid, the size and profile of the foil and the density of the fluid it's in. For a boat with hydrofoils, which will be under water, they can be much smaller than airplane foils since the density of the water is almost 800 times greater than the density of the air.

The planned designs for TSB's vessels have always been a system with 3 foils, 2 at the front and one at the rear at the bottom of the rudder, which also has the propeller incorporated. With these 3 foils there would easily be enough lift to carry the boat out of the water and having them far from the center of mass would create an easily controllable system.

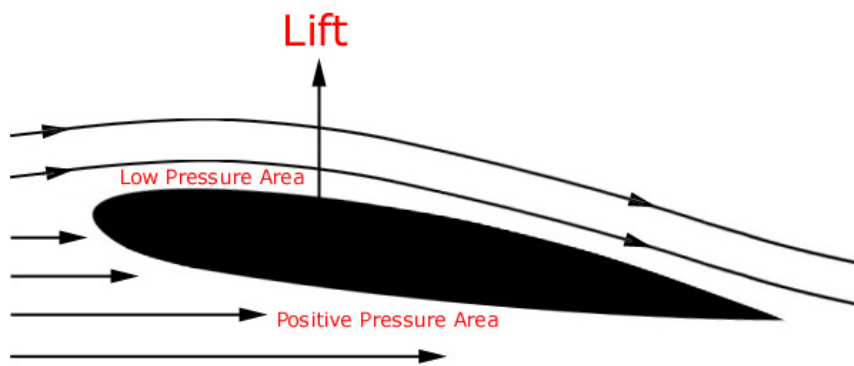


Figure 2.1: The working principle of a foil and how it generates lift.

The hydrofoils used in this project were designed by students of Aerospace Engineering who are also part of the Técnico Solar Boat project. They used data from *airfoiltools* to design the foils considering the SR01 vessel, which is similar to the SR02. These foils can be seen in figure 2.2. They have the NACA 63-412 profile.



Figure 2.2: The hydrofoils designed for SR01 that will be used on SR02.

The *airfoiltools* is a data base of known foil profiles where one can find the lift and drag coefficients of each one of them. The lift and drag of the foils depend on the Reynolds number ( $Re$ ) and the critical number ( $N_{crit}$ ), these two are normally used for CFD (Computacional Fluid Dynamics) to design airfoils.  $N_{crit}$  is used to model the turbulence of the flow or the roughness of the airfoil. The Reynolds number is a dimensionless number that defines a relation between fluid viscosity and speed of the airfoil.

Equation (2.1) shows the expression for the Reynolds number  $Re$ , where  $v$  is the speed of the foil relative to the fluid surrounding it,  $l$  is the chord of the foil and  $\nu$  is the kinematic viscosity of the fluid, that is,

$$Re = \frac{v \cdot l}{\nu} \quad (2.1)$$

For this dissertation the model used considers the kinematic viscosity of water at 20 degrees Celsius, and a fixed Reynolds number for a speed of about 7 m/s. Even though the  $Re$  number changes with the speed of the boat, figure 2.3 shows this difference has very little influence on the lift coefficient of the foil between  $-3^\circ$  and  $7^\circ$ . Since this is the range of movement these foils will have, a fixed Reynolds number is acceptable.

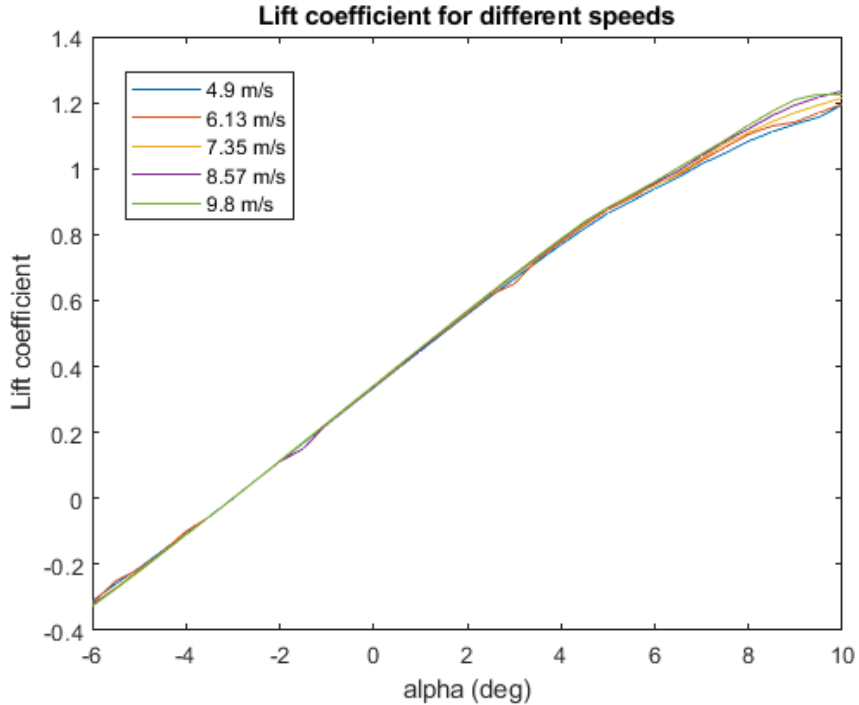


Figure 2.3: Lift coefficients for 5 different Re values, which represent 5 different speeds of the vessel. Here  $\alpha$  represents the angle of attack of the foil.

The data available directly on *airfoiltools* gives the lift coefficient for an airfoil considering a uniform and infinite foil (also known as 2-dimensional lift coefficient), this is not as in reality because finite wings have trailing vortices at their ends which create lift losses [12]. For this a correction is used, which takes into consideration the aspect ratio (AR) of the foil, defined as

$$AR = \frac{b^2}{S} \quad (2.2)$$

where  $b$  is the wingspan and  $S$  the surface area.

The correction used for this dissertation, is calculated as

$$C_L = C_l \cdot \frac{AR}{AR + 2} \quad (2.3)$$

where  $C_l$  is the 2-dimensional lift coefficient and  $C_L$  is the corrected lift coefficient, called 3-dimensional lift.

Having the lift coefficient for the wings to be used it was then linearized for the expected used range of angle of attack (AoA), again considering a speed of 7 m/s. Figure 2.4 shows the resulting linearization against its original curve.

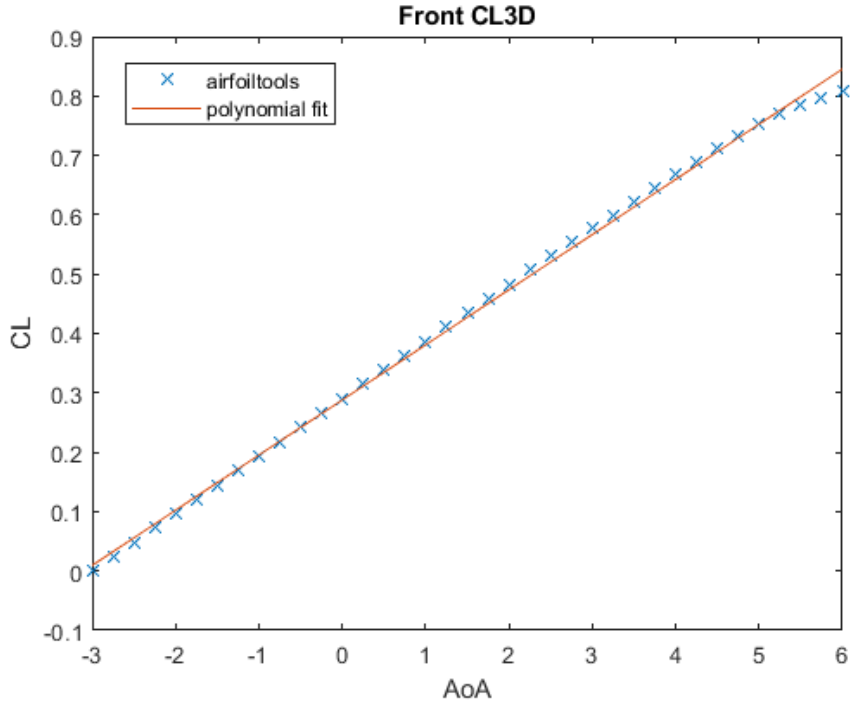


Figure 2.4: Linear curve approximation of  $C_L$  and AoA of the hydrofoils

The resulting linear regression is simply described as

$$C_L = b_1 \cdot \alpha + b_0 \quad (2.4)$$

where the constants  $b_1$  and  $b_0$  can be found in table 2.1.

The same process was done to get the drag coefficient of the foil. Data from *airfoiltools* was used and an approximated curve was obtained. For the drag the approximation is not linear but can be a 6<sup>th</sup> degree polynomial. Figure 2.5 shows the curve of the drag coefficient for the different AoA of the foil and the resulting curve approximation is

$$C_D = a_6 \cdot \alpha^6 + a_5 \cdot \alpha^5 + a_4 \cdot \alpha^4 + a_3 \cdot \alpha^3 + a_2 \cdot \alpha^2 + a_1 \cdot \alpha + a_0 \quad (2.5)$$

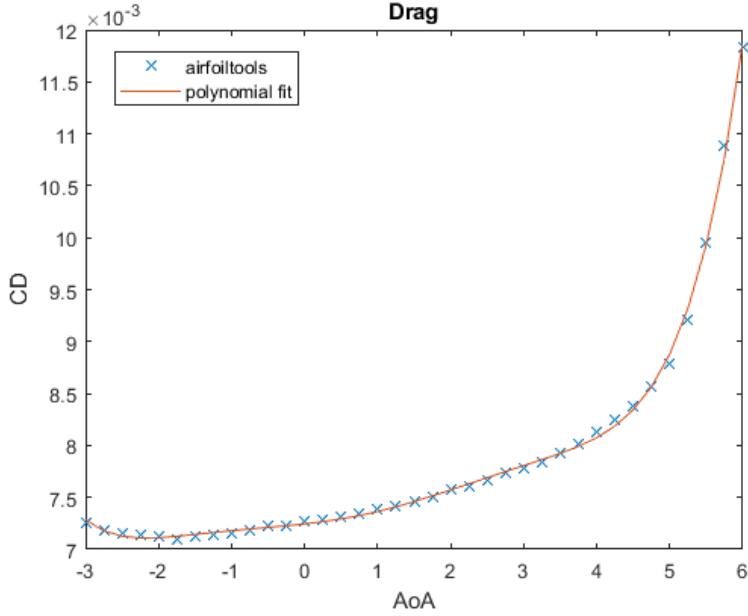


Figure 2.5: Drag curve of  $C_D$  and AoA of the hydrofoils

Since all 3 foils have the same profile, and that the AR of the front and rear foils are so similar, the polynomials for  $C_L$  and for  $C_D$  used along this work are the same for the 3 foils.

## 2.1 Theoretical Model

In this section the equations of dynamics and kinematics will be defined, assumed simplifications will be described, and all constants used for the model are presented. By the end of this chapter one can build the non-linear model that describes the motion of the vessel.

### 2.1.1 Reference frames

A model needs to have its references defined in order to have equations that are consistent. First we define two reference frames, one is the body frame, which has its origin at the center of mass of the vessel and is composed by the axis  $\{X_b, Y_b, Z_b\}$ . The second frame can be fixed anywhere on earth and will not move with the motion of the vessel, it is composed by the axis  $\{X_i, Y_i, Z_i\}$ .

For the body frame, the axis  $\{X_b, Y_b, Z_b\}$  can be described as longitudinal, transversal and normal axis, respectively. The longitudinal axis is defined from stern to bow, the transversal from portside to starboard and the normal axis from top to bottom.

Figure 2.6 shows the 6 degrees of freedom (DOF) of a boat and the two reference frames, on the image called body-fixed and earth-fixed.

To model the behavior of the boat when foilborne the movements in *yaw* and *sway* will be ignored. *Sway* velocity will always be near zero, and all simulations will be considering the vessel going straight, so *yaw* constant. This simplifies the system to a 4 DOF model.

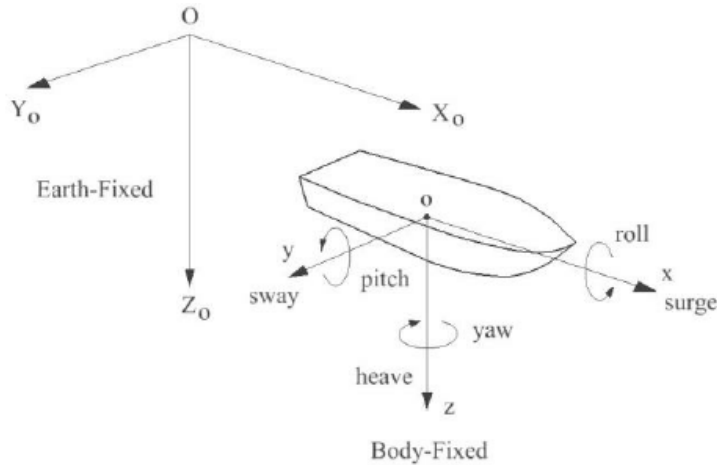


Figure 2.6: The axis orientation and the movement definitions for boats. [13]

### 2.1.2 Main forces

The forces that actuate on the boat when it is foilborne can be directly compared to the ones of an airplane. The main forces are the drag on the foils and struts, the lift generated from the foils, the thrust from the propeller and the gravitational force. Figure 2.7 illustrates those forces on a commercial airplane and on the SR02 vessel.

The boat model designed is based on these forces. Knowing all of them, and based on Newton's second law, it's possible to calculate the accelerations resulting from those forces. The vertical acceleration will result from the lift and weight forces, the horizontal acceleration will result from the drag forces and the thrust. The pitch angle will be known from the torque generated by the lift difference from the front and rear foils. Finally, the roll angle will be known from the torque generated by the lift difference from the left and right foils.

The lift and the drag equations are general equations that apply to hydrofoils just as they apply to airplane wings. Lift and drag are represented by

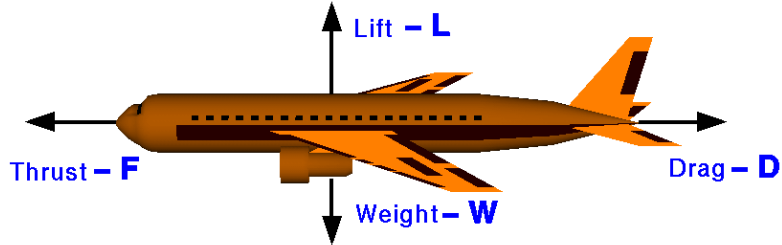
$$L = \frac{1}{2} \cdot \rho \cdot u^2 \cdot A \cdot C_L \quad (2.6)$$

$$D = \frac{1}{2} \cdot \rho \cdot u^2 \cdot A \cdot C_D \quad (2.7)$$

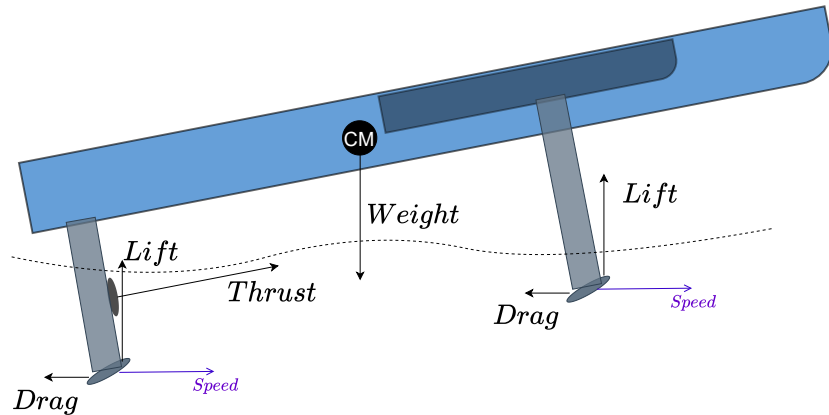
where  $A$  is the surface area of the foil,  $\rho$  is the density of the fluid surrounding the wing and  $u$  is the fluid velocity.

$C_L$  and  $C_D$  were defined in (2.4) and (2.5), respectively.

To the drag one must add the drag force of the struts that support the foils. These struts also have foil like profiles but have a zero degree AoA when the vessel is not turning. Also, the submerged area of strut varies as the vessel goes up and down a few centimeters. However, for this model the submerged strut is considered to be constant. This results in a constant drag coefficient for the struts. The coefficients for the front and rear struts can be found in table 2.1, and (2.7) is used to compute their drag.



(a) Forces acting on an airplane [14].



(b) Forces acting on the boat.

Figure 2.7: Comparison between airplane forces and foilborne boat forces.

The weight of the vessel is simply the total mass  $M$  multiplied by the gravitational acceleration  $g$ , as in

$$W = M \cdot g \quad (2.8)$$

The constants  $M$  and  $g$  can be found in table 2.1.

Finally, the thrust force comes from the propeller of the vessel. This value is controlled by the vessel's pilot. The range of thrust available has been estimated based on the whole power train system efficiency and the available power. Some simulations will be done with a fixed thrust and then some with variations.

### 2.1.3 Equations breakdown

Knowing the drag and the lift general equations, and the approximation curves for the lift and drag coefficients of the foils it is now possible to obtain all the drag and the lift forces applied to the boat.

The front foils act independently of one another, so they can control the roll of the boat. Because of this their lifts must be calculated independently.

Equations (2.9), (2.10) and (2.11) represent the lift forces exerted by the foils.

The lift forces exerted by the front left, right and rear foils can be defined as

$$L_{fleft} = \frac{1}{2} \cdot \rho \cdot u^2 \cdot A_{ffront} \cdot C_{L_{fleft}} \quad (2.9)$$

$$L_{fright} = \frac{1}{2} \cdot \rho \cdot u^2 \cdot A_{ffront} \cdot C_{L_{fright}} \quad (2.10)$$

$$L_{rear} = \frac{1}{2} \cdot \rho \cdot u^2 \cdot A_{frear} \cdot C_{L_{rear}} \quad (2.11)$$

In some cases we will refer to  $L_{front}$  as the sum of  $L_{left}$  and  $L_{right}$ .

The drag forces exerted by the front foils and struts are defined as

$$D_{left} = \frac{1}{2} \cdot \rho \cdot u^2 \cdot A_{ffront} \cdot C_{D_{left}} + \frac{1}{2} \cdot \rho \cdot u^2 \cdot A_{stfront} \cdot C_{D_{stfront}} \quad (2.12)$$

$$D_{right} = \frac{1}{2} \cdot \rho \cdot u^2 \cdot A_{ffront} \cdot C_{D_{right}} + \frac{1}{2} \cdot \rho \cdot u^2 \cdot A_{stfront} \cdot C_{D_{stfront}} \quad (2.13)$$

The drag force exerted by the rear foil and strut is defined as

$$D_{rear} = \frac{1}{2} \cdot \rho \cdot u^2 \cdot A_{frear} \cdot C_{D_{rear}} + \frac{1}{2} \cdot \rho \cdot u^2 \cdot A_{strear} \cdot C_{D_{strear}} \quad (2.14)$$

In some cases we will refer to  $D_{front}$  as the sum of  $D_{left}$  and  $D_{right}$ .

Knowing all the forces that actuate on the foils and the boat, one can deduce the vertical acceleration, for heave, the horizontal acceleration, for surge, and the angular accelerations, for the pitch and roll angles.

Based on the references of figure 2.6 it's possible to illustrate all the forces on the XZ plane, then separate their projections on the body and inertial axis, as in figure 2.8(a) and figure 2.9(a).

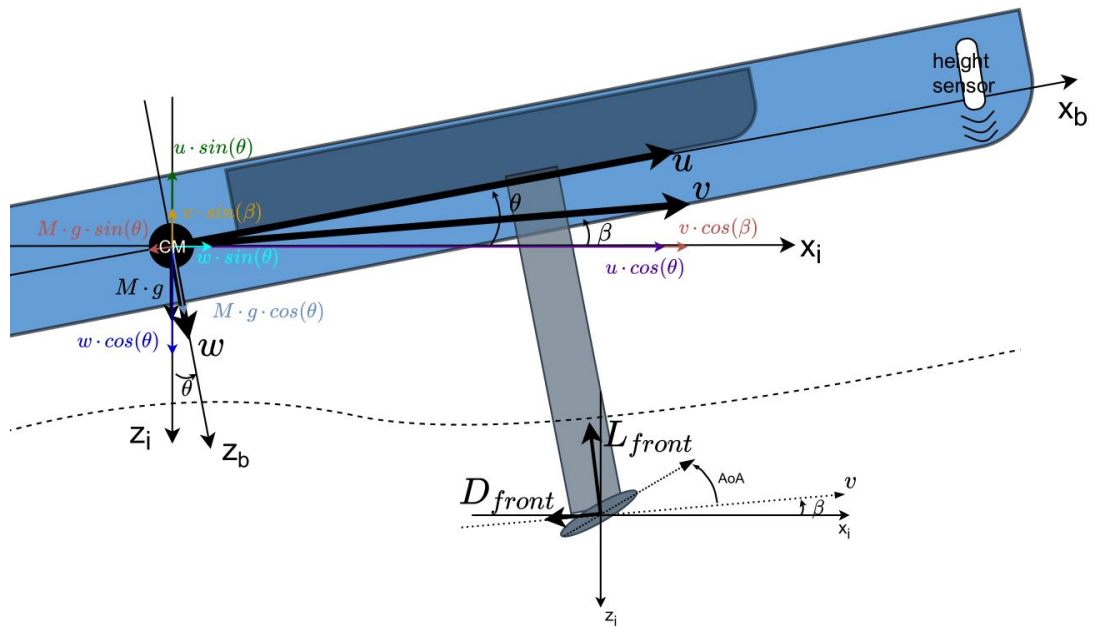
Figure 2.8(a) also shows the defined velocity vectors  $v$ ,  $u$  and  $w$ , and the angle  $\beta$  between  $v$  and the inertial axis  $x_i$ . The velocities  $u$  and  $w$  are the horizontal and vertical speeds of the boat on the body axis and  $v$  is the sum of  $u$  and  $w$ , i.e. the resulting velocity in the  $X_bZ_b$  plane.

The angle  $\beta$  is very close to zero most of the times since the boat is expected to have a very small pitch at all times. In fact it will be physically impossible for the boat to have a pitch higher than 5 degrees considering its length and the size of the struts. That allows for a simplification to be made, consider  $\beta = 0$ . This simplification results in the projections that can be seen in figures 2.8(b) and 2.9(b).

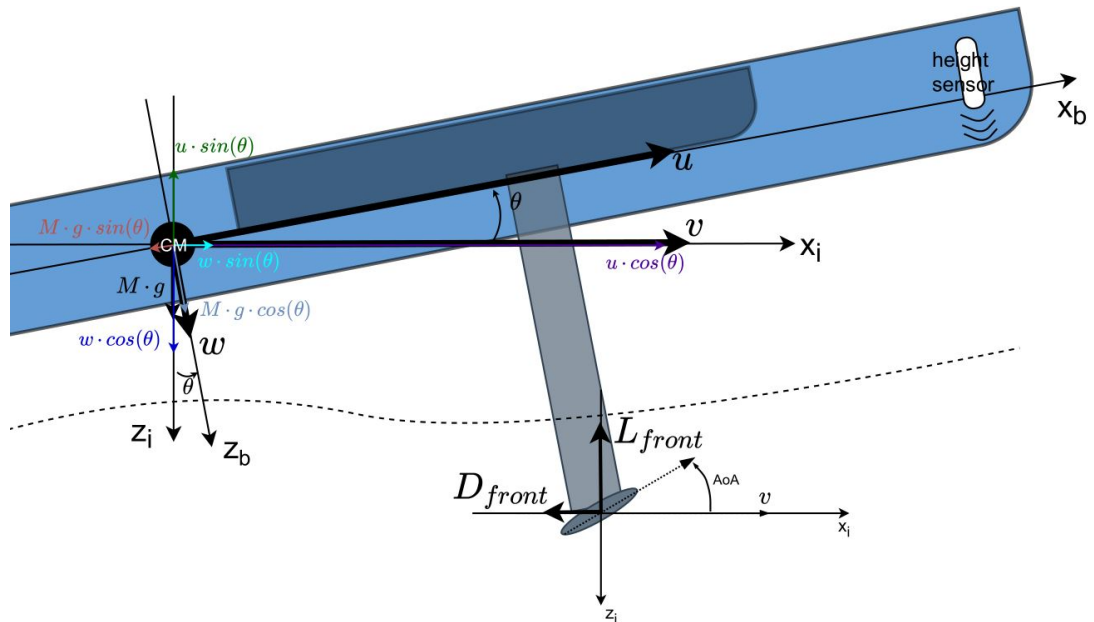
Having the projections of the forces it is possible to deduce the accelerations  $\dot{u}$  and  $\dot{w}$  on the body axis which are given by

$$\dot{u} = \frac{T - D_{rear} \cdot \cos(\theta) - D_{front} \cdot \cos(\theta) + L_{rear} \cdot \sin(\theta) + L_{front} \cdot \sin(\theta) - M \cdot g \cdot \sin(\theta)}{M} \quad (2.15)$$

$$\dot{w} = \frac{-D_{rear} \cdot \sin(\theta) - D_{front} \cdot \sin(\theta) - L_{rear} \cdot \cos(\theta) - L_{front} \cdot \cos(\theta) + M \cdot g \cdot \cos(\theta)}{M} \quad (2.16)$$

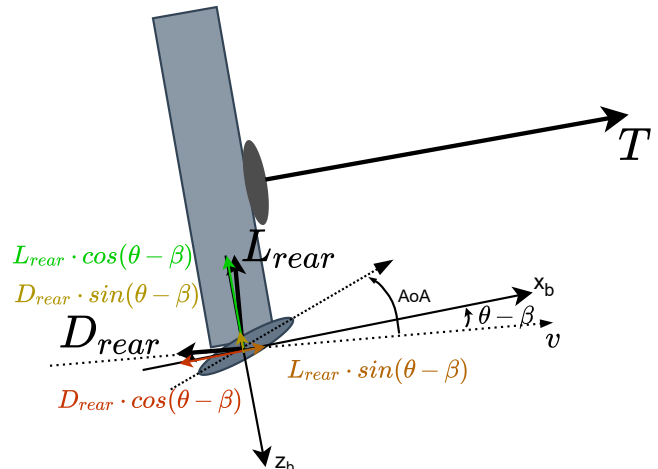


(a) Complete forces with  $\beta$  angle.

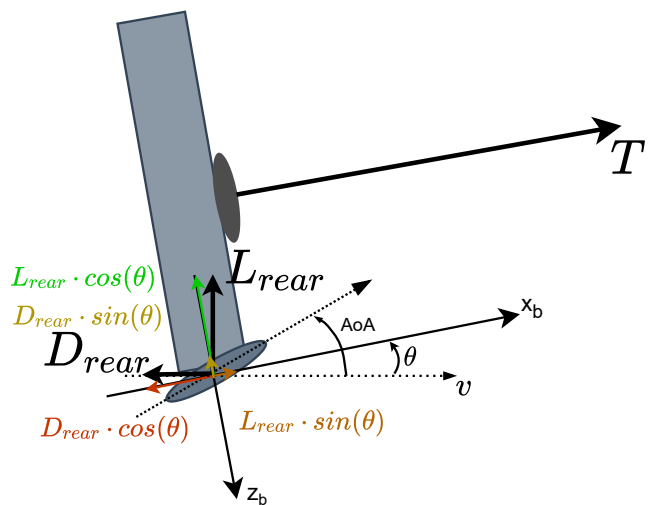


(b) Simplified forces without  $\beta$  angle.

Figure 2.8: Forces and velocities on the XZ plane and their projections with and without  $\beta$  angle.



(a) Complete forces with  $\beta$  angle.



(b) Simplified forces without  $\beta$  angle.

Figure 2.9: Foil forces on the XZ plane, angle of attack and thrust force with and without  $\beta$  angle.

Finally, the angular accelerations for roll and pitch need to be calculated. These accelerations are based on the lift and drag forces and the moments of inertia,  $I$ . The lift and drag forces have more or less influence on the resulting rotational force of the vessel depending on their distances to the centre of mass, because of that these distances are part of the equations for the angular accelerations. Figures 2.10 and 2.11 show all the distances that enter the equations and what they represent. With that it is possible to write the final equations for pitch acceleration,  $\ddot{\theta}$  and roll acceleration,  $\ddot{\phi}$ , defined as

$$\begin{aligned}\ddot{\theta} = & \frac{L_{front} \cdot \sin(\theta) \cdot d_{z_{front}} + L_{front} \cdot \cos(\theta) \cdot d_{x_{front}}}{I_y} + \\ & + \frac{D_{front} \cdot \sin(\theta) \cdot d_{x_{front}} - D_{front} \cdot \cos(\theta) \cdot d_{z_{front}} - D_{rear} \cdot \sin(\theta) \cdot d_{x_{rear}}}{I_y} + \\ & + \frac{-D_{rear} \cdot \cos(\theta) \cdot d_{z_{rear}} + L_{rear} \cdot \sin(\theta) \cdot d_{z_{rear}} - L_{rear} \cdot \cos(\theta) \cdot d_{x_{rear}} + T \cdot d_{z_{rear}}}{I_y}\end{aligned}\quad (2.17)$$

$$\ddot{\phi} = \frac{L_{left} \cdot d_{y_{front}} - L_{right} \cdot d_{y_{front}}}{I_x} \quad (2.18)$$

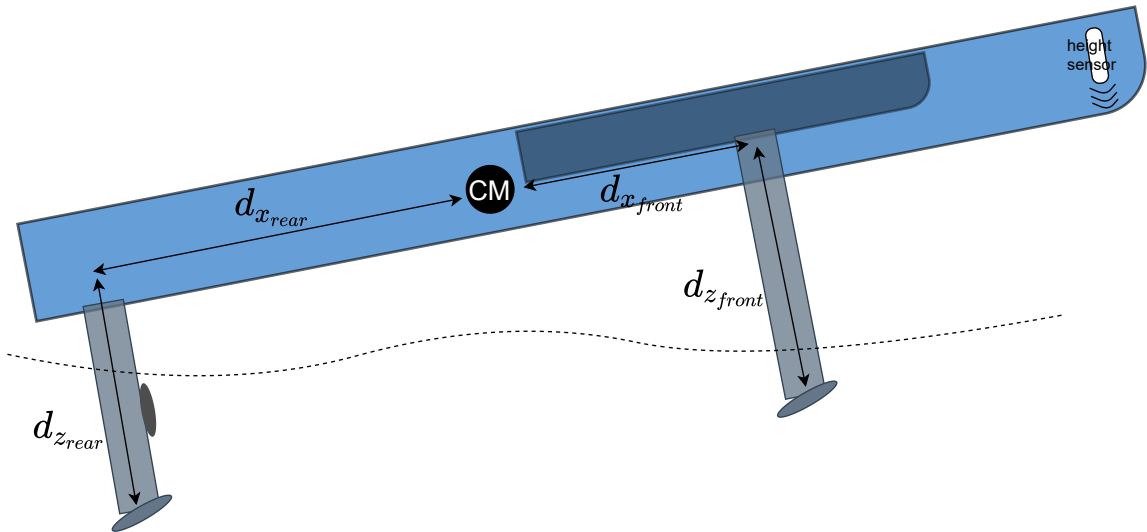


Figure 2.10: Foil distances to center of mass on the XZ plane.

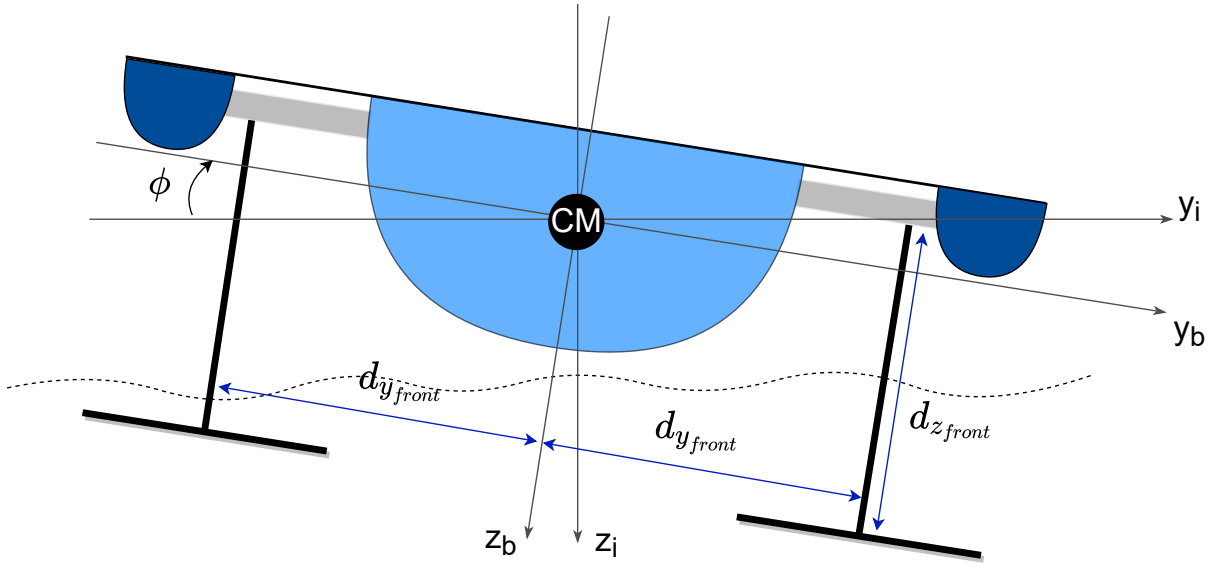


Figure 2.11: Front foils distances to center of mass on the XY plane.

Letter	Description	Value	Units
$g$	Gravitational acceleration	9.81	$m/s^2$
$\rho$	Sea water density	1025	$kg/m^3$
$M$	Boat's mass	215	$kg$
$A_{f_{front}}$	Surface area of front foil	0.048	$m^2$
$A_{f_{rear}}$	Surface area of the rear foil	0.046	$m^2$
$A_{st_{front}}$	Surface area of front strut	0.045	$m^2$
$A_{st_{rear}}$	Surface area of rear strut	0.108	$m^2$
$I_y$	Moment of Inertia about Y axis	503	$kg \cdot m^2$
$I_x$	Moment of Inertia about X axis	31	$kg \cdot m^2$
$b_0$	Constant for linearized CL	0.288	
$b_1$	Constant for linearized CL	0.090	
$a_0$	Constant for 6 <sup>th</sup> degree polynomial of CD	$7.2 \cdot 10^{-3}$	
$a_1$	Constant for 6 <sup>th</sup> degree polynomial of CD	$7.8 \cdot 10^{-5}$	
$a_2$	Constant for 6 <sup>th</sup> degree polynomial of CD	$2.9 \cdot 10^{-5}$	
$a_3$	Constant for 6 <sup>th</sup> degree polynomial of CD	$1.6 \cdot 10^{-5}$	
$a_4$	Constant for 6 <sup>th</sup> degree polynomial of CD	$-2.6 \cdot 10^{-6}$	
$a_5$	Constant for 6 <sup>th</sup> degree polynomial of CD	$-1.7 \cdot 10^{-6}$	
$a_6$	Constant for 6 <sup>th</sup> degree polynomial of CD	$3.4 \cdot 10^{-7}$	
$d_{x_{front}}$	Distance from CM to front foils on X axis	1.1	$m$
$d_{z_{front}}$	Distance from CM to front foils on Z axis	0.75	$m$
$d_{x_{rear}}$	Distance from CM to rear foils on X axis	2.45	$m$
$d_{z_{rear}}$	Distance from CM to rear foils on Z axis	0.96	$m$
$d_{z_{rear}}$	Distance from CM to front foils on Y axis	0.62	$m$

Table 2.1: Constants used for the model

# Chapter 3

## Model

### 3.1 Non-linear model

Having all the kinematic and dynamic equations of motion it's possible to describe the development of a simulation model in *Simulink*.

Before presenting the model some assumptions taken should be stated.

- The model is only valid for when the boat is foilborne,
- Only motion in the XZ plane is considered,
- The  $C_L$  and  $C_D$  of the foils are valid for a certain range of AoA and speeds,
- As said previously, yaw and sway are ignored,
- The surface area of each foil is assumed to be constant and independent of the AoA or roll of the vessel.

The model, here shown in figure 3.1, consists of a block that contains all the equations from section 2.1, integration blocks, and a block to get the  $x$  and  $z$  speeds in the inertial axis  $X_i, Z_i$ .

The block used to calculate the dynamics and kinematics of the vessel can be seen in more detail in figure 3.2. This block calculates the lift and drag of every foil and then uses these results to calculate the pitch,  $x$  and  $z$  accelerations, using the equations from 2.1.3. For roll, only the lift from the front foils is used. The block takes the foils' angles as inputs, and also thrust, pitch and speed. Pitch is fed back into this block to correct the AoA of the foils. The real AoA has two components, the actuation,  $act$ , which is the angle between the foil's chord line and the body  $x$  axis, and the pitch, which is summed to the actuation. This gives the real AoA,  $\alpha$ , as in

$$\alpha = act + \theta \quad (3.1)$$

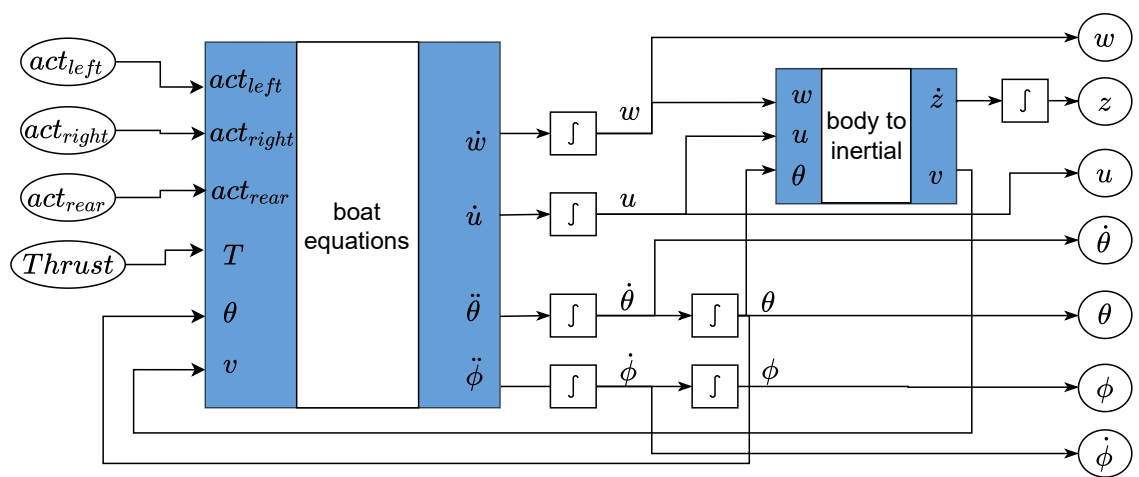


Figure 3.1: Model architecture of the boat on foils.

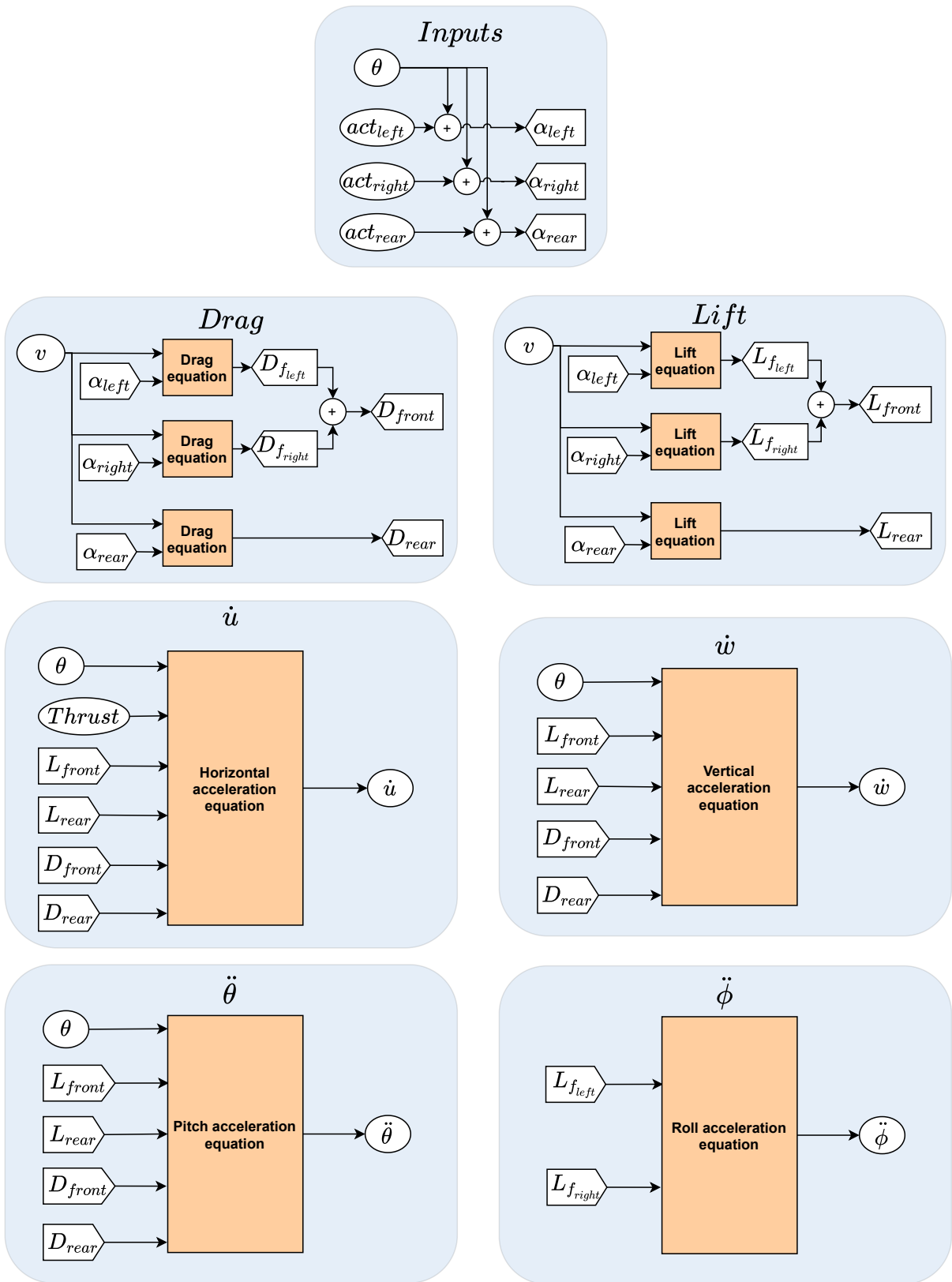


Figure 3.2: Boat equations block of the boat model.

## 3.2 Trimming of the Model

Having the model, it is possible to trim it in order to find an operating point of equilibrium. Trimming a model involves searching for a set of inputs and states that meet any specified conditions. Here the conditions will be to have the vessel over the hydrofoils, at a steady level relative to the water line, with a steady speed, roll and pitch.

This is defined as a solution to the model's equations where all variables that define the system are time-invariant. Finding such equilibrium points will allow to find an ideal steady state about which the model will be linearized and the controller will be tuned. The controller must be functioning when the system is working around this steady state.

From equations (2.15), (2.16), (2.17) and (2.18), one can understand some balances that must occur for an equilibrium to be reached.

For instance, assuming  $\theta = 0$  and  $\dot{u} = 0$ , (2.15) results in

$$T = D_{rear} + D_{front} \quad (3.2)$$

then with  $\theta = 0$  and  $\dot{w} = 0$ , from (2.16) we get

$$M \cdot g = L_{rear} + L_{front} \quad (3.3)$$

with  $\theta = 0$  and  $\ddot{\theta} = 0$ , from (2.17) results

$$T \cdot d_{z_{rear}} + L_{front} \cdot d_{x_{front}} = L_{rear} \cdot d_{x_{rear}} + D_{rear} \cdot d_{z_{rear}} + D_{front} \cdot d_{z_{rear}} \quad (3.4)$$

and finally, with  $\ddot{\phi} = 0$ , from (2.18) we get

$$L_{left} = L_{right} \quad (3.5)$$

The equilibrium points can be found analytically solving differential equations or by using computational methods. Here, the gradient descent algorithm was used, which is an iterative algorithm.

A gradient descent algorithm is used to find local minima of a function. It computes the gradient and takes steps proportional to the negative of that gradient towards the local minima. Taking steps proportional to the positive of the gradient would lead to a local maximum, and that is called the gradient ascent algorithm.

Having a multivariable function  $\mathbf{F}(\mathbf{x})$  and a point  $a$ , then  $-\nabla\mathbf{F}(a)$  is the direction the step should be taken.

Then having

$$\mathbf{a}_{n+1} = \mathbf{a}_n - \gamma \nabla \mathbf{F}(\mathbf{a}) \quad (3.6)$$

with  $\gamma$  a positive constant small enough then  $\mathbf{F}(\mathbf{a}_{n+1}) < \mathbf{F}(\mathbf{a}_n)$  and the iterations will converge.

Matlab function `findop()` runs this algorithm and finds the steady state of the model [15].

The initial values for the inputs  $u_0$ , and the state variables  $x_0$ , have to be defined and then the steady state found will be the one closest to these initial conditions.

As seen in 3.1 the input variables and the state variables can be defined as the vectors

$$\mathbf{u} = [act_{left} \quad act_{right} \quad act_{rear} \quad T]^T \quad (3.7a)$$

$$\mathbf{x} = [\phi \quad \dot{\phi} \quad \theta \quad \dot{\theta} \quad u \quad w \quad z]^T \quad (3.7b)$$

Given that, to begin the search for the steady state, the vectors  $\mathbf{u}_0$  and  $\mathbf{x}_0$  are set to

$$\mathbf{u}_0 = [act_{left}^0 \quad act_{right}^0 \quad act_{rear}^0 \quad T_0]^T \quad (3.8a)$$

$$\mathbf{x}_0 = [\phi_0 \quad \dot{\phi}_0 \quad \theta_0 \quad \dot{\theta}_0 \quad u_0 \quad w_0 \quad z_0]^T \quad (3.8b)$$

where table 3.1 shows the defined values of the constants.

Letter	Description	Value	Units
$act_{left}^0$	Initial left front foil angle for trim search	3	degree
$act_{right}^0$	Initial right front foil angle for trim search	3	degree
$act_{rear}^0$	Initial rear foil angle for trim search	3	degree
$T_0$	Initial thrust for trim search	140	N
$\theta_0$	Initial pitch angle for trim search	0	degree
$\dot{\theta}_0$	Initial pitch angular speed for trim search	0	degree/s
$\phi_0$	Initial roll angle for trim search	0	degree
$\dot{\phi}_0$	Initial roll angular speed for trim search	0	degree/s
$u_0$	Initial u speed for trim search	7	m/s
$w_0$	Initial w speed for trim search	0	m/s
$z_0$	Initial heave for trim search	-0.3	m

Table 3.1: Initial conditions used for trimming the model

Another restriction to be defined is the minimum and maximum values of each of these variables, which must be defined considering the real system limitations. Table 3.2 shows these limits, which were obtained from different studies done in the scope of the TSB project

<b>Letter</b>	<b>Description</b>	<b>Value</b>	<b>Units</b>
$act_{min}$	Minimum AoA	-2	degree
$act_{max}$	Maximum AoA	6	degree
$T_{min}$	Minimum thrust	0	N
$T_{max}$	Maximum thrust	500	N
$\theta_{min}$	Minimum pitch angle	-5	degree
$\theta_{max}$	Maximum pitch angle	5	degree
$\phi$	Roll angle always fixed	0	degree
$u_{min}$	Minimum u speed	0	m/s
$u_{max}$	Maximum u speed	14	m/s
$w$	Vertical speed always fixed	0	m/s
$z$	Heave value always fixed	-0.3	m

Table 3.2: Limits of the model for steady state search

After having these conditions the model can be trimmed. There are a few ways to trim the model since we can freely choose whether or not to fix the rear foil AoA,  $act_{rear}$ , and whether we want to specify a certain speed  $u$ , or a certain thrust  $T$ . However, if we choose to fix  $act_{rear}$  the pitch angle  $\theta$  will be zero only for a specific  $u$  speed. For other  $u$  speeds, the resulting pitch  $\theta$  will vary.

Being able to trim the model with a fixed rear AoA is important in the context of this project. The rear foil is attached to the propulsion column and for now it is not electronically controllable.

The resulting steady state points with different fixed parameters are shown in tables 3.3 and 3.4.

In table 3.3 we have the front and rear foil's AoA needed in order to have a steady state for different  $u$  speeds, with a fixed pitch  $\theta = 0$ . As we can see the faster the boat goes the smaller the actuation angles needed on the foils, for high speeds we even get negative AoA (this still gives positive lift). The table also shows the resulting thrusts needed to achieve these states.

From table 3.4 we can see the steady states for different fixed values of rear foil AoA. These have all been found for a  $u$  speed of 7 m/s. As expected, when  $act_{rear}$  raises, then  $\theta$  reduces to compensate the generated lift at the rear of the vessel.

$act_{front}$ [deg]	$act_{rear}$ [deg]	$T$ [N]	$u$ [m/s]
5.9	5.5	115	6
3.5	3.2	144	7
1.9	1.7	186	8
0.8	0.7	235	9
0.1	0	289	10
-0.5	-0.6	350	11
-0.9	-1	416	12
-1.3	-1.3	488	13

Table 3.3: Steady states values of front and rear foil's AoA and thrust for different  $u$  speeds

$act_{front}$ [deg]	$act_{rear}$ [deg]	$T$ [N]	$\theta$ [deg]
-0.8	-1	145	4.2
0.2	0	144	3.2
1.2	1	144	2.2
2.2	2	144	1.2
3.2	3	143	0.2
4.2	4	144	-0.8

Table 3.4: Steady states values of thrust and pitch for different fixed rear foil AoA and a  $u$  speed of 7 m/s

### 3.3 Linearization of the Model

The nonlinear continuous-time space state model of a given physical plant defined as a set of inputs, outputs and state variables related by first order differential equations of the form

$$\begin{aligned}\dot{x}(t) &= f(x(t), u(t), t) \\ y(t) &= g(x(t), u(t), t)\end{aligned}\tag{3.9}$$

where  $x(t)$  is the state vector,  $u(t)$  is the input vector and  $y(t)$  consists of the measured outputs.

A linear space state model is represented by the equations

$$\begin{aligned}\dot{x} &= Ax + Bu \\ y &= Cx\end{aligned}\tag{3.10}$$

The linearized model is valid in a small region about a given equilibrium point. In this case, the physical plant considered is the hydrofoil vessel. The full non linear model described before will be

linearized about trimming conditions defined by the variables listed in tables 3.3 and 3.4.

We first consider the operating condition determined by a desired speed of 7 m/s from table 3.3, this is the expected endurance speed of the vessel. For 7 m/s, we get  $\mathbf{u}_{\text{steady}}$ ,  $\mathbf{x}_{\text{steady}}$  to be

$$\mathbf{u}_{\text{steady}} = [3.5 \quad 3.5 \quad 3.2 \quad 144]^T \quad (3.11\text{a})$$

$$\mathbf{x}_{\text{steady}} = [0 \quad 0 \quad 0 \quad 0 \quad 7 \quad 0 \quad -0.3]^T \quad (3.11\text{b})$$

The linearized space state model variables are defined as

$$\begin{aligned} \delta \mathbf{x} &= \mathbf{x} - \mathbf{x}_{\text{steady}} \\ \delta \mathbf{y} &= \mathbf{y} - \mathbf{y}_{\text{steady}} \\ \delta \mathbf{u} &= \mathbf{u} - \mathbf{u}_{\text{steady}} \end{aligned} \quad (3.12)$$

Yielding the linearized space state model

$$\begin{aligned} \delta \dot{\mathbf{x}} &= A \delta \mathbf{x} + B \delta \mathbf{u} \\ \delta \dot{\mathbf{y}} &= C \delta \mathbf{x} \end{aligned} \quad (3.13)$$

where the matrices A, B and C are the Jacobians of the model computed at the trimming point

Matlab performs this linearization using numerical perturbation [16], inputs a small perturbation to each block and computes the output perturbation.

The model obtained is a linear space state model which is valid around the steady operating point in (3.11).

Considering  $\mathbf{x} = [\phi \quad \dot{\phi} \quad \theta \quad \dot{\theta} \quad u \quad w \quad z]^T$  and  $\mathbf{u} = [act_{left} \quad act_{right} \quad act_{rear} \quad T]^T$  the matrices found for the model are

$$A = \begin{bmatrix} 0 & 1 & 0 & 0 & 0 & 0 & 0 \\ 0 & 0 & 0 & 0 & 0 & 0 & 0 \\ 0 & 0 & 0 & 1 & 0 & 0 & 0 \\ 0 & 0 & -1.38 & 0 & -4.49 & 0 & 0 \\ 0 & 0 & -4 \cdot 10^{-3} & 0 & -0.19 & 0 & 0 \\ 0 & 0 & -1.50 & 0 & -2.8 & 0 & 0 \\ 0 & 0 & -0.12 & 0 & 0 & 1 & 0 \end{bmatrix}; B = \begin{bmatrix} 0 & 0 & 0 & 0 \\ 124.1 & -124.1 & 0 & 0 \\ 0 & 0 & 0 & 0 \\ 13.53 & 13.53 & -28.5 & -0.11 \\ -2.3 \cdot 10^{-3} & -2.3 \cdot 10^{-3} & -2.2 \cdot 10^{-3} & 4.7 \cdot 10^{-3} \\ -0.5 & -0.5 & -0.48 & 0 \\ 0 & 0 & 0 & 0 \end{bmatrix} \quad (3.14)$$

Since the dimension of the model is high, and the roll can be considered as an independent variable, we can separate the model from 3.14 into two models.

The first two lines of A and B, and the first two columns of A, show us that  $\phi$  and  $\dot{\phi}$  do not interfere with the other variables, and vice-versa, hence the independence. Thus, removing them gives us the A matrix for the main model.

Note that, in the matrix B,  $act_{left}$  and  $act_{right}$  have equal influence over the leftover variables, so they can be considered as one, which we call  $act_{front}$ .

Considering  $x = [\theta \quad \dot{\theta} \quad u \quad w \quad z]^T$  and  $u = [act_{front} \quad act_{rear} \quad T]^T$  the matrices for the main model are

$$A = \begin{bmatrix} 0 & 1 & 0 & 0 & 0 \\ -1.38 & 0 & -4.49 & 0 & 0 \\ 4 \cdot 10^{-3} & 0 & -0.19 & 0 & 0 \\ -1.50 & 0 & -2.8 & 0 & 0 \\ -0.12 & 0 & 0 & 1 & 0 \end{bmatrix}; B = \begin{bmatrix} 0 & 0 & 0 \\ 13.53 & -28.5 & -0.11 \\ -2.3 \cdot 10^{-3} & -2.2 \cdot 10^{-3} & 4.7 \cdot 10^{-3} \\ -0.5 & -0.48 & 0 \\ 0 & 0 & 0 \end{bmatrix} \quad (3.15)$$

The roll model will be defined with only two inputs,  $act_{left}$  and  $act_{right}$  because  $thrust$  and  $act_{rear}$  have no influence on the roll angle. Because both inputs have the same influence in modulus but with opposite signs, they can be considered as one input, which will be used for the differential control.

Considering  $x = [\dot{\phi} \quad \phi]^T$  and  $u = [act_{left} \quad act_{right}]^T$  the matrices for the roll model are

$$A_r = \begin{bmatrix} 0 & 1 \\ 0 & 0 \end{bmatrix}; B_r = \begin{bmatrix} 0 & 0 \\ 124.1 & -124.1 \end{bmatrix}; C_r = \begin{bmatrix} 0 & 1 \end{bmatrix} \quad (3.16)$$

and for the differential control we use  $u = [act_{dif}]$  with the B matrix defined as

$$B_r = \begin{bmatrix} 0 \\ 124.1 \end{bmatrix} \quad (3.17)$$

Thrust is present in the model but it is always manually controlled by the pilot. Thus, for the model used to design the controller it can be removed. The heave model will be used with only one input,  $act_{front}$ . This will be part of the input for the front foils, where both will have the same value and will be the common mode control, as will be seen further ahead in this thesis.

Considering  $x = [\theta \quad \dot{\theta} \quad u \quad w \quad z]^T$  and  $u = [act_{front}]$  the matrices for the heave model are

$$A_h = \begin{bmatrix} 0 & 1 & 0 & 0 & 0 \\ -1.38 & 0 & -4.49 & 0 & 0 \\ 4 \cdot 10^{-3} & 0 & -0.19 & 0 & 0 \\ -1.50 & 0 & -2.8 & 0 & 0 \\ -0.12 & 0 & 0 & 1 & 0 \end{bmatrix}; B_h = \begin{bmatrix} 0 \\ 13.53 \\ -2.3 \cdot 10^{-3} \\ -0.5 \\ 0 \end{bmatrix}; C_h = \begin{bmatrix} 0 & 0 & 0 & 0 & 1 \end{bmatrix} \quad (3.18)$$

The two models described define the full behaviour of the variables that we wish to control. To make sure the linear model is controllable we verify the controllability of the system. For this purpose the controllability matrix  $C_o$  and the rank of the controllability matrix need to be known.

The controllability matrix is defined as

$$C_o = \begin{bmatrix} B & AB & A^2B & \dots & A^{n-1}B \end{bmatrix} \quad (3.19)$$

where  $n$  is the dimension of the model. For the heave model  $n = 5$  and for the roll model  $n = 2$ .

It is well known that the model is controllable if and only if the matrix  $C_o$  has full rank, that is iff  $\text{rank}(C_o) = n$ . Having full rank also means that the matrix does not have linearly dependent lines.

For the heave model we get

$$\text{rank}(C_o) = 5 \quad (3.20)$$

and for the roll model we get

$$\text{rank}(C_o) = 2 \quad (3.21)$$

Having control over the front hydrofoils and since they can influence pitch, height and roll, the result is as expected, the models are controllable.

# Chapter 4

## Controller

### 4.1 Linear Quadratic Regulator

#### 4.1.1 General equations

Linear Quadratic Regulator (LQR) is a modern control technique [17] for linear space state models in the form

$$\begin{aligned}\dot{\mathbf{x}} &= A\mathbf{x} + B\mathbf{u} \\ \mathbf{y} &= C\mathbf{x} + D\mathbf{u}\end{aligned}\tag{4.1}$$

with a cost function defined as

$$J = \int_0^{\infty} (\mathbf{x}^T Q \mathbf{x} + \mathbf{u}^T R \mathbf{u}) dt\tag{4.2}$$

where  $Q$  is a real symmetric positive-definite matrix and  $R$  is a semi positive-definite matrix that penalise the state variables and the inputs , respectively.

Under suitable stabilizability and detectability conditions, there is a unique feedback stabilising solution to the minimisation problem obtained from the unique positive definite solution  $P$  to the algebraic Riccati equation

$$A^T P + PA - PBR^{-1}B^T P + Q = 0\tag{4.3}$$

from which the optimal state feedback gain  $K$  is given by

$$K = R^{-1}B^T P\tag{4.4}$$

which will itself set the gains for the state feedback law as

$$\mathbf{u} = -K\mathbf{x}. \tag{4.5}$$

Figure 4.1 shows the block diagram for a system with a simple LRQ feedback control loop.

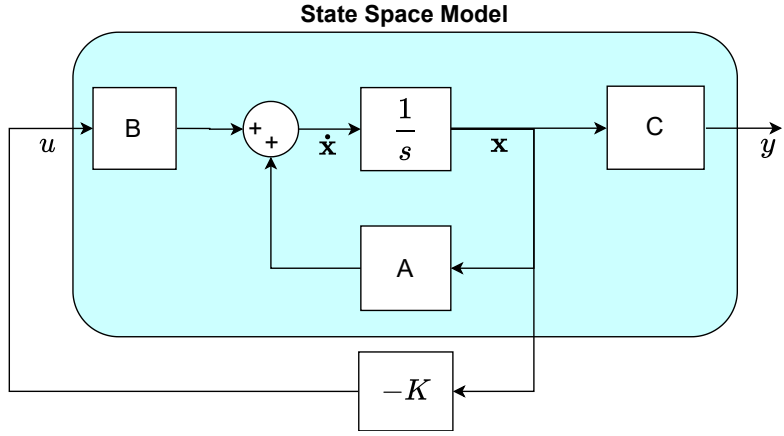


Figure 4.1: Classical LQR block diagram.

#### 4.1.2 Reference following for heave

In this system the output of the heave model needs to follow a reference value. Wherever a non-zero value is desired for a certain state variable, that state variable can be replaced by

$$x - x_d \quad (4.6)$$

where  $x_d$  is the desired value for the state variable  $x$ .

For the heave controller needed for this project, we have the  $z$  variable that has to follow a certain reference. This is because the desired height of the vessel will not be zero, but about 40 cm.

Figure 4.2 shows the modified model for reference model.

An input was added to the system from which the state variable  $z$  is subtracted and then fed back into the system. If the added input is set to zero then the system is the same as in figure 4.1.

This simple reference tracking will be have to be further improved because any bias in the system will lead to a biased tracking.

#### 4.1.3 Choosing Q and R weights

The Q and R matrices of the LQR influence the weight and thus the importance we wish to attach to a certain state or input variables.

The matrix Q penalizes the state variables and specifies which state variables must tend faster to their final value, while also equalizing the variables according to their expected range.

In its simplest form it may be chosen as a diagonal matrix of the form

$$Q = \begin{bmatrix} q_1 & & 0 \\ & \ddots & \\ 0 & & q_n \end{bmatrix}$$

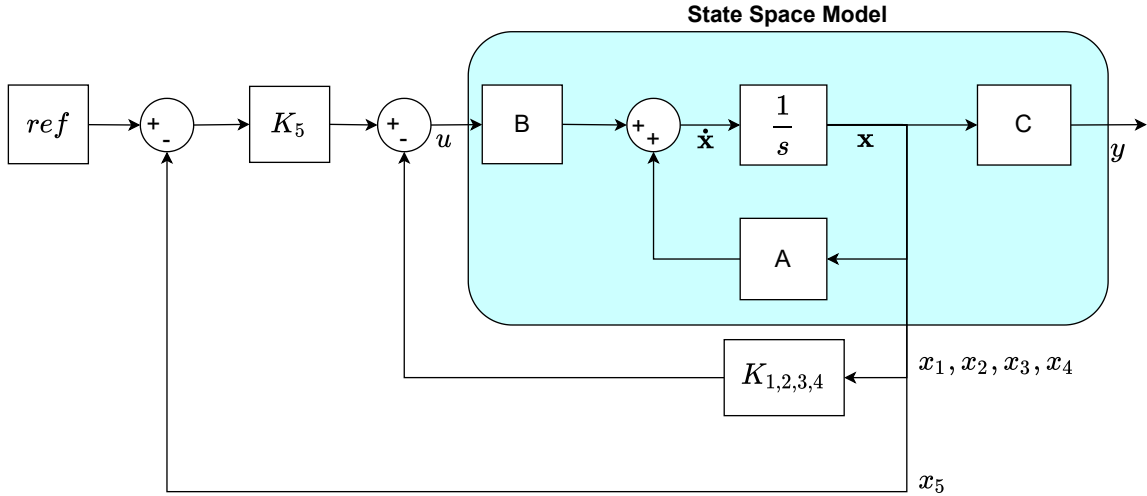


Figure 4.2: LQR model with reference following on heave.

where  $n$  equals the number of state variables of the system we are trying to control.

With this form of Q matrix, the value of each  $q_i, i = 1 \dots n$  is directly related to one single state variable.

The Q matrix can be adjusted according to Bryson' method [18], by tuning each  $q_i$  depending on the order of magnitude of each corresponding state variable. Thus making  $q_i = \frac{1}{X_{range_i}}$ , where  $X_{range_i}$  is the full range of the corresponding state variable  $x_i$ . These ranges can be found in table 4.1 and 4.2.

The R matrix represents the costs of the input control variables. There needs to be a balance between how fast the controller should react and how much energy it uses. Its simplest form will also be a diagonal matrix of the form

$$R = \begin{bmatrix} r_1 & & & 0 \\ & \ddots & & \\ 0 & & r_m & \end{bmatrix}$$

where  $m$  equals the number of input variables of the system we are trying to control.

For the controllers developed here, R is a scalar, because each model has only one input. Thus, the R value will be adjusted as a means to reach an adequate tradeoff between fast system response and energy expenditure.

Variable	Minimum	Maximum	Full range
$\theta [deg]$	-5	5	10
$\dot{\theta} [deg/s]$	-10	10	20
$u [m/s]$	4	10	6
$w [m/s]$	-1	1	2
$z [m]$	-0.2	-0.9	0.7

Table 4.1: Estimates of the full ranges of the state variables for the heave model.

<i>Variable</i>	<i>Minimum</i>	<i>Maximum</i>	<i>Full range</i>
$\phi$ [deg]	-10	10	10
$\dot{\phi}$ [deg/s]	-20	20	40

Table 4.2: Estimates of the full ranges of the state variables for the roll model.

With the values from 4.1 and 4.2 the Q matrices can be defined.

For the heave model we get

$$Q_h = \begin{bmatrix} q_\theta & 0 & 0 & 0 & 0 \\ 0 & q_{\dot{\theta}} & 0 & 0 & 0 \\ 0 & 0 & q_u & 0 & 0 \\ 0 & 0 & 0 & q_w & 0 \\ 0 & 0 & 0 & 0 & q_z \end{bmatrix} = \begin{bmatrix} 1/10 & 0 & 0 & 0 & 0 \\ 0 & 1/20 & 0 & 0 & 0 \\ 0 & 0 & 1/6 & 0 & 0 \\ 0 & 0 & 0 & 1/2 & 0 \\ 0 & 0 & 0 & 0 & 1/0.7 \end{bmatrix}$$

and for the roll model

$$Q_\phi = \begin{bmatrix} q_\phi & 0 \\ 0 & q_{\dot{\phi}} \end{bmatrix} = \begin{bmatrix} 1/10 & 0 \\ 0 & 1/40 \end{bmatrix}$$

#### 4.1.4 Step responses for heave and pitch

Now the output step response of the heave and pitch model can be analysed for different values of R. Figure 4.3 shows how R influences the step response for the heave controller, for a reference of -0.3 meters. In figure 4.4 we can see the input activity that makes state variable z converge to the desired reference. The figure shows the first second of the step response, and with a small value of R, such as  $10^{-3}$ , the controller is very reactive and overshoots. We can see in figure 4.3 that the response time for higher R values is not so different considering the vessel's time scale, and are preferable since they have less overshoot.

From what has been analysed on already existing vessels with hydrofoils they usually lift off the water in approximately 5 seconds, and so this or a lower time is what we want to achieve.

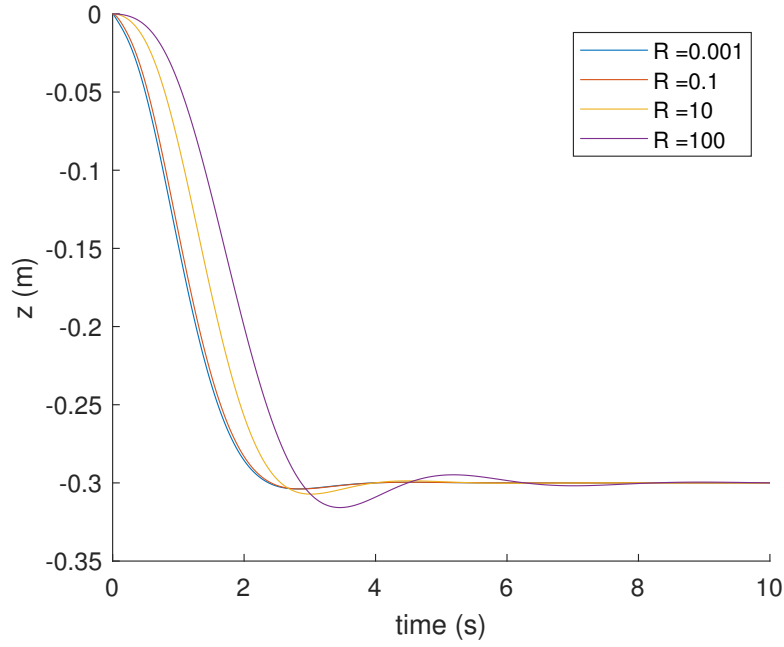


Figure 4.3: Front foil step response with LQR control for multiple  $R$  values.

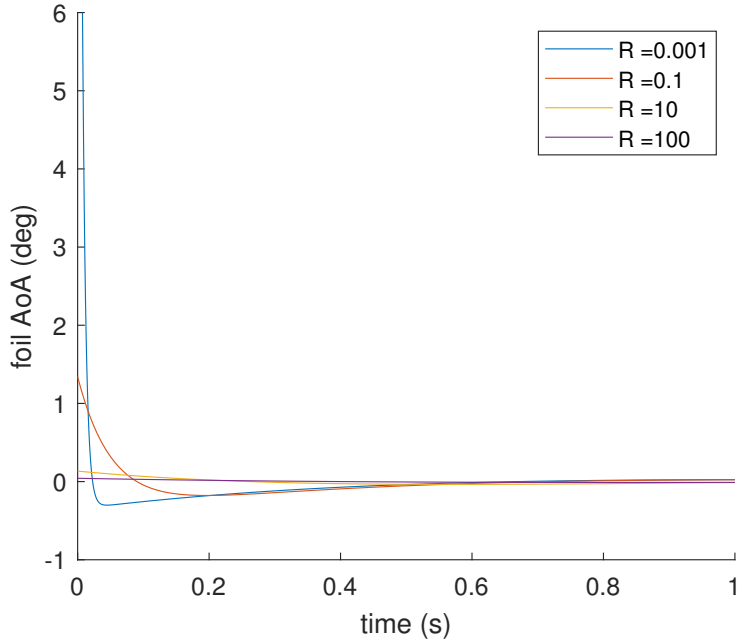


Figure 4.4: First second of the front foil input value for step response with LQR control.

Now another important variable that can be changed to adjust the performance of the step response is the  $Q_h$  entry for the state variable  $z$ . This value was set as  $1/0.7$ , now a gain  $k$  can be applied to this variable and the step response analysed again. Figure 4.5 shows the different step responses with different gains on the  $Q$  matrix value for  $z$ , with figure 4.6 showing the input reaction. Having a higher value the response is faster but has a high overshoot.

For the control of the vessel overshoot is not desired because this means pitch oscillations will

happen, as in figure 4.7, and since the vessel is over 6 meters long and stays very close to the water the bow can easily hit a wave and create a large drag. With that said, a lower  $k$  value will be used.

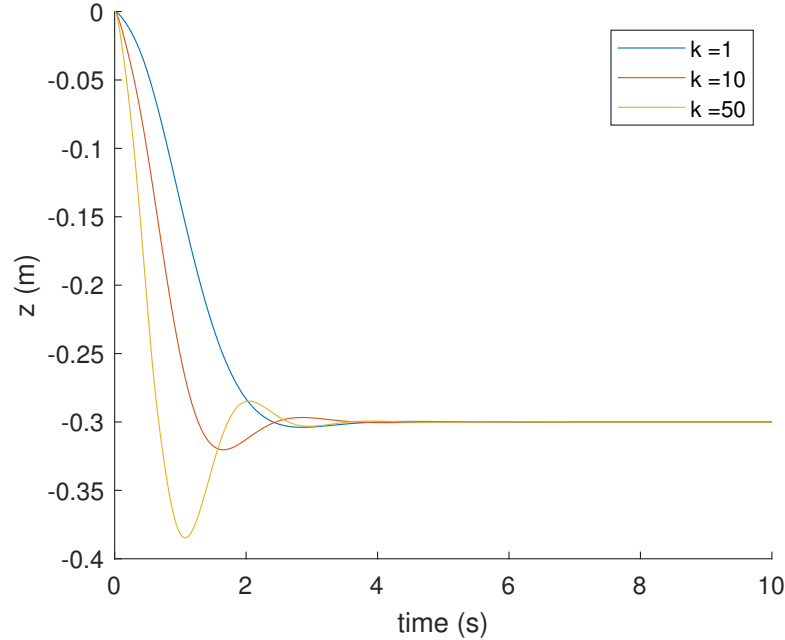


Figure 4.5: Front foil step response with LQR control for multiple gains on the  $z$  entry for the  $Q_h$  matrix.

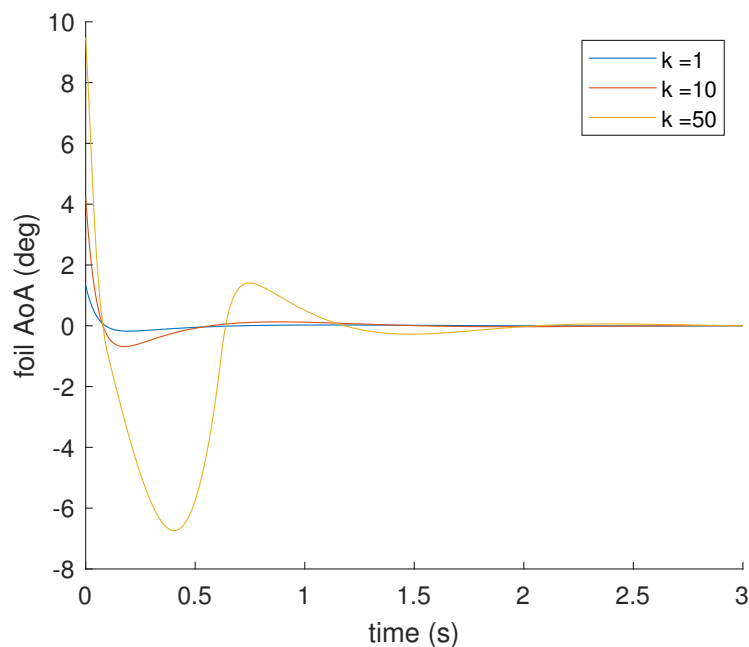


Figure 4.6: First seconds of the front foil input value for step response with LQR control for multiple gains on the  $z$  entry for the  $Q_h$  matrix.

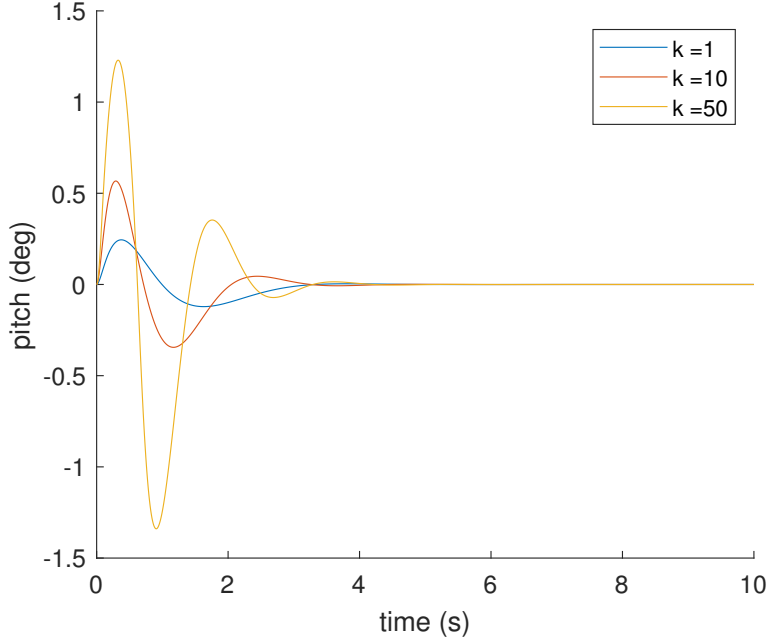


Figure 4.7: Pitch value for front foil step response with LQR control for multiple gains on the  $z$  entry for the  $Q_h$  matrix.

#### 4.1.5 Integral Action

For any controller based on a simplified model there will be uncertainty on the accuracy of the model, and even with this the goal is to have zero steady state error between the system's output and its reference. For this purpose, an integral action can be added to the controller which will guarantee the desired reference will be followed and the error will always tend to zero [19].

The idea of integral action is to add a new state, here  $x_i$ , that will be the integral of the error between the desired reference and the actual value of the state, with dynamic described by

$$\dot{x}_i = ref - z. \quad (4.7)$$

This new addition can be seen in the feedback loop of figure 4.8.

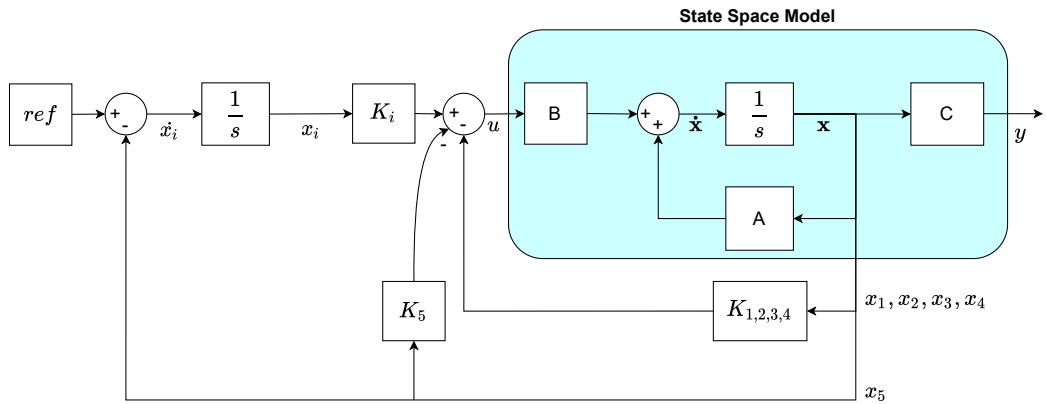


Figure 4.8: LQR model with integral action on heave.

With this new state the initial system from equation 3.10 is extended to

$$\begin{bmatrix} \dot{\mathbf{x}} \\ \dot{x}_i \end{bmatrix} = \begin{bmatrix} A\mathbf{x} + Bu \\ ref - z \end{bmatrix} = \begin{bmatrix} A\mathbf{x} + Bu \\ ref - C\mathbf{x} \end{bmatrix} \quad (4.8)$$

so the extended model with new state  $x_i$  is

$$\begin{bmatrix} \dot{\mathbf{x}} \\ \dot{x}_i \end{bmatrix} = \begin{bmatrix} A & \mathbf{0} \\ -C & 0 \end{bmatrix} \begin{bmatrix} \mathbf{x} \\ x_i \end{bmatrix} + \begin{bmatrix} B \\ 0 \end{bmatrix} u + \begin{bmatrix} \mathbf{0} \\ 1 \end{bmatrix} ref \quad (4.9)$$

and the new controller feedback is

$$\mathbf{u} = -\mathbf{K}\mathbf{x} + k_i x_i \quad (4.10)$$

where  $k_i$  is the feedback gain for the integrated output error.

Having this new model now the weight matrix Q also needs to be adapted due to the new state, yielding

$$Q_i = \begin{bmatrix} Q & \mathbf{0} \\ \mathbf{0} & q_i \end{bmatrix} \quad (4.11)$$

The new LQR gains must be computed with the additional state variable and choosing an appropriate value for  $q_i$ .

#### 4.1.6 Anti wind-up

When the controller calculates the input value necessary to go towards the desired reference output it should always stay within the limits of the actuator. This creates non-linearities that can create problems in the control loop.

When the controller sets the input of the system as a value above the limit of the actuator an effect called windup happens in the integrator of the controller.

When the windup effect happens the performance of the system is deteriorated with higher overshoot and longer settling times [20].

To solve this, the difference between the saturated and unsaturated signals is fed back into the integrator through the integral state variable  $x_i$ . This allows the saturation to discharge the integrator as if the integration was turned off until the input comes back to an acceptable range. With this the integral state variable is now

$$\dot{x}_i = ref - z - (u - \bar{u}) \quad (4.12)$$

and the new system input computed by the controller is

$$u = -\mathbf{K}\mathbf{x} + k_i \int_0^t (ref - z - (u - \bar{u})) dt \quad (4.13)$$

The implementation of this anti wind up technique can be seen in figure 4.9.

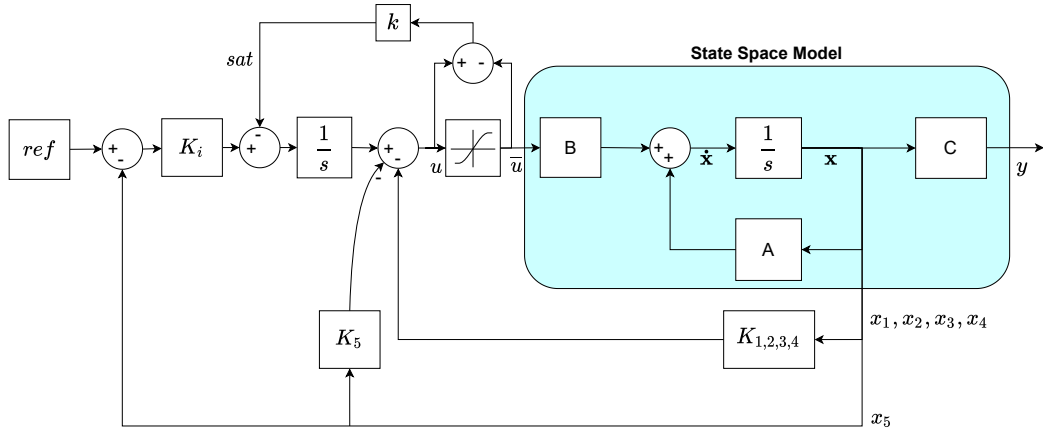


Figure 4.9: LQR model with integral action on heave.

#### 4.1.7 Delta implementation

There is an improvement that can be made to this controller which consists in having the integrator after all feedbacks, so not only integrating the error signal and saturation but all feedbacks. This allows for a better performance when a controller is designed based on a linearization of a non linear model, such as this controller, as it eliminates any biases present in the measurements of the states. This is known as delta implementation [21].

Since we linearized the model around an equilibrium point in section 3.3, this controller is made to control the system around this steady state. If the steady state has non zero state values, when applied to the non-linear model, the equilibrium points have to be subtracted from the state measurements before being multiplied by the gains  $K$ . Given that, the feedback equation becomes

$$u = -\mathbf{K}(\mathbf{x} - \mathbf{x}_{\text{steady}}) + k_i x_i \quad (4.14)$$

where  $\mathbf{x}_{\text{steady}}$  is the state vector at the equilibrium point used for the linearization. Delta implementation eliminates this part.

This method also allows to easily decide the initial input  $u$  of the system by setting the initial condition of the integrator. Without this implementation there can be larger initial oscillations at the start of the controller.

To integrate all feedback signals the solution is to derive the signals that were not originally being integrated. This way we can implement the scheme seen in figure 4.10.

The integration was moved just before the saturation block and the feedback signals  $\mathbf{K}\mathbf{x}$  goes through a derivative block.

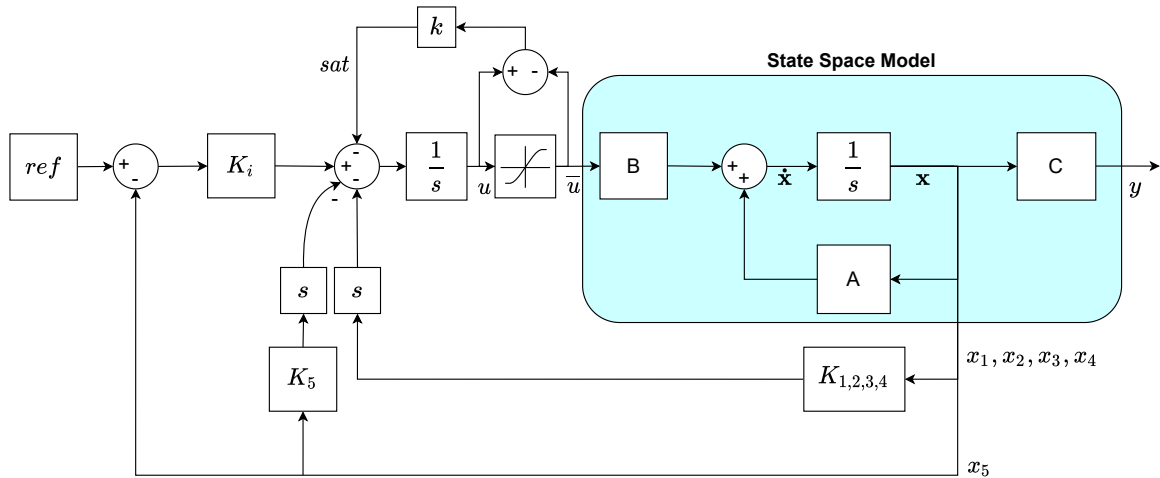


Figure 4.10: LQR model with delta implementation on heave.

#### 4.1.8 Gains recalibration

In section 4.1.3 we have seen how to find the gains for the simple LQR feedback loop with reference following. Now with the addition of the integrator, anti wind-up and delta implementation new gains must be computed.

There is a new gain  $K_i$  and a gain  $K_{sat}$  that need to be adjusted. The gain  $K_i$  is computed solving the Riccati equation for the extended system in (4.9), and adjusting the value  $q_i$  from the new matrix  $Q_i$ .

Figure 4.11 shows the step response of the heave model for different values of  $q_i$ . We can see that a higher  $q_i$  value gives a quicker response, but with  $q_i = 10$  there is already some unwanted overshoot.

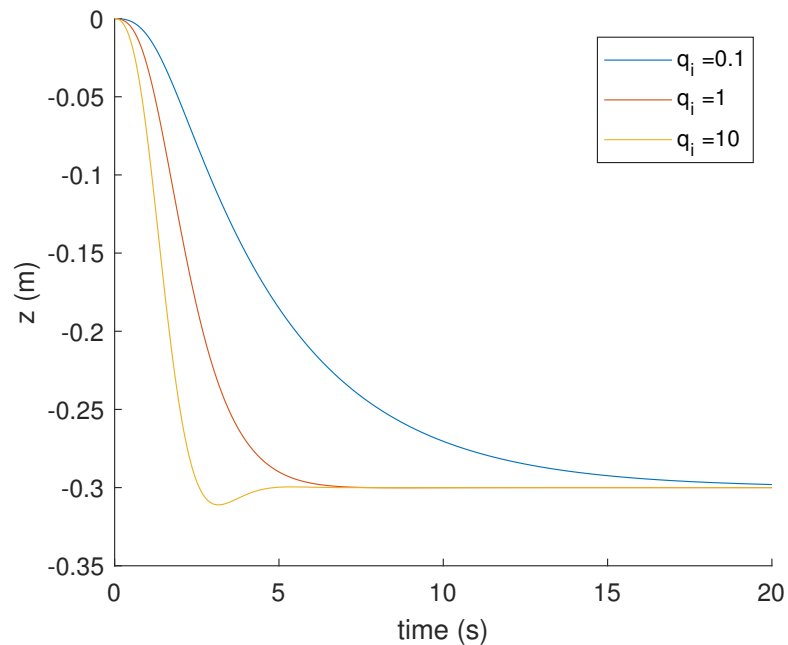


Figure 4.11: Front foil step response with LQR control for multiple gains on the  $q_i$  entry for the  $Q_h$  matrix.

With that the final gains computed are

$$K_h = \begin{bmatrix} 4.7 & 0.6 & 6.9 & -8.4 & -13.5 & -10 \end{bmatrix} \quad (4.15)$$

For the saturation different values were tried to adjust  $K_{sat}$ , and its final value was  $K_{sat} = 1$ .

We can also analyse the frequency response of the closed loop linear heave and pitch system with the bode plot from figure 4.12. The cutoff frequency is at  $\omega = 1.0825 \text{ rad/s}$ , where the magnitude drops below  $-3 \text{ dB}$ . Having a zero gain for low frequencies shows us the reference will be followed.

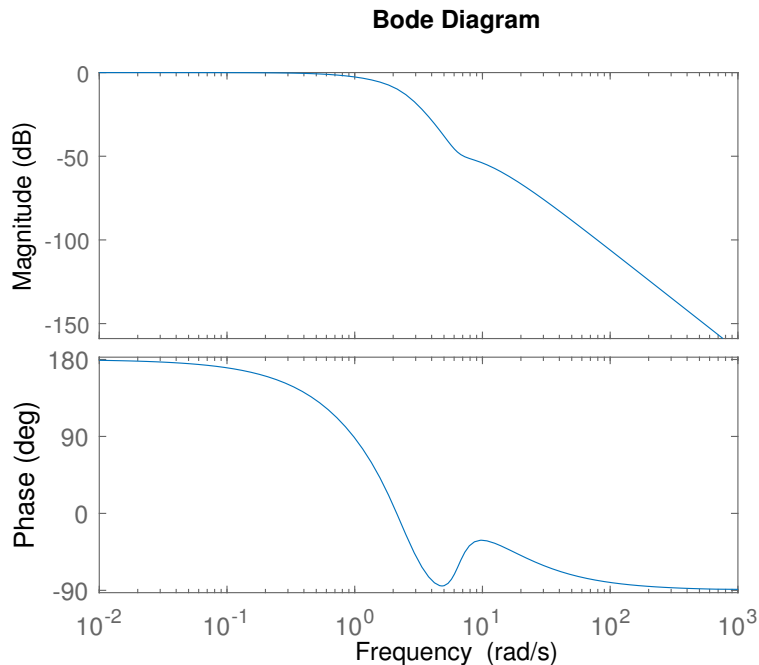


Figure 4.12: Bode plot of the closed loop linear system for heave and pitch.

#### 4.1.9 Final controller vs simple LQR

Now with the gains computed another simulation was done to see the influence of a perturbation on the velocity read by the sensor of the boat and compare the first LQR with the last with delta implementation. A bias of  $0.5m/s$  was applied to the velocity, trying to simulate a case where sea current could be present. Figure 4.13 shows how the first LQR with simple reference following reacts when this bias appears at  $t = 10s$ . Figure 4.14 the reaction of the LQR with delta implementation to the same perturbation. As we can see the final controller which has an integrator has a deviation of less than  $10cm$  and quickly goes back to the desired reference, while the simpler controller stabilizes at a completely different value.

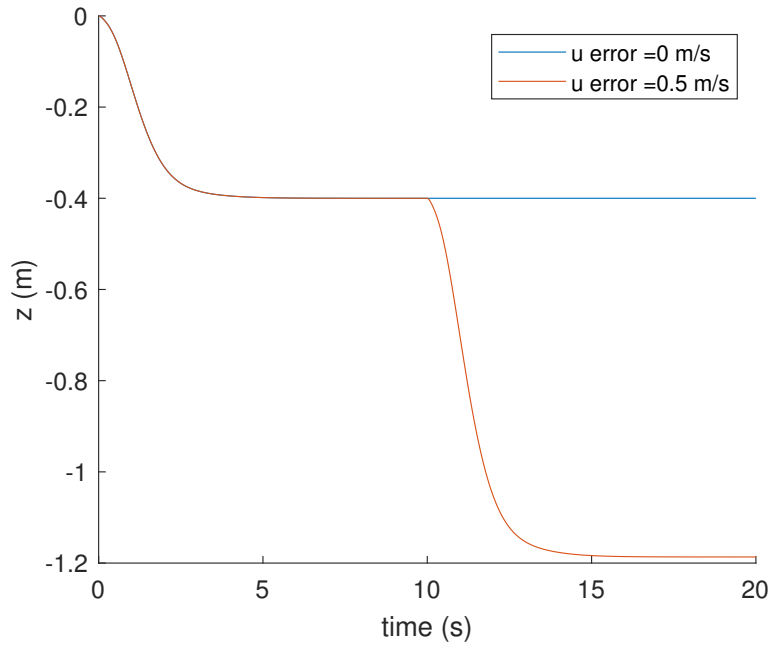


Figure 4.13: Front foil step response with LQR control as in figure 4.2 (simple reference following) with error on speed sensor value at  $t = 10s$ .

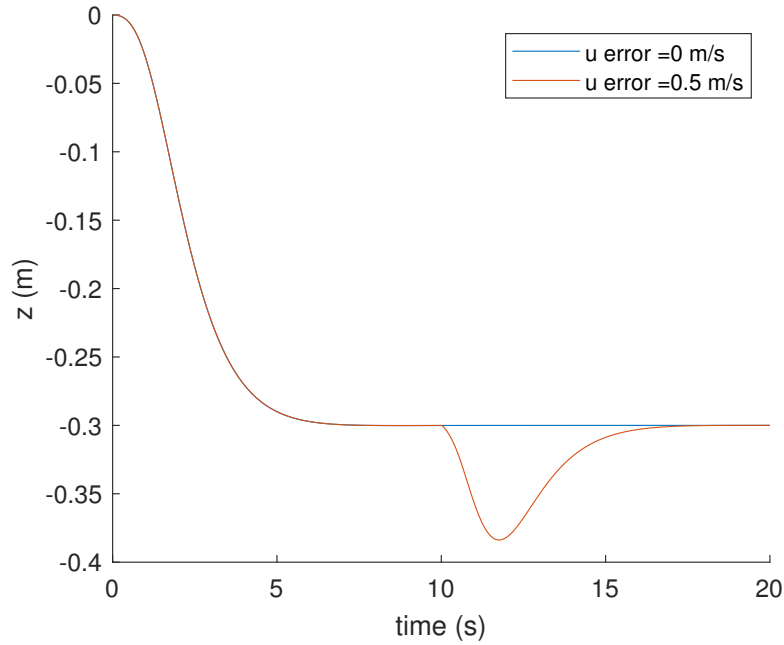


Figure 4.14: Front foil step response with LQR control as in figure 4.10 (delta implementation) with error on speed sensor value at  $t = 10s$ .

## 4.2 Controller for roll

All the simulation and equation mentioned above were done for the heave and pitch controller, which is very complex and includes non zero reference following. Because of that, a lot more work was placed on that controller compared to the roll controller. The roll controller only uses 2 state variables as inputs,

roll and roll rate, and has to maintain the roll as close as possible to zero. Besides this, all the equations are the same, and the simulation to find the optimal state feedback gains were done in a similar manner.

Figure 4.15 shows the feedback loop of the roll controller, with the state variables *GyroX* (angular velocity of roll) and *Roll* in the loop.

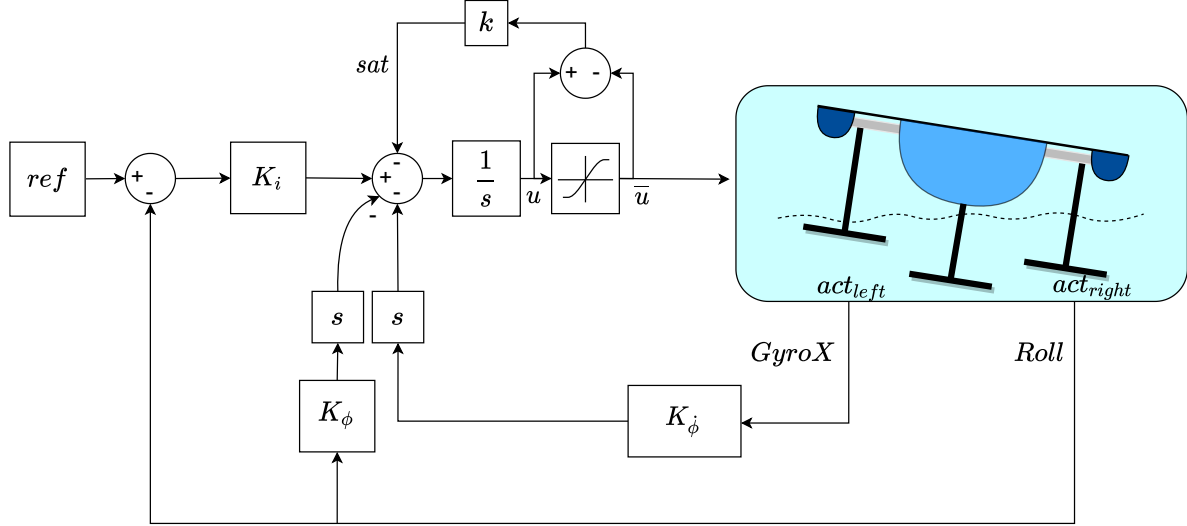


Figure 4.15: LQR model with delta implementation on roll.

After doing all the simulations, the gains computed for the differential output of the controller are

$$K_r = \begin{bmatrix} 2 & 0.25 & 1 \end{bmatrix} \quad (4.16)$$

and for the saturation,  $K r_{sat} = 1$ .

### 4.3 Common and differential modes

As said in the linearization section 3.3 the control is separated in two modes, common and differential. Common mode will control heave and pitch of the vessel by actuating with the same value on each front foil. Differential mode will actuate with symmetrical values on each front foil to maintain the vessel's roll stable.

Figure 4.16 shows how both modes are interconnected and add up to the actuation on each hydrofoil.

Regarding the ranges for each controller we need to consider the range of movement allowed for the hydrofoils' AoA. The mechanical range is from -3 to 7 degrees, but part of this range must be used for the roll control. Initially one degree was considered for roll, so the common mode would only actuate from -2 to 6, but after the first tests on roll we quickly found out that there had to be more range for roll. We ended up using 2 degrees for the differential mode's output, and the common mode was left with a range from -1 to 5 degrees. This was done in order to not exceed the physical limits of deflection of the actuators, between -3 and 7 degrees.

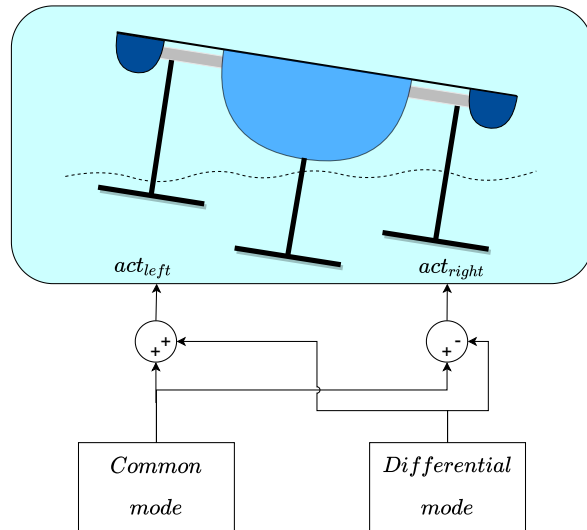


Figure 4.16: Common and differential modes combination.

# Chapter 5

## Simulations using the Non-linear Model

After having the model and the controller designed, a wide variety of simulations were done using the non-linear model of the hydrofoil vessel. The first simple simulations were done to see if the controller would hold the vessel at the steady state for which the controller was designed. Afterwards, simulations were done with variations in thrust, then with added noise extracted from real data from the sensors that have already been used in the vessel.

The simulations were mostly done looking at heave and pitch, then some more simulations were done for the roll analysis.

### 5.1 Heave and pitch control simulations

First, for heave and pitch a step was applied to the heave reference to see how the model would behave with the controller designed previously. We expected no overshoot and about 5 seconds from water to foilborne.

Figure 5.1 shows the step response simulation on the non linear model. As we can see, on the first second the model stays stable in its initial conditions. This is expected since the initial conditions were used to compute the controller gains. After the first second we can see the step on the reference, which is followed by light oscillation on pitch, and a very small variation on speed. But most importantly we can see the foils' common mode angle reacting in such way that it brings the height of the vessel to the reference. The response takes only a few seconds, and has almost no overshoot.

Other simulations were done with strong thrust variations, which can be seen directly reflected on the speed of the boat. We can see on figure 5.2 that small/slow speed changes do not compromise too much the performance of the flight, such as at time 5s and 20s. But on 5.3 at time 5s there is a larger acceleration and we can see the heave going down almost 10 centimeters. This shows how sensitive to speed the flight can be.

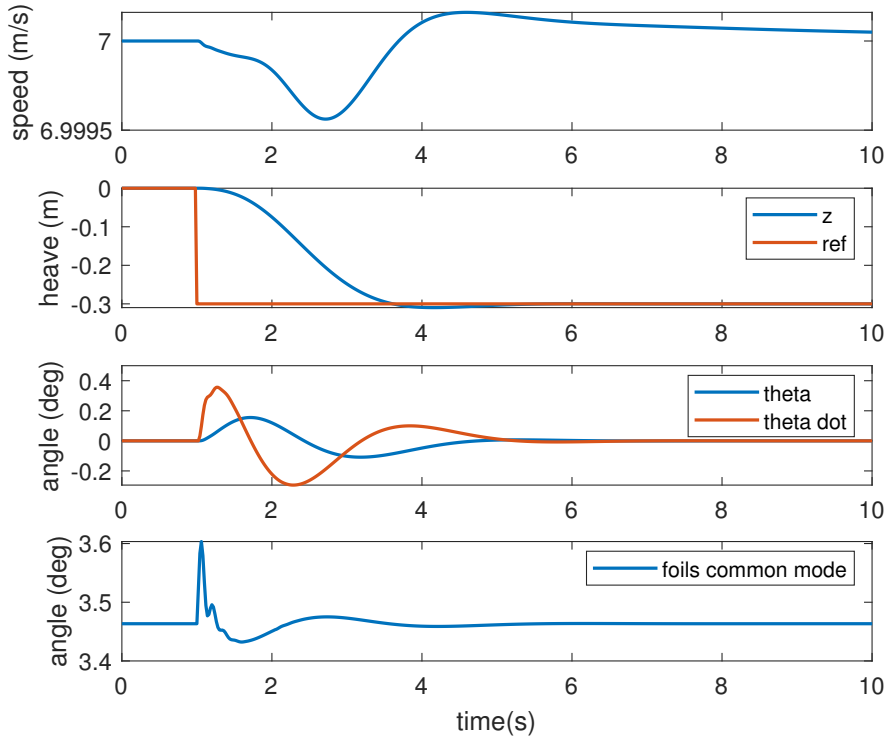


Figure 5.1: Non linear model's step response.

Due to this sensitivity some other improvements were done on the boat to control speed. This will be explained further ahead in section 7.2.1.

After having observed that the controller could maintain the vessel at equilibrium, noise was introduced in the simulation. For this purpose, real data from the sensors was used. These data were acquired during real test with the boat going close to cruise speed but without being foilborne, and without having the controller activated.

Figure 5.4 shows the data that was used as noise. This is data from an ultrasonic sensor and from an AHRS (Attitude and Heading Reference System) pitch readings. These two sensors will be used for the control, and are described in section 6. Since this was acquired while the boat had some speed changes, and the hull generates some lift, the data had to be detrended. At around time 15s and 16s some large spikes can be seen from the ultrasonic sensor readings, these were left on purpose to see how the controller would react. These spikes are usually due to bad reflections of the sonic beam on the water surface. However, when the boat is foilborne these misreads are very rare because the sensor is working closer to its optimal range.

With the data above, the simulation in figure 5.5 was obtained. As we can see the vessel's heave stays close to the reference, but it oscillates about 3 or 4 centimeters over and under the reference. Pitch (as  $\theta$ ) on the image can be seen very stable.

Finally around time 15s and 16s where the spikes happened on the ultrasonic sensor, they can be seen reflected on the common mode output of the controller, but it didn't jeopardize the vessel's heave.

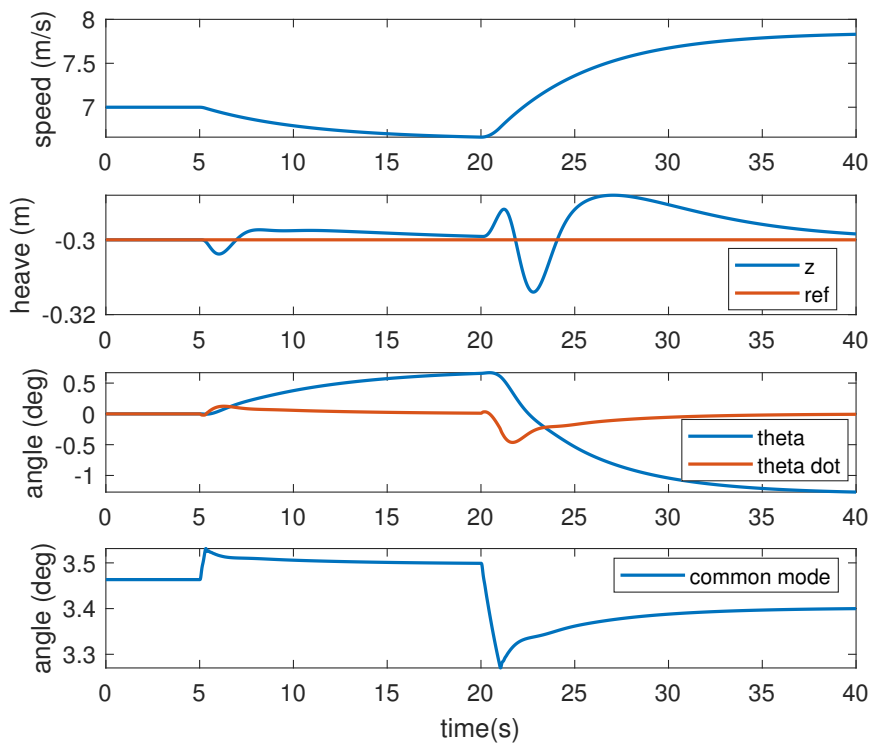


Figure 5.2: Thrust variations impact on heave and pitch control.

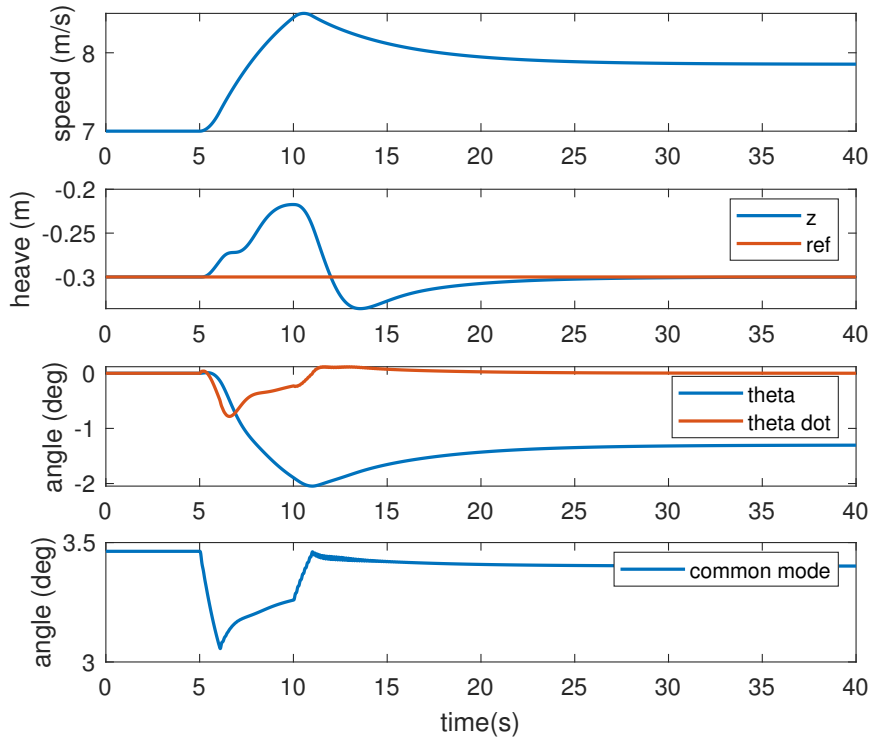


Figure 5.3: Thrust variations impact on heave and pitch control. Here with an undershoot on heave.

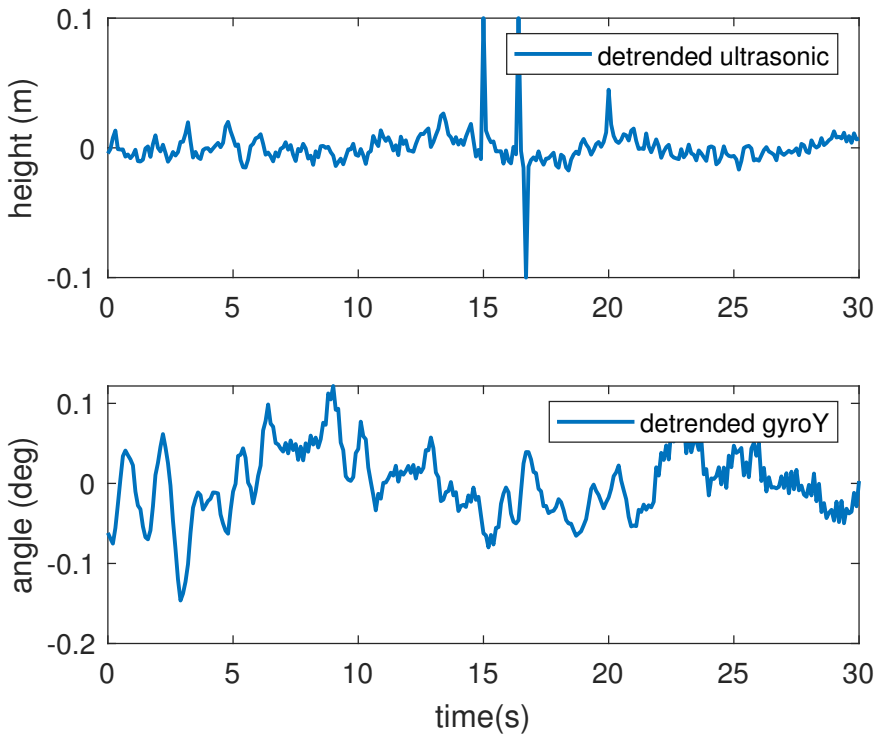


Figure 5.4: Real sensors' data detrended which was used in the simulation of figure 5.5.

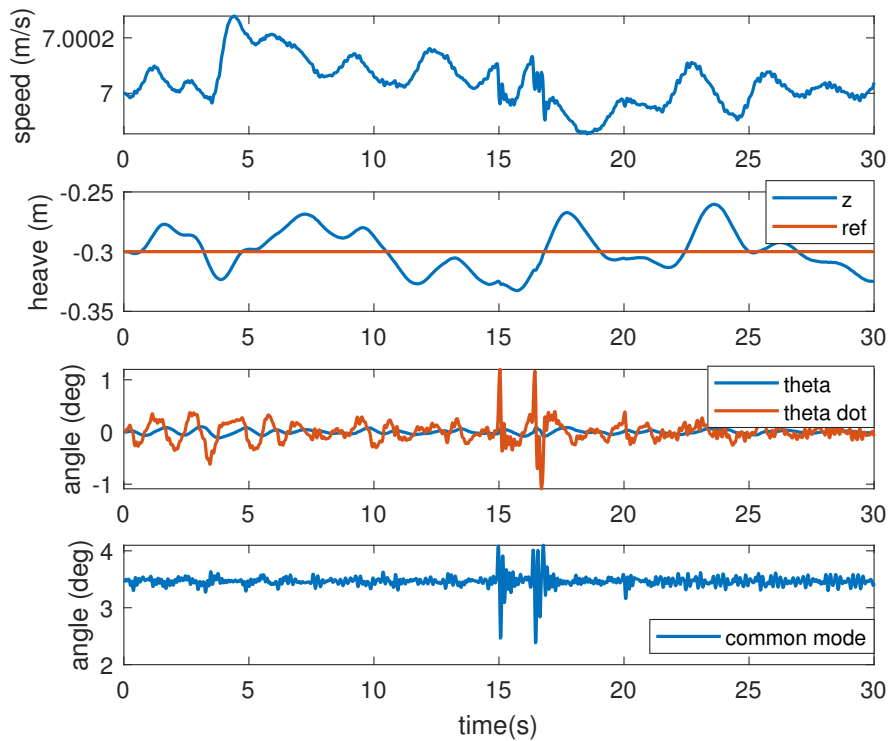


Figure 5.5: Simulations with added real sensors' data to mimic noise.

## 5.2 Roll control simulations

For roll, similar simulations to the ones above were done. Although it's unrealistic, because roll should stay zero, a step response on roll was simulated and can be seen in figure 5.6. This simulation is good to verify if the controller is doing the right thing. As we can see, the model follows the reference by slightly adjusting the foils through the differential mode.

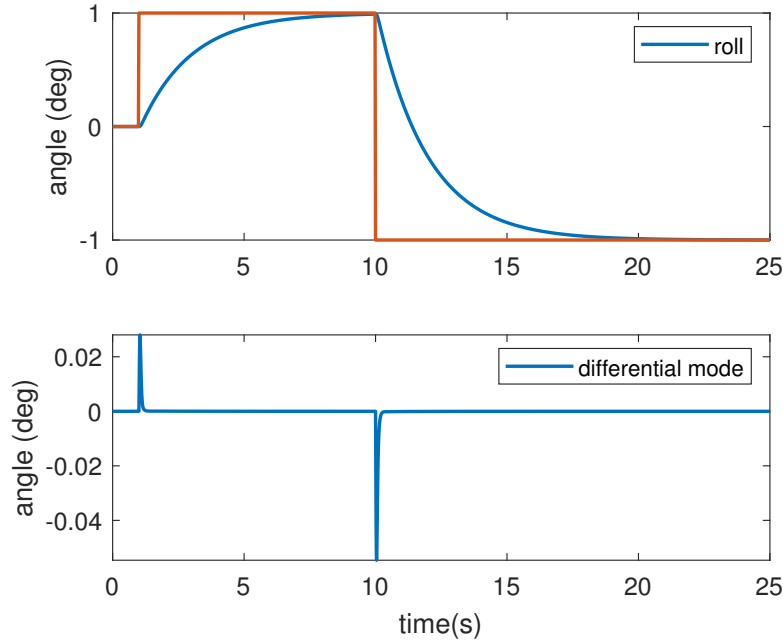


Figure 5.6: Non linear model's step response for roll.

At this point, as was done for the heave and pitch simulations, sensor readings were added to the simulation to mimic noise and external perturbations. Here the reference changes were left to better see the behaviour of the controller. Figure 5.7 shows the sensor reading that was used for the simulation, this was also obtained during real tests with the boat going close to cruise speed but without being foilborne.

Figure 5.8 shows the model behaviour with the sensor readings added and the reference changes. The result shows that the reference is followed even though there are some perturbations around the reference value. We can also see the the differential output of the controller is very reactive, but these small variations on the foils will be damped on the real system, due to all the mechanical damping. Finally on the lowest plot, we can see that simply by varying the foils' angles for roll control it has a small influence on heave.

To further analyse the influence that roll can have on the boat's heave a simulation was done with an overly perturbed roll. Figure 5.9 shows the result of this simulation. We can see that the differential mode reached an unstable regime from about 5s to 13s, and this has a very bad influence on heave, as it almost reaches a height of zero. Nonetheless it manages to recover very well from this stage.

This influence was found to be due to the slew rate limit that is present in the model's foils inputs. This slew rate represents the maximum speed at which the stepper motor can actuate on the hydrofoils.

Knowing that, the same simulation was done with the same perturbations on roll, but this time with the slew rate doubled. Figure 5.10 shows the result of this simulation, now we can see that the differential mode output doesn't reach the previous unstable regime and now the vessel's heave maintains itself really close to the reference. This means the gains must be adjusted to prevent exceeding the slew rate limits.

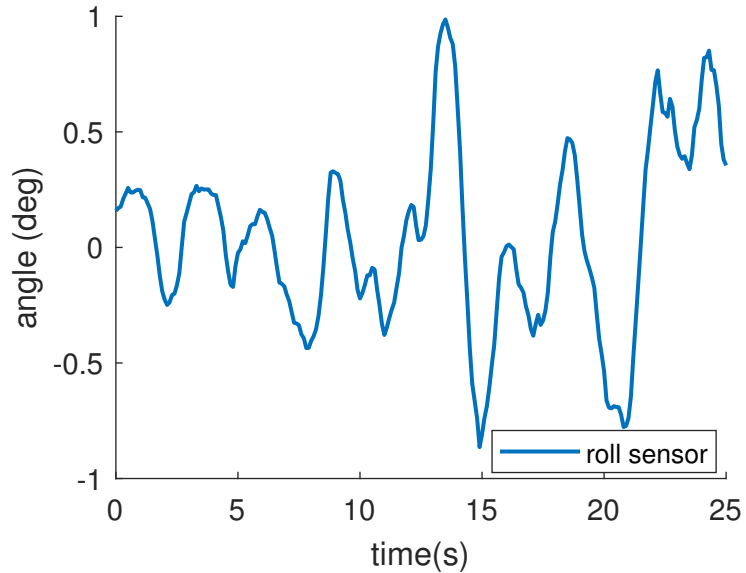


Figure 5.7: Roll readings from sensor used as perturbations for the simulation done in 5.8.

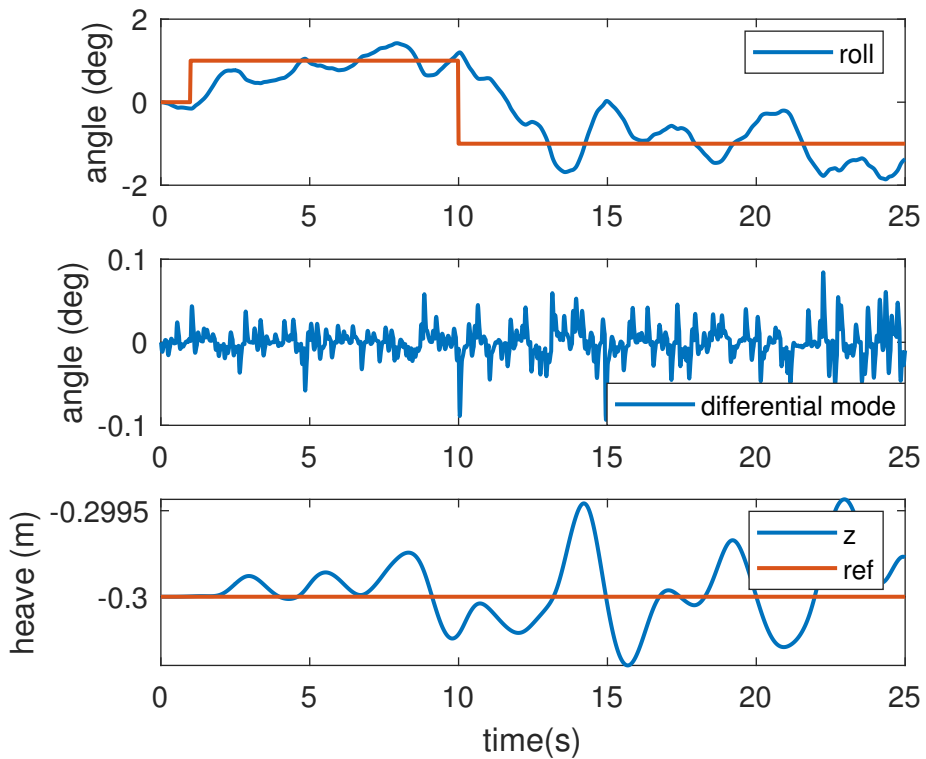


Figure 5.8: Roll control simulation with outside perturbations on roll.

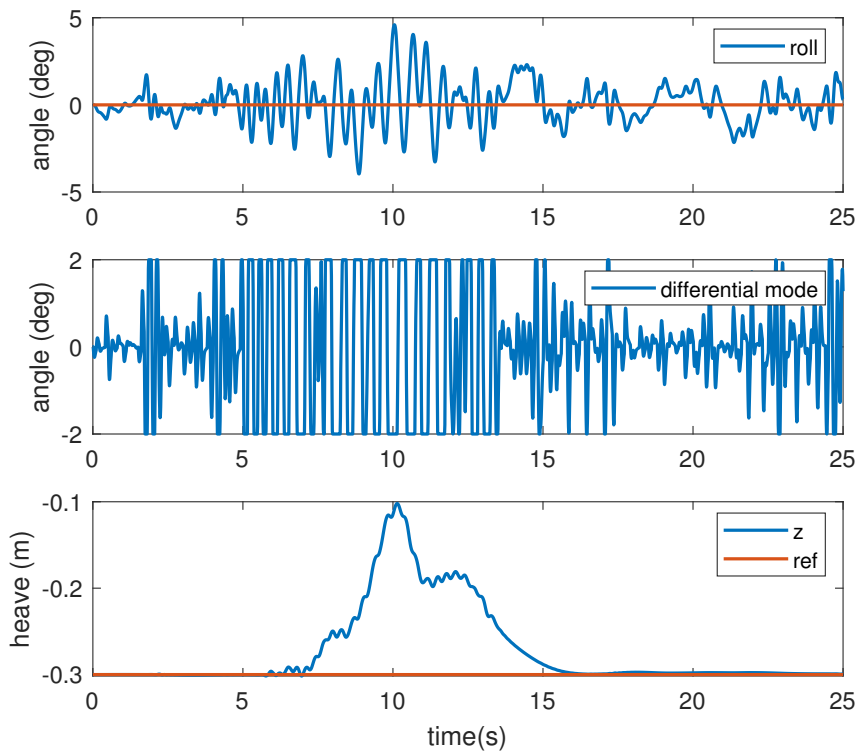


Figure 5.9: Roll control simulation with exaggerated perturbations on roll.

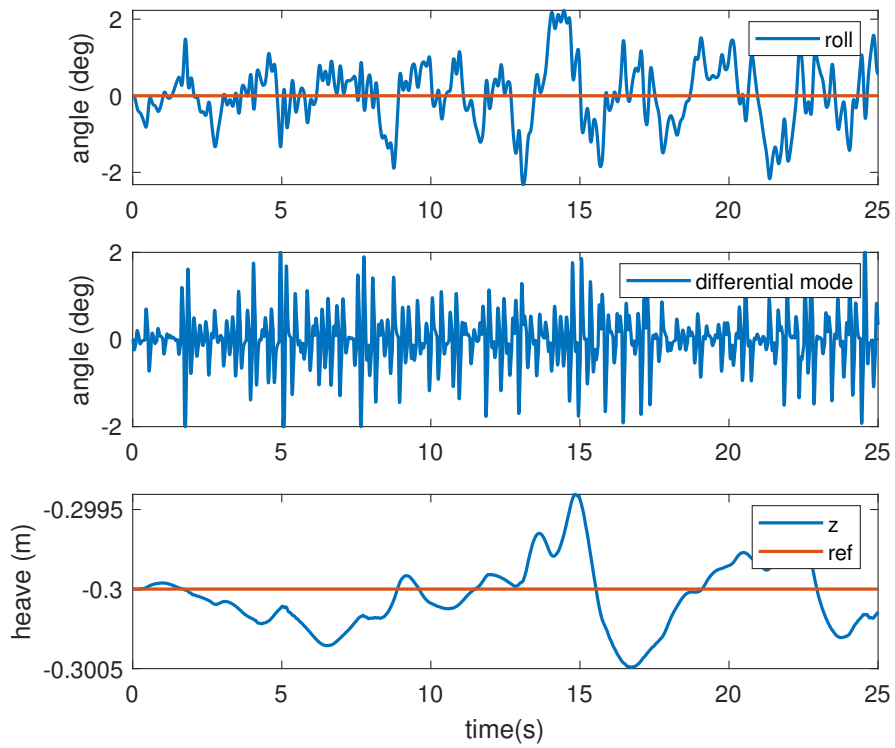


Figure 5.10: Roll control simulation with exaggerated perturbations on roll but higher slew rate on the foils' AoA.



# Chapter 6

## Implementation

This chapter is meant to give an overview on the complete system used to implement the control algorithms described before.

### 6.1 Hardware

The system is composed of

- Printed Circuit Board from appendix A
- 3 stepper motors with optical encoders, 2 for the front foils and one for the rear foil (for future use)
- 3 motor controllers
- one Attitude and Heading Reference System sensor
- one Teensy USB-based microcontroller development board
- one GPS antenna
- one ultrasonic sensor
- one RaspberryPi for remote firmware updates

The Teensy board is where all the code is implemented. This includes the LQR controller, the communication with the motor controllers, the AHRS, the ultrasonic sensor and the pilot's dashboard.

Figure 6.1 shows the connections between all the components that are used for the control of the hydrofoils.

Figure 6.2 shows the location of the AHRS and the ultrasonic sensors on the vessel. Since the ultrasonic sensor is located at the bow and the controller considers heave at the center of mass of the vessel, a small correction had to be done considering the boat's pitch. The sensor is at about 3 meters ahead towards the bow compared to the center of mass of the vessel, so the compensation for state  $z$  was computed as

$$z = US - 3 \cdot \sin(\theta) \quad (6.1)$$

where  $US$  is the sensor reading.

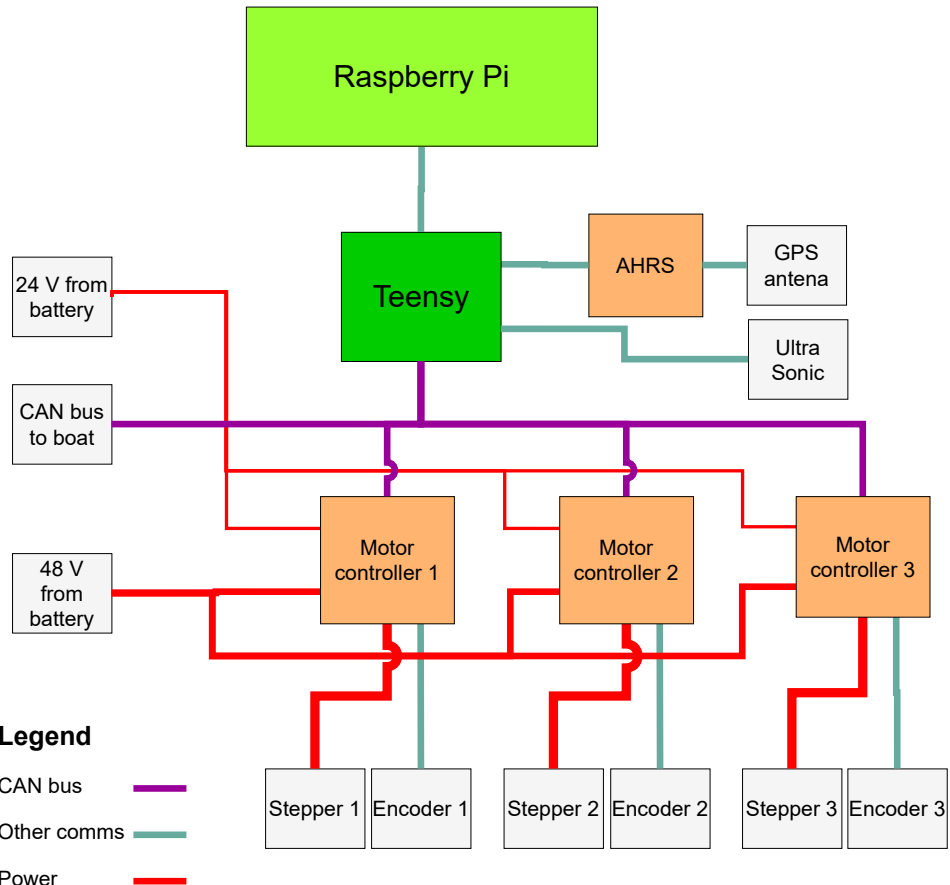


Figure 6.1: Hardware diagram of the components on the vessel that allow to control the hydrofoils.

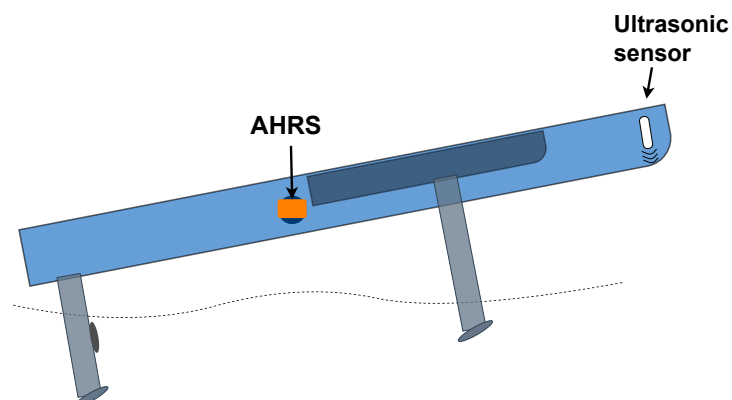


Figure 6.2: Positioning of the AHRS and the ultrasonic sensor on the vessel.

## 6.2 Software

The system was designed to be flexible, so that the pilot could change a few parameters while onboard. For this purpose, different states and functioning modes were implemented. The flowchart in 6.3 shows the functioning of the system, the changeable variables from the dashboard and the actions done by the available buttons.

- The pilot could change the following parameters
  - height reference to follow, useful for adapting to meteorological conditions
  - common mode angle for the hydrofoils when the heave controller was off
  - operating mode
  - state of operation

The different modes were implemented for testing reasons. The **Manual mode** allowed to fix a certain AoA on the foils, this was aimed to be the first test. Then the **Roll mode** allowed to activate the roll controller around a fixed common mode value. The **Heave mode** allowed to activate the heave controller without using any differential on the AoA of the foils. Finally the **Full mode** could activate both the Roll and the Heave controller.

The **homing** is a crucial routine that has to be done everytime the boat is switched back on. When the boat is off the stepper motors can rotate freely and the motor controller will loose it's reference, not knowing the exact position of the motor shaft, i.e. the foil AoA. When homing is performed the motor turns until hitting the maximum AoA and saves this as its reference. This is why the optical encoders are used.

Another important feature was implemented on the vessel to facilitate testing. A Raspberry Pi was connected to the Teensy and connected to the WiFi network present in the boat to allow remote modifications of the core code of the Teensy. This allowed us to change the LQR gains, the takeoff speed, and any other code we would want to change without needing to be close to the boat.

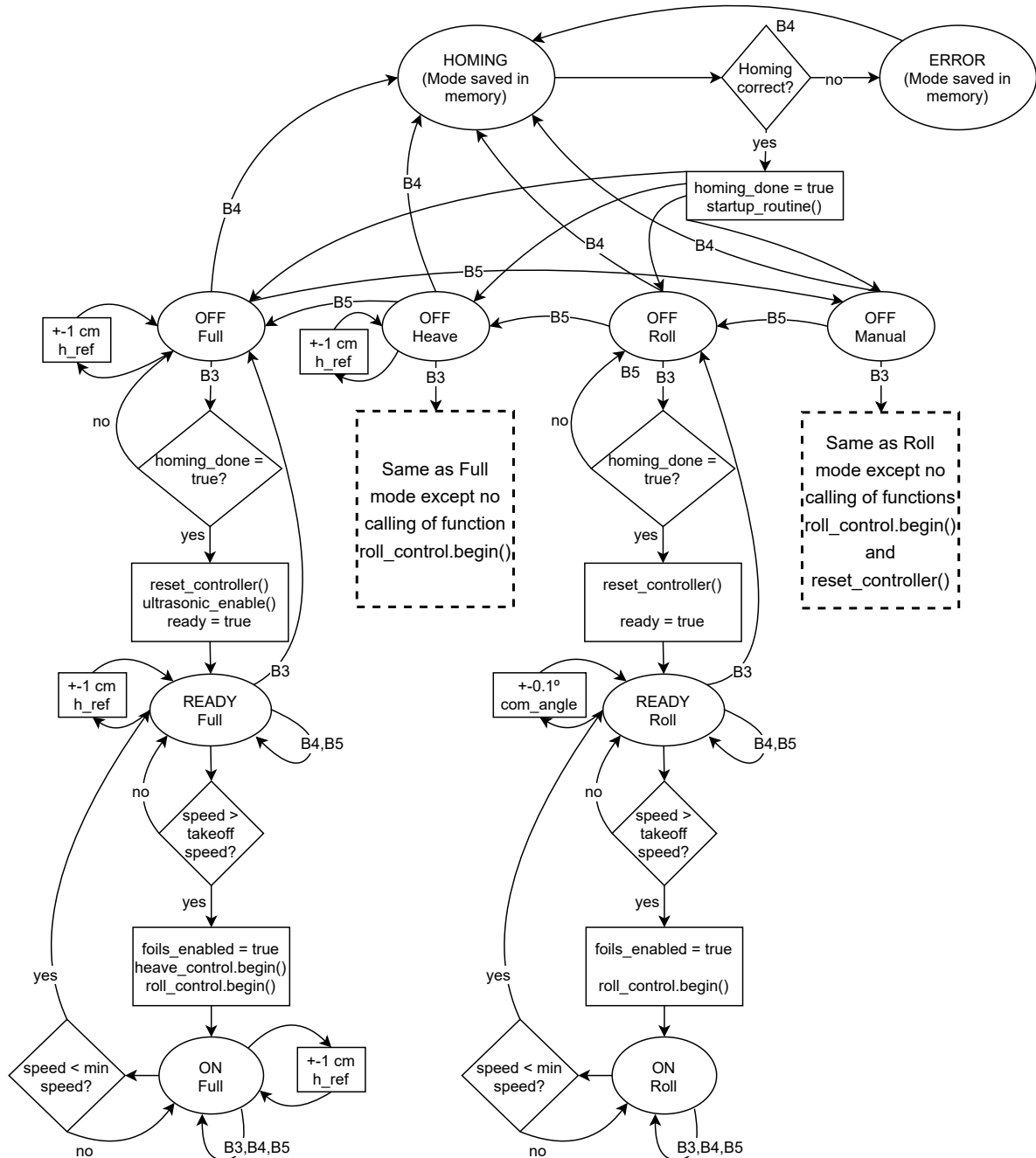
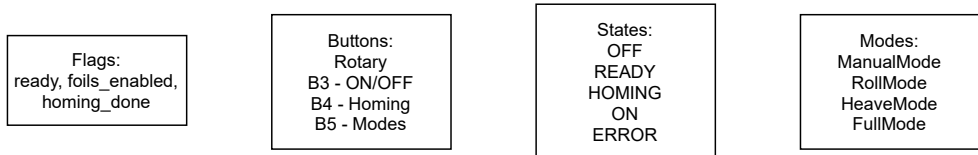


Figure 6.3: Flowchart of the different states and operating modes.

### 6.3 Hardware in the loop test

After programming the microcontroller with all the code necessary for the LQR controller, test data were generated using *Simulink*. These data were fed into the microcontroller and the outputs generated from the *Simulink* and the microcontroller were then compared.

The test data consisted of data points of all state variables that go into the LQR controller. These data points were extracted from simulations that had perturbations that also created saturation on the controller. This was done on purpose to confirm that the LQR code was properly done.

Figure 6.4 shows the result of these tests. The data follows the same behavior on both platforms even though there is a small bias, but since the test on the microcontroller didn't have feedback this could be expected.

Since the code for the roll controller had the same structure as the heave controller this test was only done for the heave controller and considered acceptable for both controllers.

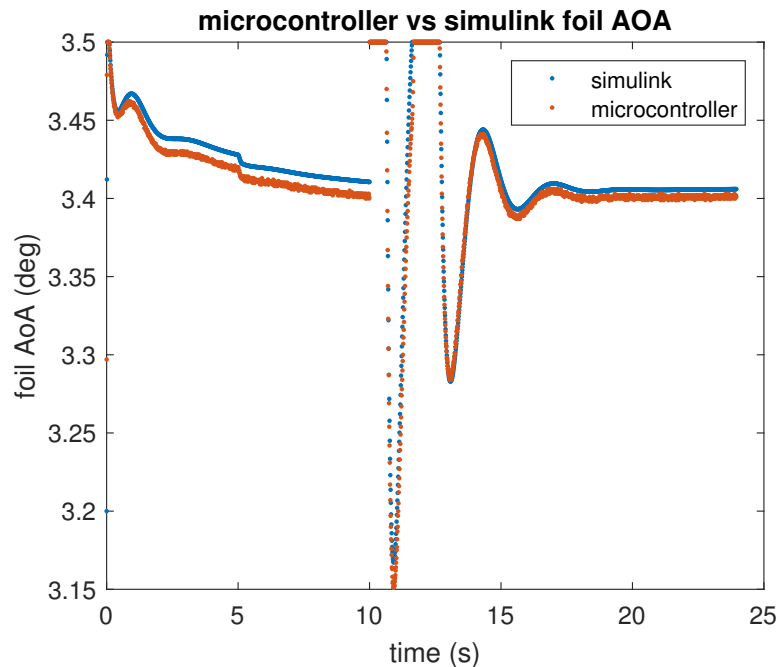


Figure 6.4: Comparison between LQR controller output on the microcontroller and *Simulink* for heave control.



# Chapter 7

## Results and upgrades

### 7.1 Roll controller tests

After having everything implemented tests were done with the vessel in the water. This was the first time that this system (including the mechanical part) was put to test. With this we didn't know what to expect so we started slowly.

First we fixed the AoA of the front foils and tried to reach a decent speed and see if lift was generated. The problem with this was that there was too much unevenness between the left and right front foils and this caused lateral imbalance. This can be seen in figure 7.1, where peaks in speed show different runs. There are many mechanical factors can cause this imbalance, like the control rods cut by hand, or the struts that can be mounted with different angles relative to the vertical body axis  $z_b$ . So we quickly realized we needed the roll controller.

The first gains used for the roll controller were very small, we had

$$K_r = \begin{bmatrix} 0.15 & 0.01 & 0.001 \end{bmatrix} \quad (7.1)$$

These gains were adjusted during dry tests simply moving the AHRS by hand, and were small to start testing slowly and see if everything would go as planned. Here we only had one degree on the differential output.

The roll controller worked as planned and gave some stability to the vessel, more than it had without the hydrofoils.

Figure 7.2 shows the first test done with active roll control. The controller can be seen starting at a speed of 5 m/s and taking approximately 5 seconds until stabilizing. It then turns off at 3 m/s, as it was programmed. To stabilize quicker, it was important to start the controller at an earlier speed and so it was reprogrammed to start at 2 m/s. Starting at a later speed was more important for the heave controller.

The limitation here was when turning too hard and falling sideways, the vessel had to slow down to recover. To make it possible to turn harder the gains had to be adjusted and/or a larger differential angle had to be allowed.

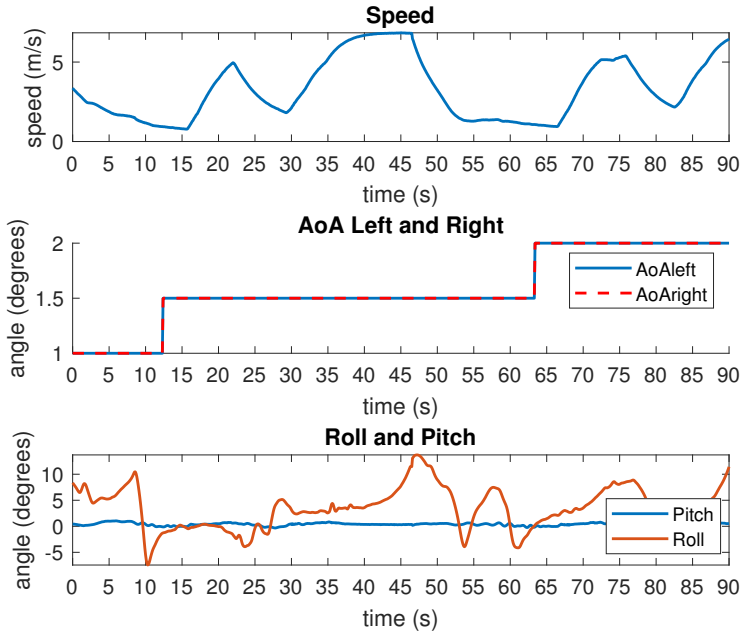


Figure 7.1: First tests where no control was active and high rolls can be seen in multiple runs.

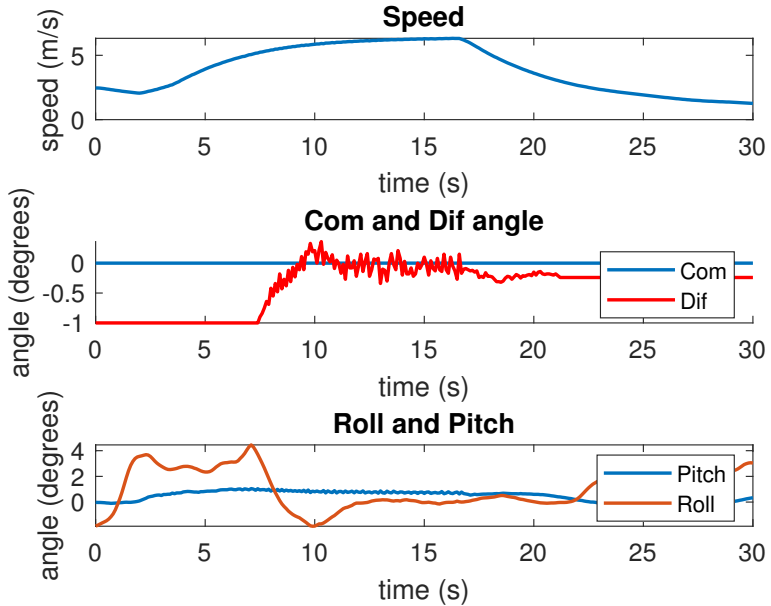


Figure 7.2: First test with active roll control.

We first tried only adjusting the gains. Testing showed that the gains had to be larger than what we initially used. But even with higher gains we couldn't do tight turns. So we added one more degree for the differential angle.

Our final gains for the roll controller were

$$K_r = \begin{bmatrix} 0.8 & 0.25 & 1 \end{bmatrix}. \quad (7.2)$$

Figures 7.3 and 7.4 show the results of these gains for the roll controller. The data shows that the boat was going close to its cruise speed, maintaining a steady roll. The map figure shows that it was doing a relatively tight loop.

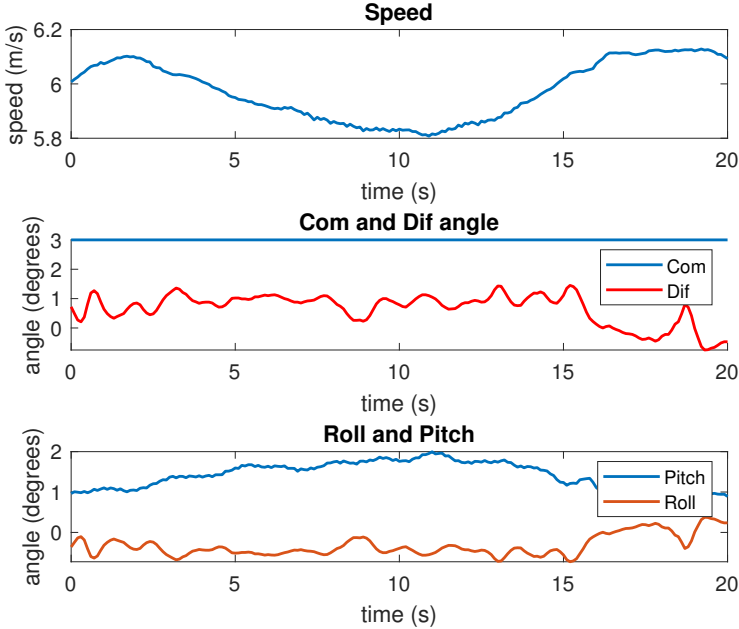


Figure 7.3: Roll controller active and turning at cruise speed.

We eventually had a big problem that seemed to come from the roll control, but was found to be due to the actuators lacking power. What was visible was the boat falling sideways about 50% of the times we tried to take off, and always to the same side. We tested different configurations, exchanged the whole struts from one side to the other, and still got the vessel falling to the same side, so it seemed to be an electronic or software problem. To test that we exchanged the left and right controllers, and still got the same result.

Eventually we contacted the manufacturers of the actuators and they guided us to find the source of the problem: the stepper motors don't have enough force to move the hydrofoils under certain conditions. Since the actuators are at their limit, sometimes they manage to control the foils but at certain speeds, angles of pitch, AoA position it may get stuck.

In figure 7.5 the boat can be seen falling sideways (very large roll), and the right angle asked by the LQR controller is different than the real angle from about time 7s to 11s. Since the stepper gets stuck it stops following the orders of the LQR. After slowing the vessel down, the lift generated by the foil decreases a lot and so the force of the stepper is enough to start moving again.

The reason for the vessel to always fall to the same side continues to be unknown but it may be due to a small dissymmetry of the hull, or a misalignment of the beam where the struts that hold the foils are fastened.

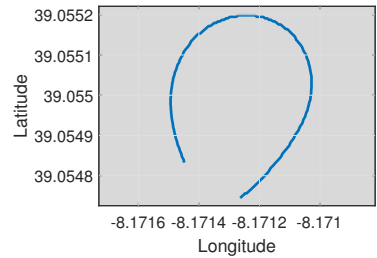


Figure 7.4: Bird view of the course taken by the boat for data of figure 7.3.

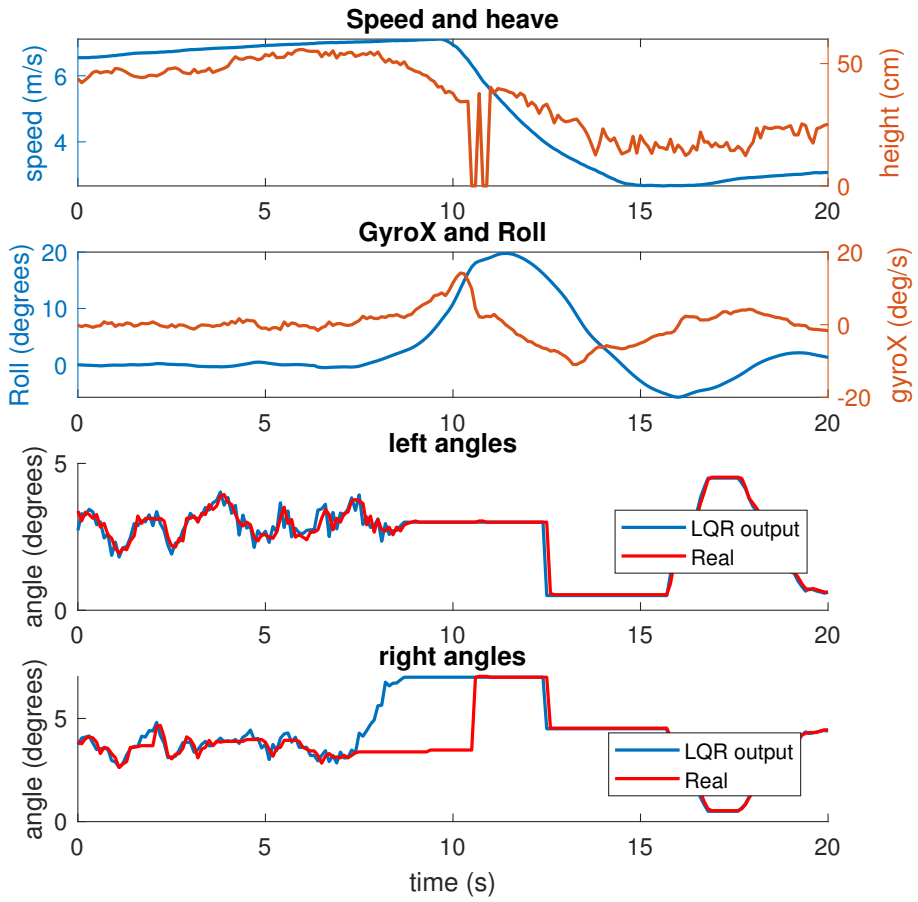


Figure 7.5: First test with active roll control.

## 7.2 Heave and pitch controller tests

The heave and pitch control tests were very interesting and made us progress along the different times we had test days. We had about 10 full days of tests, spread over 3 months, dedicated to this.

A lot of upgrades were done in between the different trips to the test site. This had implications on the data that could be shown here. For example, initial tests were done only saving the LQR's output. Eventually the real position on the actuator was saved to compare the commanded position of the steppers and their real position. In the last tests, we had a CAN bus datalogger that would save 16GB of messages in 2 days of tests, we could see the torque component of the current going to the steppers, we had an ethernet switch connected to the stepper controllers to access them remotely using the manufacturers integrated web server.

On the first trials of heave and pitch control, we tried to take off at low speeds (using only one of the two motors onboard) and with a low height reference, trying to stay as safe as possible. However, the speeds we were reaching were not enough to take off, so we went for higher speeds (using both motors) and managed to take off.

Figure 7.6 shows how the boat was reacting during the first height control tests. The figure shows 3 different runs, and each one of them shows the same behavior, when a certain speed is reached the

boat takes off and keeps accelerating until there is too much lift on the rear foil and the vessel "bow dives". We can see that from the pitch plot and the height, the height suddenly goes down and the pitch goes to negative values. This can be seen very clearly in the images of figure 7.7.

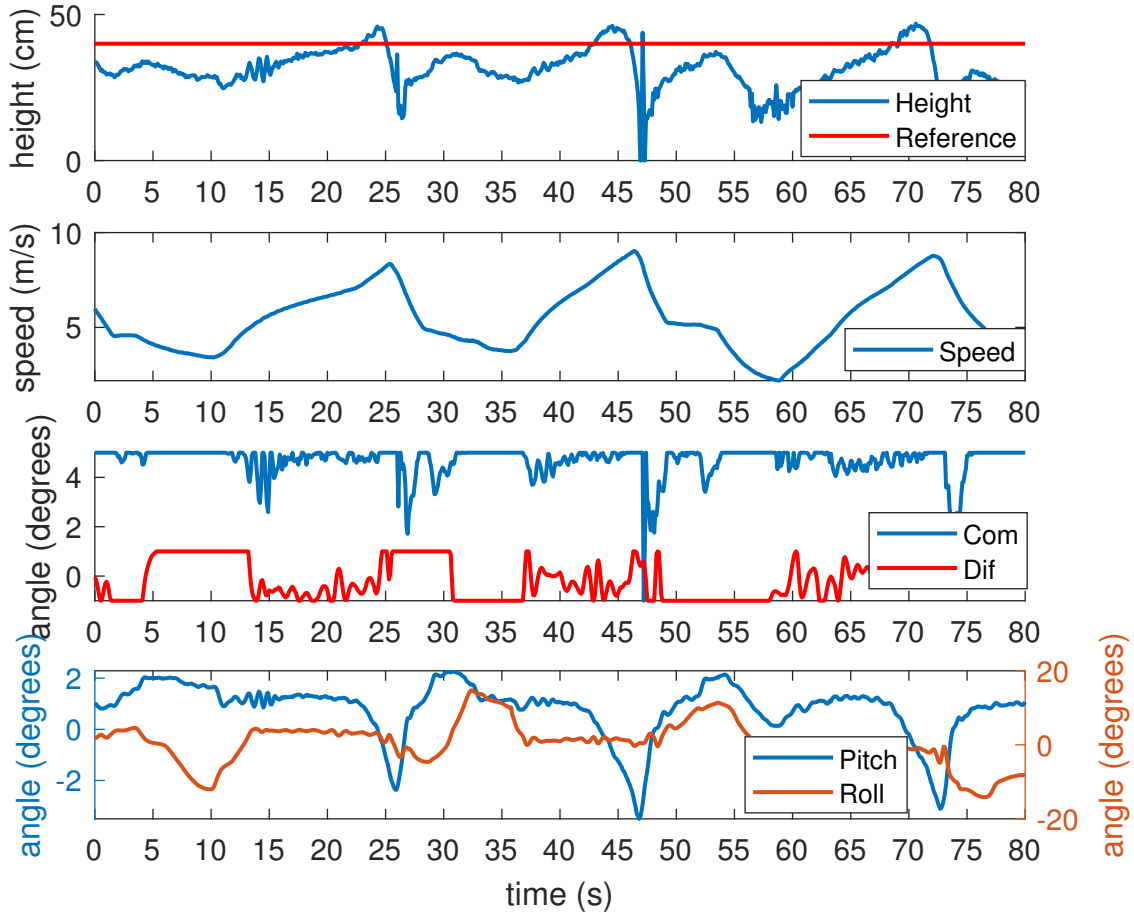


Figure 7.6: First tests with active height control.



(a) Flight just after takeoff and before "bow diving". (b) Moment where the boat "bow dives".

Figure 7.7: Sequence where the boat can be seen flying and then "bow diving".

When this happened we first tried to reduce the rear angle of attack, but this wasn't a good idea and

wouldn't solve the problem because the vessel would still over accelerate after taking off. Ideally the pilot would have had time to reduce the power on the motors after take off so the vessel would stay at the right speed, but this happens too fast for the pilot to control it without a lot of training.

After reducing the rear foil's AoA, we didn't have enough lift and so only the bow would lift off. Even though the pitch was far from the equilibrium point around which the controller was designed, the vessel would stay very stable and could go like this for long period of time. Image 7.8 shows the position the vessel would maintain. Since this angle was not enough for the rear foil we eventually went back to the angle we had initially.



Figure 7.8: Flying with small rear AoA.

Looking at the data we could see that with a single motor, the common mode angle would saturate and the foils wouldn't generate enough lift to take off. To solve this the struts were moved around their attachment axis to have the foils' range of AoA shifted up a few degrees. After that it was possible to take off at speeds just under 7 m/s. With that we could fly at 7 m/s and with only one motor, as was planned from the beginning, getting closer to the expected values from tables 3.3 and 3.4.

Now even though we managed to takeoff at speeds lower than 7 m/s and had the rear foil at an appropriate angle we still had the problem of overshooting speed that caused the "bow diving" described above. Because of that we implemented a simple PID that would adjust the power to the motors automatically to maintain a constant speed. See subsection 7.2.1 to see how this was implemented

### 7.2.1 Motor's PID upgrade

To maintain a constant speed with hydrofoils the power has to be reduced as soon as the takeoff has happened. Since the drag is reduced after takeoff, if the power is not reduced then the boat will accelerate.

On the first tests of the boat the pilot controlled the power of the motors with the boat's throttle, as shown in figure 7.9. The throttle would send a command to the motor controller, and that command was

interpreted as the desired power on the motor.

To automatically adjust the power a PID was used between the throttle and the motor controller, as shown in figure 7.10. The throttle's command is now interpreted as the desired speed, which is compared to the real speed of the boat and the PID computes the adequate power that is then sent to the motor controller. The actual vessel has 2 motors, but for simplicity this PID was implemented for single motor. To use both motors and the PID more care has to be taken because the power distribution between the 2 motors has its own algorithm.

The actual PID was coded inside a microcontroller which is equal to the one in the hydrofoils system, but this one is only used to make a bridge between the throttle, the boat's CAN bus and the motor controllers. Since this microcontroller is widely used there are PID libraries available, ready to use, and the one used implements the PID controller that can be seen in figure 7.11. This library uses a different method to prevent wind-up effect. It simply limits both the output, and the integral term to the limits chosen by the user [22].

To find the best PID gains we first tried gains that were sound to use considering the order of magnitude of both the power command and the desired speeds. After implementing the PID and running quick tests on dry land we tested the PID and fine tuned the gains. After a few runs the gains were adjusted to

$$K_P = 35 \quad K_I = 5 \quad K_D = 15. \quad (7.3)$$

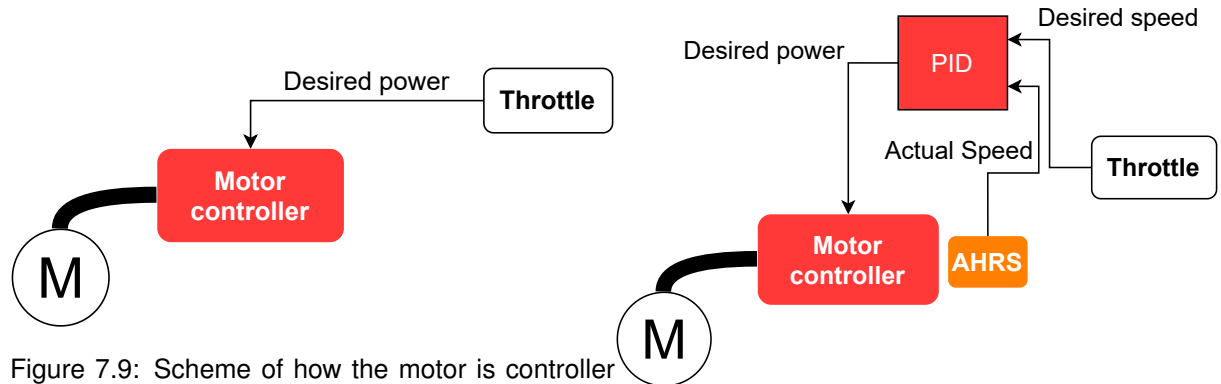


Figure 7.9: Scheme of how the motor is controlled without PID.

Figure 7.10: Scheme of how the motor is controlled with the new PID.

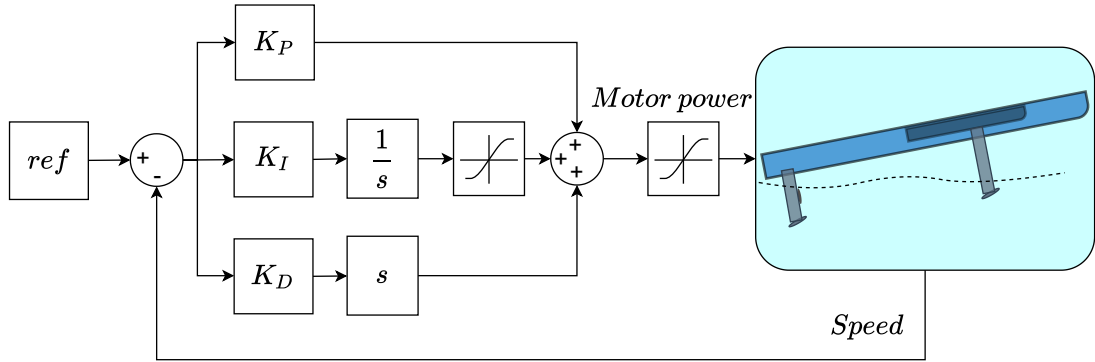


Figure 7.11: PID feedback loop that was implemented to keep a constant speed.

After implementing the PID we had trouble with the steppers lacking power, as mentioned in 7.1. We did a lot of runs trying to takeoff but the vessel would fall sideways, so we spent a lot of time repeating this to find exactly when it happened. After many tries we found out that if we stayed under a certain speed, with a slow acceleration, the problem didn't happen. With this strategy we obtained the results from figures 7.12 and 7.13, which are time matched. We can see that the speed stays very close to the desired speed, with some oscillations. Furthermore, by looking at the height and pitch data we can see that the speed oscillations match the ups and downs of the boat. These ups and downs are due to the fact that the common mode angle is very close to its upper limit, and so sometimes the lift at the front is not sufficient. Flying faster would solve this, but again, we would get one of the steppers stuck and fall sideways.

Even though the vessel would go up and down every 20 seconds, it was enough to see it fly very well and even doing some turns. Image 7.14 shows the vessel flying and slightly turning.

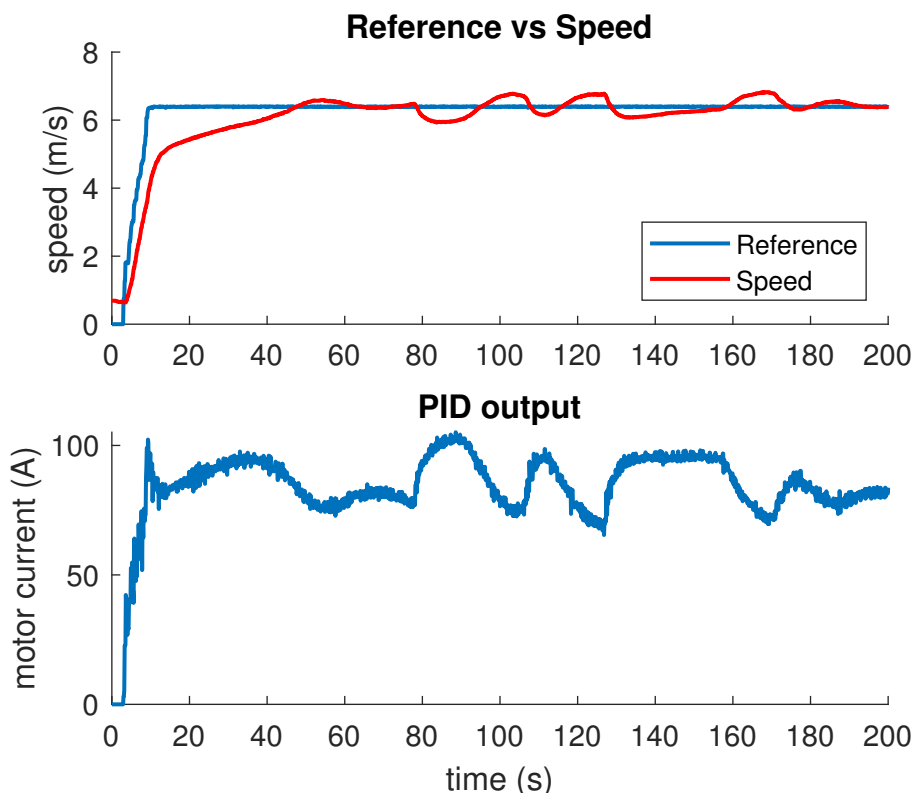


Figure 7.12: PID speed control results.

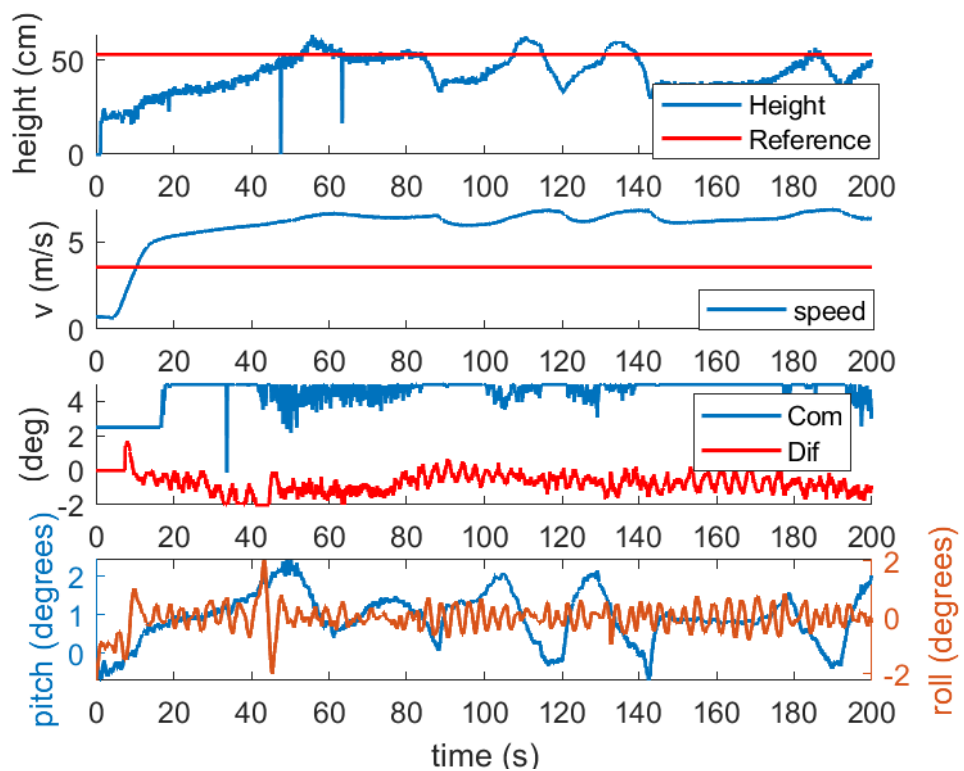


Figure 7.13: Flight data with PID speed control corresponding to figure 7.12.



Figure 7.14: Flying stable and doing a small turn (drone view).

### 7.3 Active roll reference

When we managed to get reasonably stable flights we started to test the limits of curvature. When there was wind coming from the inside of the curve the vessel would easily fall to the outside of the curve, the wind force added to the centrifugal force. Figure 7.15 shows the boat falling sideways (high roll), and this time the LQR output is matched with the actual stepper angle, so the actuator is not stuck.

Because the roll controller would try to maintain the boat level the wind could get under the side panels that support the solar modules. This triggered the idea of using a non-zero roll reference. Changing the roll reference could allow the boat to lean towards the inside of the curve, not letting the wind penetrate, and also realign the lift force with the centrifugal force.

To implement an active roll reference we need to know when the boat is turning. For this, and to not have to add sensors to the boat, we can use the yaw rate,  $\dot{\psi}$ , that comes from AHRS sensor that is present on the vessel. To adjust the sensitivity of the reference the yaw rate is multiplied by a gain, as in equation

$$ref = K_{ref} \cdot \dot{\psi} \quad (7.4)$$

After the gain a saturation block is used to limit the roll reference to an acceptable value, this is adjusted by testing. Figure 7.16 shows the adapted feedback loop for the new addition on the roll controller.

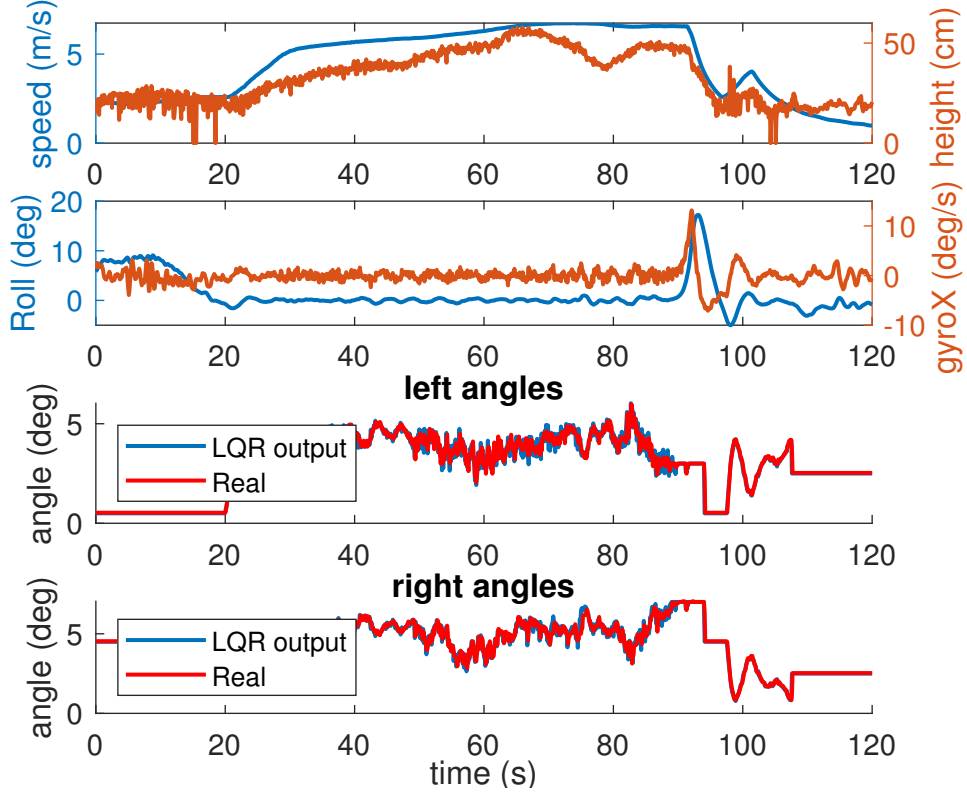


Figure 7.15: Flight data where the boat can be seen falling sideways due to the wind.

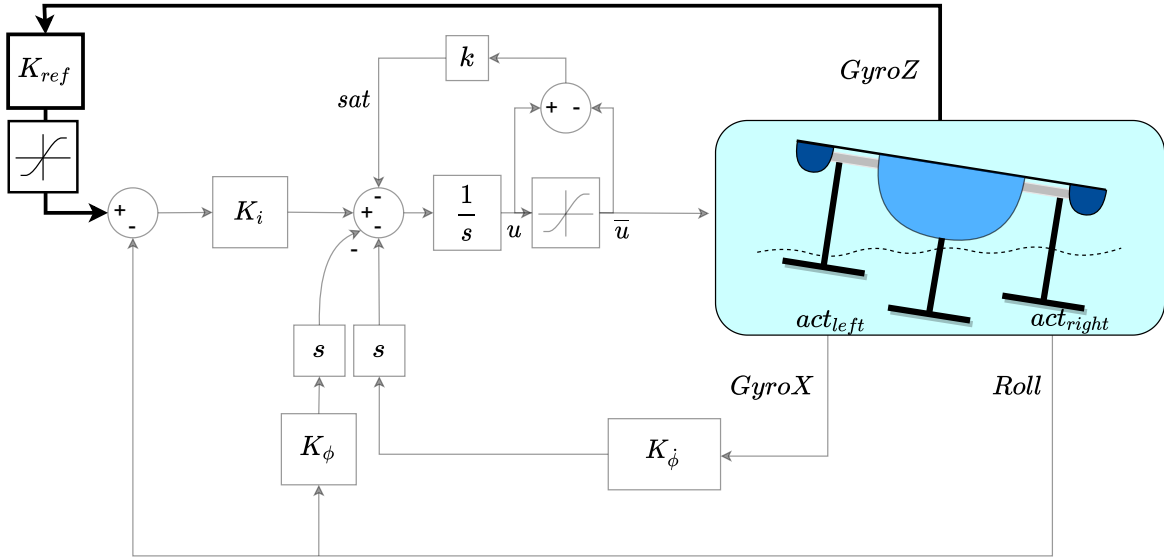


Figure 7.16: Upgrade done on the roll controller with yaw rate (here GyroZ) fed back to the reference.

Before implementing this on the vessel, real data was used to adjust the gain  $K_{ref}$ . Simulations were done to see if the controller would follow the reference. Figure 7.17 shows the real data tested, and the yaw rate can be seen very noisy when the boat is foilborne. Because of this some filtering was done.

Different filters were tested on the real data acquired during previous tests. Such as simple moving average, exponential moving average and median filter. Figure 7.18 shows the different filters compared and plotted over the raw data. For this application any one of the three filters would smooth out the

control in a similar way. So the simple moving average filter was used, being very simple and appearing to be more reactive than the other two filters.

With the filtered data the simulation could be run, and the result can be seen in figure 7.19. The roll can be seen following the reference very closely with the gains previously chosen in (7.2).

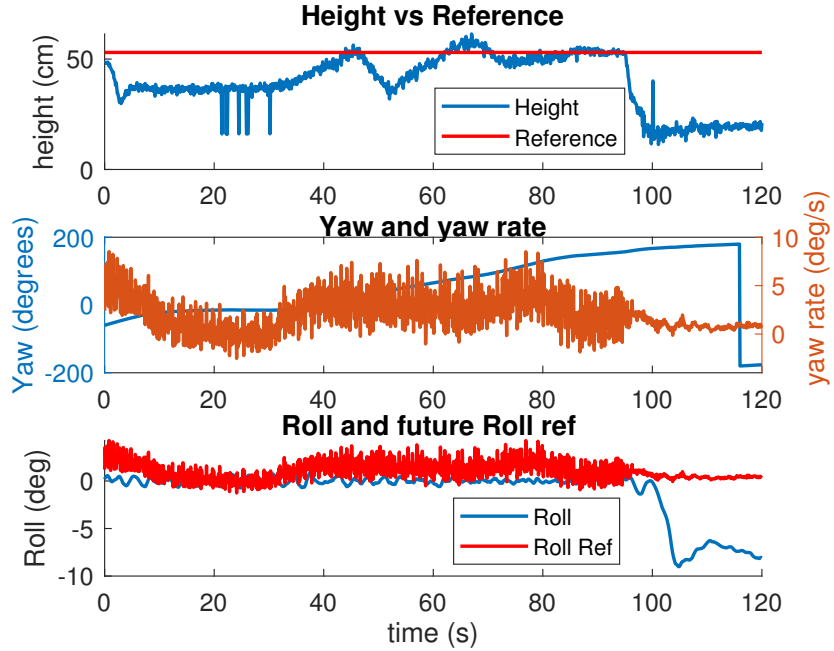


Figure 7.17: Real data used to simulate how the roll reference would look like. As can be seen here, a lot of noise comes from the sensor.

With the simulation done to validate the control this was tested on the vessel. After some trials the gain was set to

$$K_{ref} = 0.8 \quad (7.5)$$

and the maximum roll set to 5 degrees.

This control worked well and can be seen on figure 7.20. The course done on this figure is also represented in figure 7.21. The data shows the roll reference being followed while doing loops starting at time 300s, and the filtered yaw rate can also be seen very similar to 7.18.

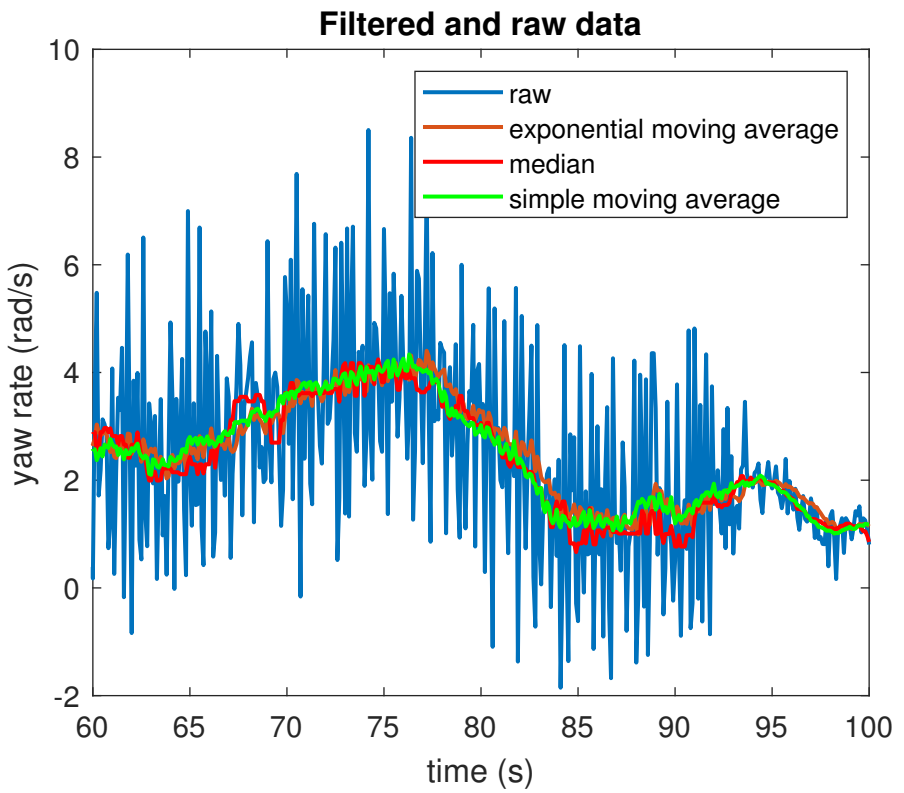


Figure 7.18: Yaw rate filtered data over the raw data from the sensor.

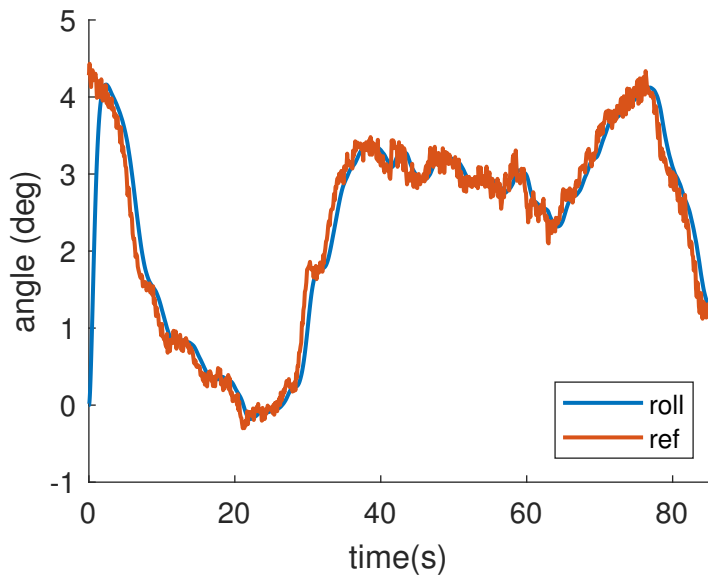


Figure 7.19: Active roll reference simulation with filtered yaw rate as reference.

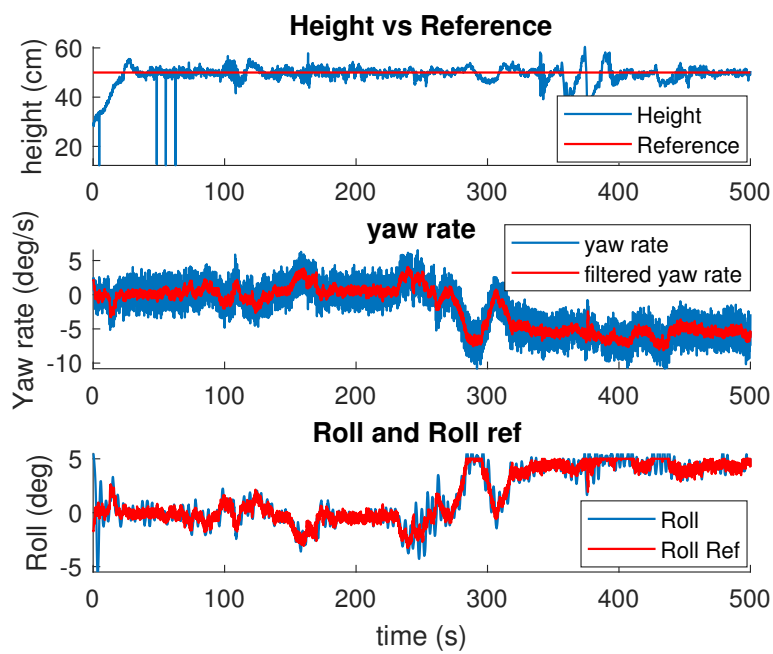


Figure 7.20: Real data with active roll reference implemented on the vessel and doing loopings at cruise speed.

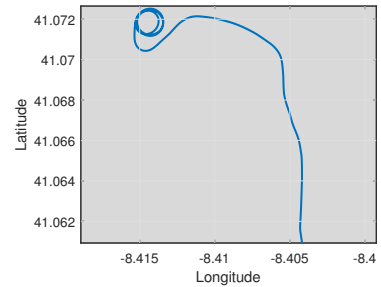


Figure 7.21: Bird view of the course taken by the boat for data of figure 7.20.

## 7.4 Técnico Solar Boat Odisseia 2020

After all the implementations and tests the Técnico Solar Boat team did a tour of Portugal to show the vessel to the public. At each stop of this tour there was at least one test day, and this allowed to do some more improvements on the vessel. One improvement was on the smoothness of the mechanical parts that control the AoA of the hydrofoils. This allowed to reduce the times that the steppers would get stuck by lack of power. That allowed the vessel to fly faster and stay foilborne for periods of 10 minutes non-stop. Figure 7.22 shows the data from one of those moments and figure 7.23 shows images of the vessel successfully cruising on hydrofoils.

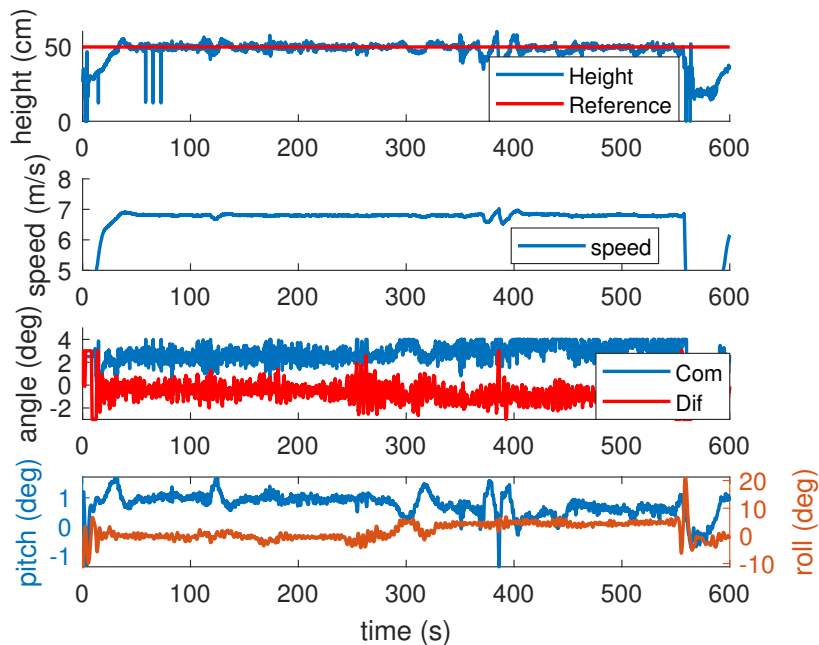


Figure 7.22: Long flight during the Odisseia 2020 event.

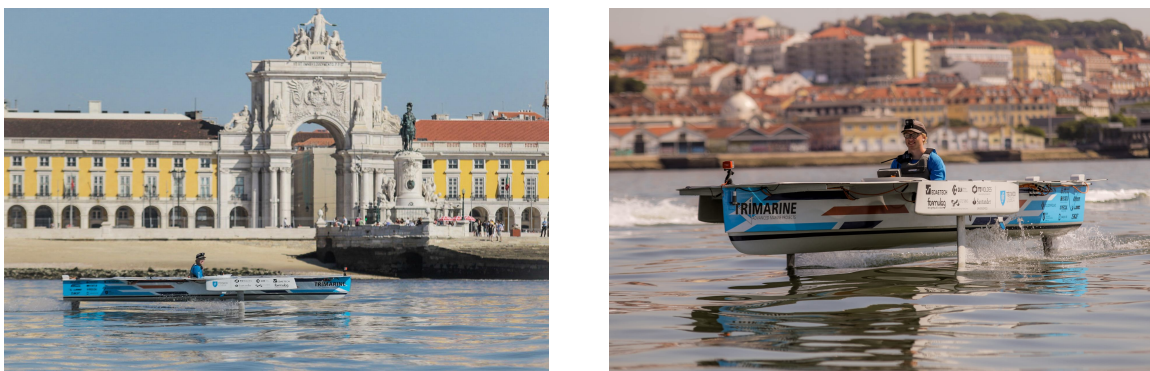


Figure 7.23: Images of the boat during the Odisseia 2020 tour.



# Chapter 8

## Conclusions

### 8.1 Summary

The main goal of this project was to implement hydrofoils on an existing solar powered vessel, SR02, which had hydrofoils already designed, but was yet to test those foils.

A first introduction was done about hydrofoils, their history and how they work. The motivation to implement hydrofoils on this vessel was talked about. Going through other existing vessels that compete directly with the Técnico Solar Boat team. Different kinds of control were shown, such as electronic control versus mechanical control.

After having the theme introduced, the hydrofoils to be used on the SR02 were analysed, from their profile to their lift and drag coefficients. CFD numbers such as  $N_{crit}$  and  $Re$  number were introduced and the equations that describe lift of the airfoils were compared for different speeds to see what simplifications could be done. The concept of 2 and 3 dimensional lifts was also introduced.

Having described the foils we could focus on the model that would describe the behaviour of the vessel when foilborne. For this model we first defined the reference frames and the DOF of a vessel. Knowing what would be done in this work, the movements for this vessel were simplified to 4 DOF. Having the reference frames, the forces that act on the vessel were described, and all simplifications and assumptions were exposed. From here the base non linear model was obtained.

Having the non linear model we could start thinking how it could be controlled. For that the usual steps to compute optimal control gains were taken: trim the model, linearize it about the trimmed equilibrium point and finally compute the gains for an LQR controller. With those gains computed the model's response to input steps were seen. However, before trying to optimize the gains, some improvements to the LQR controller were done. First a reference following for heave was implemented, then integral action, anti wind-up, and finally a delta implementation. All these improvements were done to make the controller as robust as possible. Having the full implementation of the controller, it was compared to the classical LQR controller and proven to be better at following a reference when a bias was applied to one of the state variables.

All this was done considering the model and controller for the main model, that describes pitch and

heave behaviour, but even though roll is independent from these variables, a very similar controller was projected to control roll. Having the roll controller, the concept of differential and common mode interconnection was seen.

To prove that the controller was well designed it was put to test on the non linear model that was initially built. Simulations on this model were done now including the controller, and the results were acceptable to implement the controller on the real vessel.

The implementation of the controller was successfully tested with hardware in the loop tests. A flowchart was presented to explain the functioning of the system and the interactions the pilot could have with it, what could be changed or not.

Having the implementation done it was time to test the vessel in the water in real conditions. First tests were done slowly as no one in the Técnico Solar Boat team had experience with hydrofoils and we knew from other teams that things could go wrong. Luckily most tests went smoothly and on the first day that both controllers (common and differential) were tested, the vessel took off and stayed foilborne for a few seconds. This was an event of great excitement since it proved that it could be possible to have the whole vessel over the hydrofoils.

After the first tests the data were analysed and we could see there needed to be some sort of control on the motor to be able to maintain the speed close to the speed at which the controller was designed. This control was implemented and worked well, it allowed the vessel to stay over the hydrofoils for longer periods of time. After this a problem arised, which was related to the actuators. The actuators would get stuck and the vessel would fall sideways. This was a great impasse, and it took almost one month of tests to discover the origin of this problem because some important data was not being acquired. Luckily after finding out about this problem the mechanical parts could be improved and at this stage we managed to finally get great results. The vessel then took part in a tour around Portugal to show everyone what the team had pulled off.

## 8.2 Future Work

Having had a lot of difficulties on the mechanical implementation of the vessel we could not fully test the controller to its limits at high speeds nor with larger waves. Most tests were done in very good conditions which allowed the vessel to fly smoothly and without large perturbations.

A very interesting work to be done in the future is to improve the mechanical part of the foils' control to push the vessel to the limits. This would allow to test the controller at speeds of over 10 m/s. This would be interesting to test the real range of operation of the controller, considering it was designed at 7 m/s it may be unstable at 10 m/s. If that is the case then gain scheduling could be done, where the gains are adjusted depending on the speed at which the vessel is going.

More tests should also be done with more waves and maybe some adjustments to the gains will be needed.

Another major improvement to be made is to have a controllable rear foil and implement the controller for such vessel.

Some higher security features could be implemented, such as a detection of too high reading of the ultrasonic sensor for a certain period of time could warn the pilot, or send a signal to the motor controller to stop the vessel.

Finally, the model could be improved to consider movement in yaw and sway to simulate the vessel turning.

This work was proven to be successful but it can definitely be improved in some very interesting ways.



# Bibliography

- [1] G. Trincheiras. Técnico solar boat (tsb): Electrical propulsion system improvement featuring a dual motor drive. Master's thesis, Instituto Superior Técnico, 2018.
- [2] V. Energy. Solar boat racing: Clafis victron energy unstoppable - victron energy. <https://www.victronenergy.com/blog/2017/09/08/solar-boat-racing-clafis-victron-energy-unstoppable/>, Sept. 2017. Accessed on 1-6-2019.
- [3] YCM. Solar & energy boat challenge. <https://mcsebc.org/>, 2019. Accessed on 6-6-2019.
- [4] J. Meyer and J. Wilkins. In *Hydrofoil development and applications*. High Performance Marine Vehicles Conference and Exhibit, 1992.
- [5] J. Eickmeier, M. Dalanaj, J. Gray, and M. Kotecki. *OCE Hydrofoil Development Team Spring/Summer 2006: Final Report*. 2006.
- [6] Quadrofoil. <https://quadrofoil.com/en/>, 2019. Accessed on 1-6-2019.
- [7] Tu delft solar boat team. <https://solarboatteam.nl/en/over/>, 2018. Accessed on 4-6-2019.
- [8] D. S. Oiling and R. G. Merritt. Patrol combatant missile hydrofoil design development and production - a brief history. *High-Speed Surface Craft*, 1980.
- [9] R. J. JOHNSTON and W. C. O'NEILL. 'the development of automatic control systems for hydrofoil craft. *Hydrofoil Development Program Office Naval Ship Research and Development Center*, 1975.
- [10] Candela speed boat. <https://candelaspeedboat.com/>, 2019. Accessed on 3-6-2019.
- [11] G. P. van Marrewijk and J. K. Schonebaum. An experimentally validated dynamical model of a single-track hydrofoil boat. 2017.
- [12] C. E. Brennen. An internet book on fluid dynamics - finite span performance. <http://brennen.caltech.edu/FLUIDBOOK/FLUIDBOOK.htm>, 2006.
- [13] M. Altosole, G. Benvenuto, M. Figari, and U. Campora. Real-time simulation of a cogag naval ship propulsion system. *Proceedings of The Institution of Mechanical Engineers Part M-Journal of Engineering for The Maritime Environment*, 223:47–62, 02 2009. doi: 10.1243/14750902JEME121.

- [14] NASA. L/d ratio. <https://www.grc.nasa.gov/www/k-12/VirtualAero/BottleRocket/airplane/ldrat.html>, 2019. Accessed on 30-5-2019.
- [15] MathWorks. Steady-state operating point from specifications (trimming) or simulation. [https://www.mathworks.com/help/slcontrol/ug/findop.html?s\\_tid=doc\\_ta](https://www.mathworks.com/help/slcontrol/ug/findop.html?s_tid=doc_ta), 2019. Accessed on 1-6-2019.
- [16] MathWorks. Exact linearization algorithm - matlab & simulink. <https://www.mathworks.com/help/slcontrol/ug/exact-linearization-algorithm.html#bspks1b>, 2019. Accessed on 5-6-2019.
- [17] J. Azinheira. *Sebenta de Controlo de Voo MEAer*. DEM, IST, 2019.
- [18] R. Murray. *Optimization Based Control*. 2009.
- [19] K. J. A. Richard Murray. *Feedback Systems*. Princeton University Press, 2009.
- [20] S. Al-Haddad and H. Wahid. Decoupled integral lqr controller with anti- windup compensator for mimo two rotor aerodynamical system (tras). *Journal of Engineering Science and Technology*, 14: 1374–1397, 06 2019.
- [21] P. P. K. ISAAC KAMINER, ANTONIO M. PASCOAL and E. E. COLEMAN. A velocity algorithm for the implementation of gain-scheduled controllers. *Pergamon Press*, 1995.
- [22] Improving the beginner's pid: Reset windup. <http://brettbeauregard.com/blog/2011/04/improving-the-beginner%E2%80%99s-pid-reset-windup/>, 2011. Accessed on 25-8-2020.

## **Appendix A**

### **Controller PCB**

Schematic and top layer of the PCB used for the hydrofoils' control. The PCB connects to the CAN bus and to all the sensors used for the control.

